

N-7034 Trondheim, Norway

Telephone: (+ 47 7) 59 30 00
Telex: 55 620 SINTEF N
Telefax: (+ 47 7) 59 24 80

Rev. 1993-04-02

Rev. 1992-02-01

Rev. 1991-03-01

Rev. 1990-07-01

| | |
|---|--|
| Title of report USFOS - A Computer Program for Progressive Collapse Analysis of Steel Offshore Structures. Theory Manual | Date 1988-10-21 |
| | No. of pages/appendices 83 |
| Author(s) <i>Tore H. Søreide, Jørgen Amdahl, Ernst Eberg Tore Holmås and Øyvind Hellan</i> | Divisional responsibility (sign.) <i>Nils Spidsøe</i> |
| Division Division of Structural Engineering | Project no. 710690 |
| ISBN no. | Price group |

| | |
|--|---------------|
| Client/sponsor of project Multiclient | Clients' ref. |
|--|---------------|

Abstract

The theoretical basis for the computer program USFOS is described. The program is aimed at ultimate strength and progressive collapse analysis of framed offshore structures. The basic idea of the technique is to represent one physical element in the structure by one finite element. Nonlinear geometric - and material properties are accounted for, the latter by means of yield hinge theory and interaction formulas for stress resultants.

At present the program allows for concentrated - and linearly distributed loads, as well as thermal loads.

An element model for a tube with local dent and lateral distortion is included. This makes the program well suited for residual strength analysis of damaged offshore structures.

| | Indexing terms: English | Norwegian |
|---------------------------------|-------------------------|--------------------|
| Group 1 | Marine Tehcnology | Marinteknikk |
| Group 2 | Platform | Plattform |
| Key terms selected by author(s) | Progressive Collapse | Sammenbrudd |
| | Computer Program | Regnemaskinprogram |
| | Theory Manual | Teorimanual |

CONTENTS

| | Page |
|---|------|
| 1. INTRODUCTION | 1.1 |
| 1.1 General | 1.1 |
| 1.2 Previous Work on the Idealized Structural Unit Method | 1.2 |
| 1.3 Aim of Present Study | 1.4 |
| 2. FUNDAMENTAL CONTINUUM THEORY FOR ELASTIC BEAM | 2.1 |
| 2.1 Large Displacement Theory | 2.1 |
| 2.1.1 Description of Motion | 2.1 |
| 2.1.2 Strain Measure | 2.2 |
| 2.1.3 Stress Measure | 2.3 |
| 2.2 Strain-Displacement Relations for Beam | 2.3 |
| 2.2.1 Reference System | 2.4 |
| 2.2.2 Strain-Displacement Relations | 2.4 |
| 2.2.3 Comments on the Accuracy of the Strain-Displacement Relations | 2.5 |
| 2.3 Variational Principles | 2.6 |
| 2.3.1 Principle of Virtual Work | 2.7 |
| 2.3.2 Incremental Form of the Virtual Work Principle | 2.9 |
| 2.4 Initial Stress Free Deflections | 2.10 |
| 2.4.1 Effective Strain | 2.10 |
| 2.4.2 Modification of Stiffness Matrix | 2.13 |
| 3. PLASTIC HINGES | 3.1 |
| 3.1 Basic Assumptions | 3.1 |
| 3.2 Elastic-Perfectly-Plastic Model | 3.1 |
| 3.3 Elasto-Plastic Models with Strain Hardening | 3.4 |
| 3.4 Partial Yielding and Strain Hardening Model | 3.6 |
| 3.5 The Hardening Matrix | 3.10 |
| 3.6 Plastic Potentials for Beams | 3.14 |
| 3.6.1 Interaction Surface for Thin-Walled Tube | 3.14 |
| 3.6.2 Interaction Surface for Symmetric I-Profiles | 3.15 |
| 3.6.3 Interaction Surface for Box Sections | 3.16 |

| | | |
|-------|---|------|
| 4. | IMPLEMENTATION OF THE IDEALIZED STRUCTURAL UNIT METHOD | 4.1 |
| 4.1 | General Description | 4.1 |
| 4.2 | Coordinate Systems | 4.2 |
| 4.2.1 | Spatial Coordinates | 4.2 |
| 4.2.2 | Local Element System | 4.4 |
| 4.2.3 | Geometric Transformations | 4.5 |
| 4.3 | Incremental Stiffness for Elastic Beam | 4.9 |
| 4.3.1 | Variational Formulation | 4.9 |
| 4.3.2 | Interpolation Functions Satisfying the Differential Equations | 4.12 |
| 4.3.3 | Third Order Polynomials as Interpolation Functions | 4.17 |
| 4.3.4 | Final Stiffness Matrix | 4.18 |
| 4.4 | Modification for Plastic Hinges | 4.21 |
| 4.4.1 | Plastic Hinge at Element Ends | 4.21 |
| 4.4.2 | Plastic Hinge at Element Midspan | 4.28 |
| 4.5 | Accumulation of Stress Resultants | 4.29 |
| 5. | SOLUTION ALGORITHM | 5.1 |
| 5.1 | Step-by-Step Method | 5.3 |
| 5.2 | Equilibrium Iteration | 5.6 |
| 5.3 | Arch Length Control | 5.7 |
| 5.4 | Convergence Criterion | 5.11 |
| 5.5 | Increment Scaling | 5.12 |
| 5.6 | Bifurcation Analysis | 5.12 |
| 6. | MODELLING OF DENTED TUBULAR MEMBERS | 6.1 |
| 6.1 | Introduction | 6.1 |
| 6.2 | Idealization of Dented Tube | 6.1 |
| 6.3 | Plastic Potential for Dented Section | 6.3 |
| 6.4 | Extension to 3 Dimensions | 6.4 |
| 7. | TEMPERATURE EFFECTS | 7.1 |
| 7.1 | Introduction | 7.1 |
| 7.2 | Beam Element Formulation | 7.1 |
| 7.2.1 | Basic Assumptions | 7.1 |
| 7.2.2 | Equilibrium Equations | 7.3 |
| 7.2.3 | Incremental Equations | 7.4 |
| 7.2.4 | Modification Due to Yield Stress Degradation | 7.6 |
| 7.3 | Plate Element Formulation | 7.7 |
| 7.4 | Mechanical Properties | 7.12 |
| 7.4.1 | Mechanical Properties | 7.12 |

Contents

| | | |
|-----|---|-------|
| 8. | LINEAR DEPENDENCY | 8.1 |
| | 8.1 Introduction | 8.1 |
| | 8.2 Derivation of Kinematic Constraints | 8.1 |
| 9. | LOCAL FLEXIBILITY | 9.1 |
| | 9.1 Introduction | 9.1 |
| | 9.2 Basic | 9.2 |
| | 9.3 Modelling of a Brace/Chord Connection | 9.2 |
| | 9.4 Stiffness Matrix for Degrees of Freedom on the Chord Shell Surface | 9.4 |
| | 9.5 Examples | 9.9 |
| | 9.6 Conclusion | 9.15 |
| 10. | FRACTURE CRITERIA | |
| | 10.1 Introduction | 10.1 |
| | 10.2 Rotation in Elasto-Plastic Region | 10.2 |
| | 10.2.1 Rectangular Cross-Section | 10.2 |
| | 10.2.2 Tubular Cross-Section | 10.4 |
| | 10.3 Rotation in Strain Hardening Region | 10.6 |
| | 10.3.1 Bending | 10.6 |
| | 10.3.2 Membrane Strain | 10.11 |
| | 10.4 Fracture Criterion | 10.15 |
| 11. | LOCAL BUCKLING OF RECTANGULAR CROSS-SECTIONS | |
| | 11.1 Introduction | 11.1 |
| | 11.2 Buckling Criterion | 11.5 |
| | 11.3 Residual Plastic Capacities | 11.5 |
| | 11.4 Interaction Function for Stress Resultants | 11.10 |
| | 11.5 Elasto-plastic Constitutive Equations | 11.10 |
| 12. | DECK PLATING | 12.1 |
| 13. | SHIP COLLISION | |
| | 13.1 Introduction | 13.1 |
| | 13.2 Local denting of tube wall | 13.1 |
| | 13.3 Implementation in the plasticity formulation | 13.3 |
| | 13.4 Ship indentation characteristics | 13.4 |
| 14. | DYNAMIC COLLAPSE ANALYSIS | |
| | 14.1 Introduction | 14.1 |
| | 14.2 Mass matrix | 14.1 |
| | 14.3 Damping | 14.2 |
| | 14.4 The α -method of time integration | 14.2 |
| | 14.5 Equilibrium iteration | 14.5 |
| | 14.6 The predictor-corrector method | 14.6 |
| | 14.7 Time step scaling | 14.7 |
| 15. | EXTERNAL HYDROSTATIC PRESSURE | |
| | 15.1 Introduction | 15.1 |
| | 15.2 Tube section interaction curves | 15.1 |
| | 15.3 Implementation in the plasticity formulation | 15.3 |
| | 15.4 Limitations | 15.5 |
| 20. | REFERENCES | 20.1 |

LIST OF REVISIONS

| Section | Date | Contents |
|---------|------------|-------------------------------------|
| 0 | 1993-04-01 | Abstract / Contents |
| 1 | 1988-10-01 | Introduction |
| 2 | 1988-10-01 | Fundamental Continuums Theory |
| 3 | 1992-02-01 | Plastic Hinges |
| 4 | 1992-02-01 | Implementation of ISUM |
| 5 | 1992-02-01 | Solution Algorithm |
| 6 | 1988-10-01 | Modelling of Dented Tubular Members |
| 7 | 1993-04-01 | Temperature Effects |
| 8 | 1989-12-01 | Internal Hinges |
| 9 | 1989-12-01 | Local Flexibility |
| 10 | 1991-03-01 | Fracture Criteria |
| 11 | 1991-03-01 | Rectangular Cross-Section |
| 12 | 1991-03-01 | Deck Plating Element |
| 13 | 1991-03-01 | Ship Collision |
| 14 | 1993-04-01 | Dynamic Collapse Analysis |
| 15 | 1993-04-01 | External Hydrostatic Pressure |
| 20 | 1993-04-01 | References |

1. INTRODUCTION

1.1 General

The implementation of accidental loads as a design load category in offshore rules /1/ has strengthened the need for rational tools for accidental load effect analysis. In design and operation of the structure it is of interest to know the amount of damage as well as the residual strength in damaged condition.

Related to the prediction of damage due to impact loading a new design philosophy is developed in the sense that structural capacity is given as energy absorption capability rather than as ultimate load. The DnV rules for mobile offshore units /2/ specify 14 MJ (Mega Joule) as impact energy for beam collision and 11 MJ for bow or stern collision, corresponding to a supply vessel of 5000 tonnes displacement with impact speed 2.0 ms^{-1} .

The extent of damage caused by accidental loads ranges from total collapse of the structure to small damages which may not have serious consequences at the time of accident. However, such a small damage may effect the ability of the structure to withstand extreme loads, thus having an influence on the safety. Newer general structural design codes include a progressive collapse limit state /3/. The philosophy behind this design limit state is to assure that a structural system has sufficient resistance to tolerate some local damage without catastrophic consequences.

Fjeld /4/ has presented the philosophy of limit state of progressive collapse for fixed offshore structures. However, accidental loads are covered only to a small extent in present codes. The British rules /5/ assume that the conventional types of structures have sufficient extra resistance to sustain accidental loads while the American Petroleum Institute code /6/ contains no criteria on accidental loads. The regulations for fixed platforms by the Norwegian Petroleum Directorate /7/ require the residual strength to be checked in damaged condition. Local damage is accepted in case of sufficient post-damage capacity. The Norwegian Maritime Directorate has started a major research project to improve the ability to do a rational design against accidental loads

on mobile platforms. The first results from this project have already been given /8/. This presentation describes a procedure for progressive collapse strength evaluation.

In the case of damage of a bracing element in an offshore structure, the simplest procedure for checking residual strength would be to eliminate the damaged element from the structural frame model and to perform a new linear analysis of nominal stresses. However, such an analysis is conservative in the sense that the post-damage strength of the damaged element is neglected together with the effects of stress redistribution in the structure. These factors can only be taken care of by an elasto-plastic large displacement type of analysis.

The choice of design impact situations must be done under consideration of probability of occurrence /9/. The size of design vessel is to be determined on the basis of the vessels intended to operate in the area, such as service vessels, tankers for offshore loading and by-passing ships.

1.2 Previous Work on the Idealized Structural Unit Method

Ueda and Rashed /10/ have described a procedure which combines plastic methods of structural analysis with local buckling of web for ultimate strength analysis of transverse frames in ship structures. Rashed /11/ has extended this procedure, called the Idealized Structural Unit Method (ISUM), to be used for ultimate strength analysis of tubular frame structures. The beam-column behaviour of slender members is taken care of by using an element stiffness formulation presented by Livesley /12/, where the stiffness terms are nonlinear functions of the axial force. Plastic hinges are introduced at locations where the element cross section reaches its ultimate capacity. The stiffness matrix is modified to account for the plastic hinge, and the load increased until the next cross section reaches its ultimate capacity. This process continues until a complete mechanism is formed and the load cannot be increased any further.

The Idealized Structural Unit Methods has been further developed and adopted to progressive collapse analysis of mobile offshore platforms /13/. Incremental equations are derived from energy potentials by variation of the total energy

and subsequent differentiation of the equilibrium equations /13/. The main advantage of the derivation based on energy expressions is that it results in a symmetric matrix while the derivation in /11/ from the differential equation gave almost identical but nonsymmetric expression.

The structure stiffness matrix is assembled from element stiffnesses calculated in an updated geometry. The effect of large nodal point displacements is thus included.

The load is applied incrementally. For each load step the structure stiffness is assembled and the global displacement increment calculated. The element force increment is calculated by using the tangential stiffness matrix and the element displacement increment. At each level all elements are checked to see whether buckling or plastic capacity has been reached. If such an event is predicted the step is reduced to being the response to just reach that event. A plastic hinge is introduced in the element at the position where the capacity was reached. A modified stiffness matrix accounting for the plastic hinge is calculated and the process proceeds to the next load step. A cross section that has reached the plastic capacity remains on the plastic interaction surface and move tangentially to this surface. The previous formulation does not include the possibility of elastic unloading from a plastic stress state.

Buckling is accounted for by standard column buckling strength formula. The effective length l_e of the beam-column element depends on the stiffness of adjacent elements. Approximate expressions based upon the relative stiffness of the adjacent members at each end is used /11/. The effective length calculated by this approach will always be less than the actual length of the element. If the rigidity in some direction is small at a nodal point this may be completely misleading. Fortunately, a criteria for global buckling in most cases will detect such type of failure, by checking the incremental stiffness matrix.

Analysis of progressive collapse of structures with dented tubular members /14/ has been performed by replacing the dented region by an eccentric circular cylinder with equivalent cross section properties.

1.3 Aim of Present Study

The previous versions of the program USFOS /11, 13/ have worked well for problems with moderate nonlinearity. The version in /11/ was capable of handling only linear geometry while van Aanhoud implemented updating of global coordinates and thereby allowed large global deformations. But the program still was restricted to linear geometric behaviour on element level. The present version has built in large deflection formulation on element level and thus allows moderate deflections of elements between nodal points.

This has a major implication on the buckling phenomenon. Buckling is now a result of the energy state of the system. Hence, there is no longer need to introduce this artificially by comparison with standard column buckling strength formula. The event check on element level now only concerns detection of plastic hinges.

The step-by-step solution technique has so far been based upon pure Euler-Cauchy incrementation. It is the aim of this study to describe the procedure for equilibrium iterations based on the residual between external loads and internal stress resultants. This modification would also include Euler-Cauchy incrementation with equilibrium correction at each step. The variational foundation of the program is also rewritten in the way that it is now totally based upon the principle of virtual displacements for equilibrium control. The incremental stiffness is derived from the corresponding incremental form of the virtual work principle. These new considerations on the variational principles result in modifications of the computer program on the calculation of element stiffnesses and equilibrium forces.

A new model for dented tubular cross-sections is implemented. It is based upon the work of J. Taby /24/. By this model, the local dent is accounted for by reducing the plastic capacity of the cross-section. The overall distortion is handled as an initial stress free deflection.

A new interaction formula for I-profiles is implemented. The main advantage as compared with the previous formulation is its continuity over the entire force

space. A plastic interaction formula for box-sections is also provided.

Finally, a model for temperature loads has been developed. It comprises the effects of E-modulus and yield strength degradation and thermal expansion.

The present study ends in a progressive collapse analysis program for frames capable of handling large displacements and the formation of plastic hinges. The element model is parallel to the real structure in the way that one element in the numerical model corresponds to one physical bracing element. Hence, the problem for the designer to choose a relevant element mesh is eliminated.

2 FUNDAMENTAL CONTINUUM THEORY FOR ELASTIC BEAM

2.1 Large Displacement Theory

The formulation behind the program is valid for large displacements but restricted to small strains. This means that second-order effects from displacements are considered, but the structure is so slender that the strains are still in the range of some percent.

2.1.1 Description of Motion

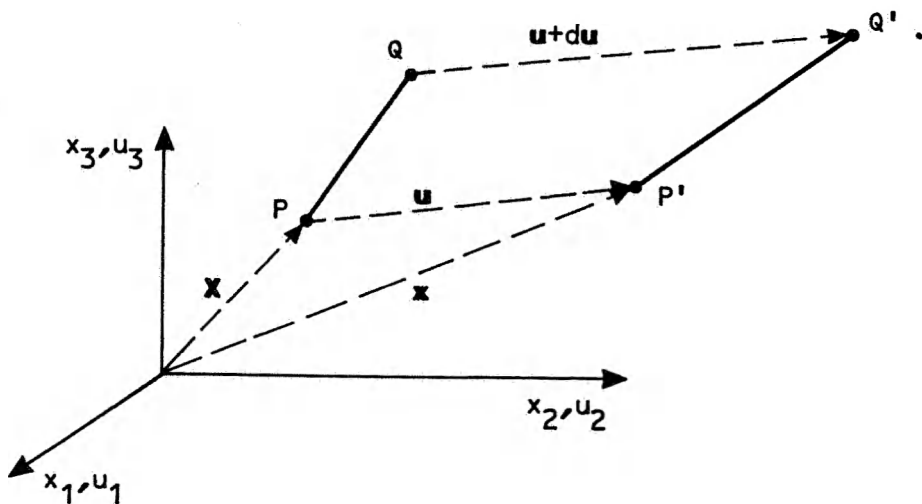


Figure 2.1 Reference system for motion

A spatial Cartesian Coordinate system X_i is given for measuring global displacement u . Denoting the initial coordinates of point P by capital letters X_i and the current coordinates after deformation by x_i the displacement components come out of

$$x_i = X_i + u_i \quad (2.1)$$

In the computer program the coordinates x_i are accumulated at each node and updated during deformation by Eq. (2.1). The displacements u_i are the

global changes in nodal point coordinates during deformation. The relation (2.1) is used for updating the global coordinates of the structure while the evaluation of element stiffnesses is first carried out in local element systems and thereafter transformed into the common global reference system when establishing displacement continuities at nodal points.

2.1.2 Strain Measure

The program is aimed for the analysis of trusses and frames and is restricted to uniaxial strain for tubular sections. For I- and box profiles shear strain is included.

The Green strain component E_x is derived from the definition /15/

$$E_x = \frac{ds^2 - ds_0^2}{2ds_0^2} \quad (2.2)$$

where ds_0 and ds are infinitesimal line segments in initial and current configuration, respectively.

From the definition (2.2) it is clear that self-straining at rigid-body motion is excluded. Self-straining is further discussed in Section 2.3.3 for incomplete strain-displacement relations introduced for the beam elements. It should, however, be emphasized that by Eq. (2.2) and complete strain-displacement expressions self-straining is no problem.

The relation between Green strain and engineering strain

$$\epsilon_x = \frac{ds - ds_0}{ds_0} \quad (2.3)$$

comes out of Eqs. (2.2 and 2.3) as

$$E_x = \epsilon_x + \frac{1}{2} \epsilon_x^2 \quad (2.4)$$

For small strains the higher order term in Eq (2.4) may be neglected and Green strain and engineering strain coincide.

In subsequent derivations the engineering strain notation ϵ_x is used.

The strain measure is related to initial length ds_0 of the line segment. This means that differentiation of shape functions needs to be performed only once in initial coordinates and therefore used at each configuration. For linear elastic material behaviour, the linear part of the element stiffness matrices is kept constant at deformed configurations and only the deflection-dependent stiffness terms need be updated.

2.1.3 Stress Measure

The stress tensor energy conjugate to the Green strain tensor is the second Piola-Kirchhoff stress S_{ij} with uniaxial component S_x . S_{ij} is referred to initial volume and along the convective axes. This means that in the case of small strain S_{ij} approaches the Cauchy stress σ_{ij} in the directions of the convective axes. This is also seen from energy considerations.

In the subsequent stiffness derivations for small strains no distinction is made between second Piola-Kirchhoff stress S and Cauchy stress σ . The symbol σ is used in the formulas.

2.2 Strain-Displacement Relations for Beam

The present section gives the basis for establishing strain-displacement relations for a beam element. The accuracy and restrictions on the assumed relations are also discussed.

2.2.1 Reference System

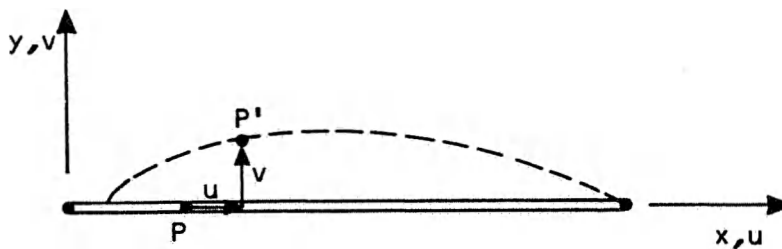


Figure 2.2 Local element xy-system

Fig 2.2 shows the local set of axes x, y for a beam element with the deflected element shape dotted. The total displacement of a point P is decomposed into axial displacement $u(x)$ and lateral deflection $v(x)$ (and $w(x)$ in three dimensions).

The complete expression for strain is subsequently established in local element xy -system and the element stiffness is also derived in local system.

2.2.2 Strain-Displacement Relations

The complete expression for Green's strain (or engineering strain for small strains) reads /15/

$$\epsilon_x = u_{,x} + \frac{1}{2} u_{,x}^2 + \frac{1}{2} v_{,x}^2 + \frac{1}{2} w_{,x}^2 \quad (2.5)$$

For moderate local deflections on element level ϵ_x is simplified into /16/

$$\epsilon_x = u_{,x} + \frac{1}{2} v_{,x}^2 + \frac{1}{2} w_{,x}^2 \quad (2.6)$$

The inaccuracy introduced by this simplification is discussed in the next section. However, it is clear that self-straining is a consequence, and that restrictions are put on the magnitude of local rotations related to the line between end points of the element.

2.2.3 Comments on the Accuracy of the Strain-Displacement Relations

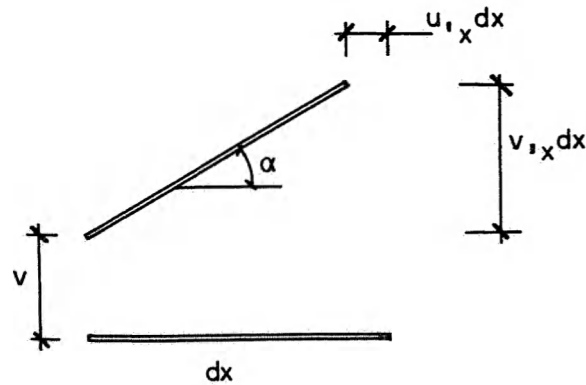


Figure 2.3 Rigid body rotation

Consider the infinitesimal element dx in Fig 2.3 subjected to rigid body motion. The angle of rotation is denoted α , and under rigid body motion the following relations hold /16/

$$v_{,x} = \sin\alpha \quad (2.7)$$

$$u_{,x} = \cos\alpha - 1 \quad (2.8)$$

Combining Eqs. (2.7 and 2.8) and using series expansion gives

$$u_{,x} = (1 - \sin^2\alpha)^{\frac{1}{2}} - 1 \approx -\frac{1}{2} v_{,x}^2 + \frac{1}{8} v_{,x}^4 - \dots \quad (2.9)$$

According to the simplified expression 2.6 the rigid body motion gives a self-straining

$$\epsilon_x = u_{,x} + \frac{1}{2} v_{,x}^2 \approx \frac{1}{8} v_{,x}^4 \quad (2.10)$$

This artificial strain should be compared to the magnitudes of operating strains in the structure. The yield strain for steel is in the range of 0.001 and accepting one percent selfstraining gives an allowable rotation $v_{,x}$ equal to

$$v_{,x} = (8 \cdot 0.00001)^{\frac{1}{4}} \approx 0.1 \text{ rad} \\ = 5.7 \text{ degrees} \quad (2.11)$$

With practical slendernesses of bracing elements the above restriction on local deformation is considered to be no problem.

2.3 Variational Principles

The present section deals with equilibrium equations between external loads and internal stresses on two levels. First, the first variation of potential energy (or its equivalent principle of virtual displacements) is used to establish the total force equilibrium. This formulation is the basis for the process of equilibrium iteration which is carried out between total external loads and total internal stresses at each level of loading.

The second variation of potential energy (or its equivalent principle of virtual displacements on incremental form) is the basis for calculation of incremental stiffness. As it is demonstrated in Section 2.2.2 this procedure is based on a linearization of the incremental strain and thus must be completed by equilibrium iterations in order to find the true solution.

2.3.1 Principle of Virtual Work

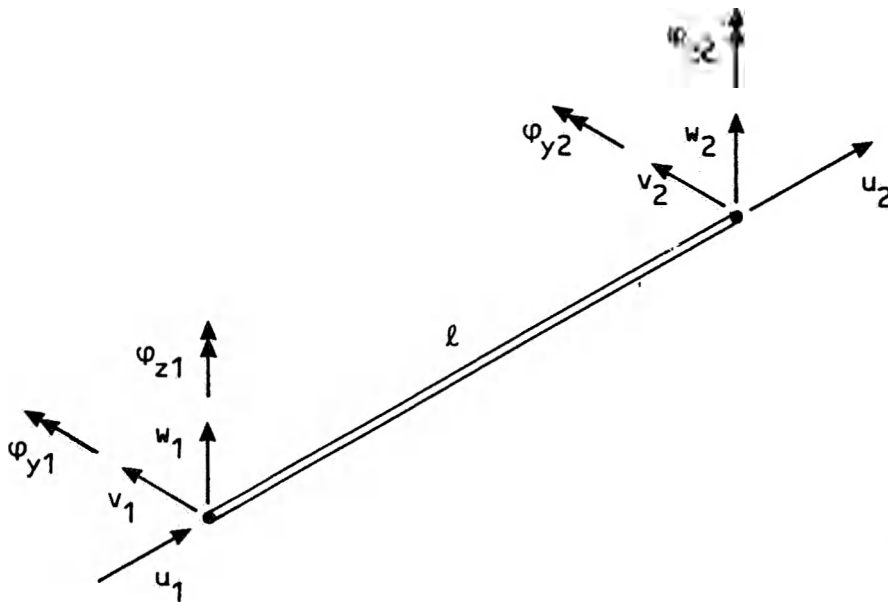


Figure 2.4 Local element displacements

Using the notation in Fig 2.4 for displacements in local element system, the internal strain energy for the elastic element reads

$$\begin{aligned}
 U = & \frac{1}{2} \int_0^l EA (u_{,x} + \frac{1}{2} v_{,x}^2 + \frac{1}{2} w_{,x}^2)^2 dx \\
 & + \frac{1}{2} \int_0^l EI_z v_{,xx}^2 dx + \frac{1}{2} \int_0^l EI_y w_{,xx}^2 dx
 \end{aligned} \tag{2.12}$$

where the first integral represent axial straining and the two last integrals are the contributions from bending. Torsion is not included.

In Eq. (2.12) comma denotes differentiation with respect to the subsequent indice (s).

The potential of external loads is written as

$$H = -(F_i u_i + \int_0^l q_x \cdot u dx + \int_0^l q_y \cdot v dx + \int_0^l q_z \cdot w dx) \tag{2.13}$$

The total potential π comes out of

$$\pi = U + H \tag{2.14}$$

The first variation of internal strain energy is found from Eq. (2.12) as

$$\begin{aligned} \delta U = & \int_0^1 EA(u_{,x} + \frac{1}{2} v^2_{,x} + \frac{1}{2} w^2_{,x}) (\delta u_{,x} + v_{,x} \cdot \delta v_{,x} + w_{,x} \cdot \delta w_{,x}) \\ & + \int_0^1 EI_z v_{,xx} \delta v_{,xx} dx + \int_0^1 EI_y w_{,xx} \delta w_{,xx} dx \end{aligned} \quad (2.15)$$

Introducing now the axial force in the element equal to

$$N = -EA(u_{,x} + \frac{1}{2} v^2_{,x} + \frac{1}{2} w^2_{,x}), \quad (2.16)$$

positive for compression, and rearranging Eq (2.15), the first variation of strain energy becomes

$$\begin{aligned} \delta U = & \int_0^1 EAu_{,x} \delta u_{,x} dx \\ & + \int_0^1 EI_z (v_{,xx} \delta v_{,xx} - \frac{N}{EI_z} v_{,x} \delta v_{,x}) dx \\ & + \int_0^1 EI_y (w_{,xx} \delta w_{,xx} - \frac{N}{EI_y} w_{,x} \delta w_{,x}) dx \\ & - \int_0^1 (N + EAu_{,x}) \delta u_{,x} dx \end{aligned} \quad (2.17)$$

The first term in Eq. (2.17) is the conventional linear contribution from axial strain. The two next integrals represent bending deformation including magnification due to axial compression. The corresponding stiffness matrix elements are represented by the Livesley's functions /12/. The last integral of Eq. (2.17) comes from the nonlinear axial strain contribution from lateral deflections v and w . This is seen to give a contribution to the equilibrium vector of axial loads in addition to the linear relation $EAu_{,x}$ in the first term of Eq. (2.17).

Implementing the following interpolation of element displacements

$$\begin{aligned}
u(x) &= \varphi_u^T(x) u \\
v(x) &= \varphi_v^T(x) v \\
w(x) &= \varphi_w^T(x) w
\end{aligned} \tag{2.18}$$

The first variation of the total potential energy for an elastic element reads

$$\begin{aligned}
\delta\pi &= \delta u^T \left(\int_0^l EA \varphi_{u,x} \varphi_{u,x}^T dx \right) u \\
&+ \delta v^T \left(\int_0^l EI_z (\varphi_{v,xx} \varphi_{v,xx}^T - \frac{N}{EI_z} \varphi_{v,x} \varphi_{v,x}^T) dx \right) v \\
&+ \delta w^T \left(\int_0^l EI_y (\varphi_{w,xx} \varphi_{w,xx}^T - \frac{N}{EI_z} \varphi_{w,x} \varphi_{w,x}^T) dx \right) w \\
&- \delta u^T \left(S_u + \int_0^l (N + EA \cdot u_{,x}) \varphi_{u,x} dx \right) \\
&- \delta v^T S_v - \delta w^T S_w
\end{aligned} \tag{2.19}$$

2.3.2 Incremental Form of the Virtual Work Principle

The aim of the present section is to come up with incremental load-displacement relation for an elastic beam element. The derivation is based upon the variational equations in the previous section.

Denote by Δu_i the increment in displacement between two adjacent deformed configurations C_n and C_{n+1} . Letting δU be the variation in strain energy in C_n the corresponding expression for C_{n+1} may be written.

$$\begin{aligned}
\delta(U+\Delta U) &= \int_0^l EA (u_{,x} + \Delta u_{,x} + \frac{1}{2} (v_{,x} + \Delta v_{,x})^2 + \frac{1}{2} (w_{,x} + \Delta w_{,x})^2) \\
&\quad \cdot (\delta u_{,x} (v_{,x} + \Delta v_{,x}) \delta v_{,x} + (w_{,x} + \Delta w_{,x}) \delta w_{,x}) dx \\
&\quad + \int_0^l EI_z (v_{,xx} \Delta v_{,xx}) \cdot \delta v_{,xx} dx \\
&\quad + \int_0^l EI_y (w_{,xx} \Delta w_{,xx}) \cdot \delta w_{,xx} dx
\end{aligned} \tag{2.20}$$

Incorporating δU from Eg. (2.17) gives

$$\begin{aligned}
\delta U &= \delta(U+\Delta U) - \delta U \\
&= \int_0^1 EA\Delta u_{,x} \delta u_{,x} dx \\
&+ \int_0^1 EI_z (\Delta v_{,xx} \delta v_{,xx} - \frac{N}{EI_z} \Delta v_{,x} \delta v_{,x}) dx \\
&+ \int_0^1 EI_y (\Delta w_{,xx} \delta w_{,xx} - \frac{N}{EI_y} \Delta w_{,x} \delta w_{,x}) dx \\
&+ \int_0^1 EA(\Delta u_{,x} v_{,x} \delta v_{,x} + \Delta v_{,x} v_{,x} \delta u_{,x}) dx \tag{2.21} \\
&+ \int_0^1 EA(\Delta u_{,x} w_{,x} \delta w_{,x} + \Delta w_{,x} w_{,x} \delta u_{,x}) dx \\
&+ \int_0^1 EA(\Delta v_{,x} v_{,x}^2 \delta v_{,x}) dx \\
&+ \int_0^1 EA(\Delta w_{,x} w_{,x}^2 \delta w_{,x}) dx \\
&+ \int_0^1 EA(\Delta v_{,x} v_{,x} w_{,x} \delta w_{,x} + \Delta w_{,x} w_{,x} v_{,x} \delta v_{,x}) dx \\
&+ \text{higher order terms of } \Delta v_{,x} \text{ and } \Delta w_{,x}. \text{ These are neglected.}
\end{aligned}$$

The corresponding variation of the increment in external potential gets the form

$$\delta \Delta H = -\Delta F_i \delta u_i - \int_0^1 \Delta q_x \delta u dx - \int_0^1 \Delta q_y \delta v dx - \int_0^1 \Delta q_z \delta w dx \tag{2.22}$$

The incremental stiffness matrix is obtained by incorporating interpolation of element displacements. It is seen from Eq. (2.21) that this procedure results in a symmetric incremental stiffness matrix.

2.4 Initial Stress Free Deflections

2.4.1 Effective Strain

In the case of initial stress free deflections the strain ϵ_x in Eq. (2.6) is modified into an effective strain as /16/:

$$\epsilon_x = \epsilon_x^{\text{total}} - \epsilon_x^{\text{initial}} \quad (2.23)$$

where $\epsilon_x^{\text{total}}$ is the strain according to Eq. (2.6) with total displacements inserted, that means initial plus load-dependent deformations, $\epsilon_x^{\text{initial}}$ is the value from Eq. (2.6) with initial displacements inserted.

Using notation \bar{v} and \bar{w} for initial deflections and v and w for additional deflections, the following relation emerges:

$$\epsilon_x = u_{,x} + \bar{v}_{,x} \cdot v_{,x} + \bar{w}_{,x} \cdot w_{,x} + \frac{1}{2} v_{,x}^2 + \frac{1}{2} w_{,x}^2 \quad (2.24)$$

The first variation of strain ϵ_x reads

$$\delta \epsilon_x = \delta u_{,x} + (\bar{v}_{,x} + v_{,x}) \delta v_{,x} + (\bar{w}_{,x} + w_{,x}) \delta w_{,x} \quad (2.25)$$

and the increment

$$\Delta \epsilon_x = \Delta u_{,x} + (\bar{v}_{,x} + v_{,x}) \Delta v_{,x} + (\bar{w}_{,x} + w_{,x}) \Delta w_{,x} + \frac{1}{2} \Delta v_{,x}^2 + \frac{1}{2} \Delta w_{,x}^2 \quad (2.26)$$

In Eq. (2.25) δ is the variation symbol and Δ is the incremental symbol in Eq. (2.26).

It is seen in Eqs. (2.25 - 26) that the total slopes $(\bar{v} + v)_{,x}$ and $(\bar{w} + w)_{,x}$ come in as the large deflection effects on local element level. It is later demonstrated how these geometric terms influence the incremental stiffness matrix.

The effect from initial slope on strain increment is illustrated in Fig. 2.5 showing initial configuration C_{01} with no initial deflection and C_{02} with initial slope $\bar{v}_{,x}$.

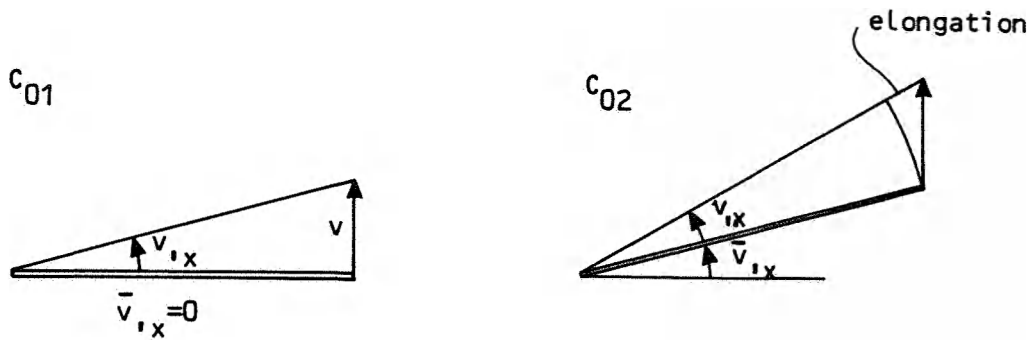


Figure 2.5 Effect of initial slope on strain

From Eq. (2.24) to Eq. (2.25) only the load-dependent displacements u , v and w are varied. It is also clear that from the considerations in Sect. 2.2.3 the relations (2.25 - 26) are valid only for moderate rotations due to the von Karman simplification eliminating higher order terms of the axial displacement from Eq. (2.5) to Eq. (2.6).

A physical illustration of the geometric stiffening from initial lateral deflection is given in Fig. 2.6 for a cable element.

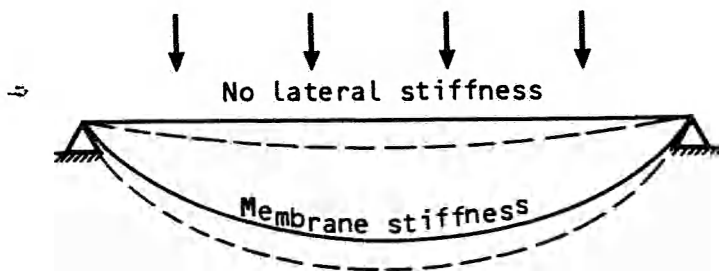


Figure 2.6 Cable element with lateral load

2.4.2 Modification of Stiffness Matrix

In the case of initial deflections $\bar{v}(x)$ and $\bar{w}(x)$ Eq. (2.12) for elastic strain energy turns into

$$\begin{aligned}
 U = & \frac{1}{2} \int_0^l EA(u_{,x} + \bar{v}_{,x} \cdot v_{,x} + \bar{w}_{,x} \cdot w_{,x} + \frac{1}{2} v_{,x}^2 + \frac{1}{2} w_{,x}^2)^2 dx \\
 & + \frac{1}{2} \int_0^l EI_z v_{,xx}^2 dx + \frac{1}{2} \int_0^l EI_y w_{,xx}^2 dx
 \end{aligned} \tag{2.27}$$

The variation $\delta(U + \Delta U)$ reads

$$\begin{aligned}
 \delta(U + \Delta U) = & \int_0^l EA\{u_{,x} + \Delta u_{,x} + \bar{v}_{,x} \cdot (v_{,x} + \Delta v_{,x}) + \bar{w}_{,x} \cdot (w_{,x} + \Delta w_{,x}) \\
 & + \frac{1}{2} (v_{,x} + \Delta v_{,x})^2 + \frac{1}{2} (w_{,x} + \Delta w_{,x})^2\} \cdot \\
 & + \{\delta u_{,x} + (\bar{v}_{,x} + v_{,x} + \Delta v_{,x}) \delta v_{,x} + (\bar{w}_{,x} + w_{,x} + \Delta w_{,x}) \delta w_{,x}\} \cdot dx \\
 & + \int_0^l EI_z (v_{,xx} + \Delta v_{,xx}) \cdot \delta v_{,xx} dx + \int_0^l EI_y (w_{,xx} + \Delta w_{,xx}) \cdot \delta w_{,xx} dx
 \end{aligned} \tag{2.28}$$

and the stiffness terms of Eq. (2.21) get the form

$$\begin{aligned}
 \delta \Delta U = & \delta(U + \Delta U) - \delta U \\
 = & \int_0^l EA \Delta u_{,x} \delta u_{,x} dx \\
 & + \int_0^l EI_z (\Delta v_{,xx} \cdot \delta v_{,xx} - \frac{N}{EI_z} \Delta v_{,x} \cdot \delta v_{,x}) dx \\
 & + \int_0^l EI_y (\Delta w_{,xx} \cdot \delta w_{,xx} - \frac{N}{EI_y} \Delta w_{,xx} \cdot \delta w_{,xx}) dx \\
 & + \int_0^l EA \{\Delta u_{,x} \cdot (\bar{v}_{,x} + v_{,x}) \cdot \delta v_{,x} + \Delta v_{,x} \cdot (\bar{v}_{,x} + v_{,x}) \cdot \delta u_{,x}\} dx \\
 & + \int_0^l EA \{\Delta u_{,x} \cdot (\bar{w}_{,x} + w_{,x}) \cdot \delta w_{,x} + \Delta w_{,x} \cdot (\bar{w}_{,x} + w_{,x}) \cdot \delta u_{,x}\} dx \\
 & + \int_0^l EA \cdot \{\Delta v_{,x} \cdot (\bar{v}_{,x} + v_{,x})^2 \cdot \delta v_{,x}\} dx
 \end{aligned} \tag{2.29}$$

$$\begin{aligned}
& + \int_0^l EA \cdot \{\Delta w_{,x} \cdot (\bar{w}_{,x} + w_{,x})^2 \cdot \delta w_{,x}\} dx \\
& + \int_0^l EA \cdot \{\Delta v_{,x} \cdot (\bar{v}_{,x} + v_{,x}) \cdot (\bar{w}_{,x} + w_{,x}) dw_{,x} \\
& + \Delta w_{,x} (\bar{w}_{,x} + w_{,x}) \cdot (\bar{v}_{,x} + v_{,x}) dv_{,x}\} dx \\
& + \text{higher order terms of } \Delta v_{,x} \text{ and } \Delta w_{,x}.
\end{aligned}$$

The variation of increment in external potential comes out on the same form as in Eq. (2.22). The conclusion from these considerations is that the initial deflections affect the incremental stiffness. However, the correct values are obtained by using the total deflection (initial + additional) in the nonlinear expressions.

Again, it ought to be emphasized that the derivations are valid for moderate rotations.

3 PLASTIC HINGES

3.1 Basic assumptions

The present chapter deals with the theoretical formulation for the modification of flow theory of plasticity to application on M/N type interaction curves instead of σ type yield functions. The chapter also deals with some problems associated with numerical implementation of the modified flow theory.

In the conventional flow theory of plasticity three basic assumptions are made. These are

- a. There exists an initial yield condition which in stress space can be illustrated by an initial yield surface.
- b. There exists a flow rule relating plastic strain increment to stress increment
- c. A hardening rule is defined relating the translation of the yield surface to the amount of plastic deformation.

3.2 Elastic-Perfectly-Plastic Model

In this case the first condition above is expressed by the interaction formula of the cross section in the way

$$F(s_i) = 0, \quad s_i = \frac{s_i}{\sigma_y W_i} \quad (3.1)$$

where the parameters are:

$$s_1 = \frac{N}{\sigma_y A} = \text{normalized axial force}$$

$$s_2 = \frac{Q_y}{\tau_y A_y} = \text{normalized shear force in local y-direction}$$

Plastic Hinges

$$s_3 = \frac{Q_z}{\tau_y A_z} = \text{normalized shear force in local z-direction}$$

$$s_4 = \frac{M_x}{\tau_y W_x} = \text{normalized torsion moment}$$

$$s_5 = \frac{M_y}{\sigma_y W_y} = \text{normalized bending moment about local y-axis}$$

$$s_6 = \frac{M_z}{\sigma_y W_z} = \text{normalized bending moment about local x-axis}$$

Eq. (3.1) defines the plastic state of stress while elastic conditions are characterized by

$$F(s_i) < 0 \quad (3.2)$$

This derivation is restricted to non-hardening materials so that the yield surface remains the same throughout plastic deformation. This means that by loading from one plastic stress state to another plastic state the following equation is valid

$$dF = \frac{\partial F}{\partial N} dN + \frac{\partial F}{\partial Q_y} dQ_y + \frac{\partial F}{\partial Q_z} dQ_z + \frac{\partial F}{\partial M_x} dM_x + \frac{\partial F}{\partial M_y} dM_y + \frac{\partial F}{\partial M_z} dM_z = 0 \quad (3.3)$$

which is equivalent to the consistency condition in conventional flow theory for non-hardening materials.

It should be emphasized that Eq. (3.3) above as well as other derivations in the present section 3.2 are restricted to infinitesimal increments. Modifications for finite increments in plastic region are presented in section 4.4.1.

An associated flow rule is applied in the sense that the yield function in Eq. (3.1) is used as plastic potential. Denoting by \mathbf{v}^p the plastic deformation vector associated with the plastic hinge, the flow rule reads

$$d\mathbf{v}^p = d\lambda \cdot \frac{\partial F}{\partial \mathbf{S}} = d\lambda \cdot \mathbf{g} \quad (3.4)$$

Plastic Hinges

where the vector S contains the section forces at the plastic hinge

$$S = [N, Q_y, Q_z, M_x, M_y, M_z]^T \tag{3.5}$$

The parameter $d\lambda$ in Eqs. (3.4) is a non-negative scalar quantity which is zero at pure elastic deformation and g is the gradient $\frac{\partial F}{\partial S_i}$ to the yield surface

On component from Eq. (3.4) may for a typical hinge be written as:

$$\begin{bmatrix} du^P \\ du^P \\ dw^P \\ d\theta_x^P \\ d\theta_y \\ d\theta_z^P \end{bmatrix} = d\lambda \cdot \begin{bmatrix} \partial F / \partial N \\ \partial F / \partial Q_y \\ \partial F / \partial Q_z \\ \partial F / \partial M_x \\ \partial F / \partial M_y \\ \partial F / \partial M_z \end{bmatrix} \tag{3.6}$$

The deformation vector v^P is equivalent to conventional strain in the sense that it is a deformation measure at the plastic hinge. It gives the adjacent displacements between the two sides of the hinge so that rigid body motion of the hinge is not making any contribution. An illustration of the exclusion of rigid body rotation is given in Fig. 3.1.

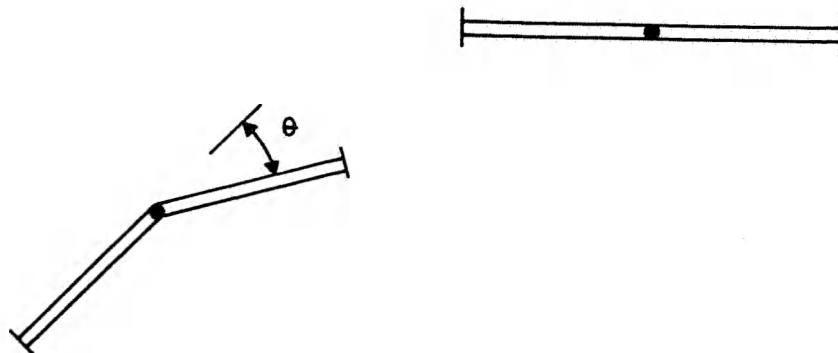


Figure 3.1 Elimination of rigid body rotation at plastic hinge

3.3 Elasto-plastic models with strain hardening

The introduction of hardening in the plasticity modelling represents an generalization of the deviation in the previous section.

At each state of plastic deformation at the hinge it is postulated that there exists a unique yield surface in the normalized force space given by:

$$F(s_i) = 0, \quad s_i = \frac{S_i - \alpha_i}{\sigma_y W_i z_y} \quad \text{and } i = 1, 6 \quad (3.7)$$

where

α_i represents the yield surface offset components in the force space and z_y denotes the yield surface extension in the normalized force space.

Strain hardening takes place when $F(s_i) > 0$.

The yield surface $F(s_i)$ generally depends both on the current state of forces and on the displacement history.

In the current formulation kinematic hardening will be assumed, so that the extension parameter z_y and the shape of the yield surface are kept constant while its origo α_i is allowed to move. Isotropic hardening, which would imply increasing z_y , is not considered here.

→

The following formulations will be written on a form using finite increments. Consider the stage of loading shown in Figure 3.2

Plastic Hinges

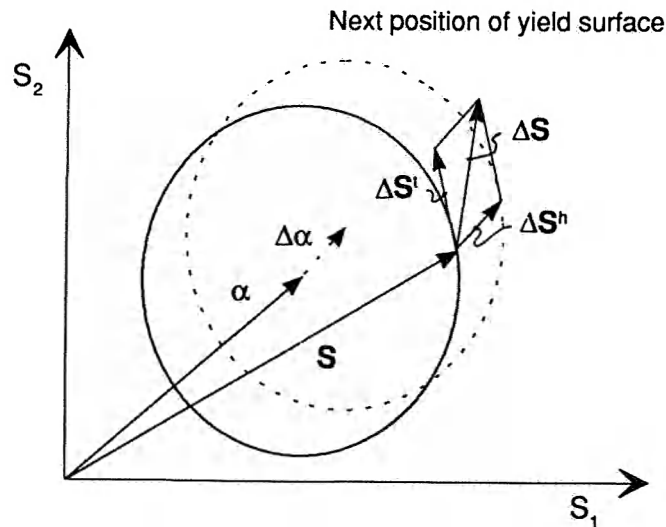


Figure 3.2 Force decomposition

The current force vector is denoted by S . The total force increment, ΔS during a load step can be split into two components; ΔS^t , which is tangential to the yield surface and produces no plastic flow and ΔS^h which is not tangential to the yield surface and causes a shift of the yield surface offset $\Delta\alpha$. Written as a vector in the 6 dimensional normalized force space this gives:

$$\Delta S = \Delta S^t + \Delta S^h \tag{3.8}$$

$$\Delta\alpha = \Delta S^h \tag{3.9}$$

For the tangential force component the consistency criterion is written in the form:

$$g^T \cdot \Delta S^t = 0 \tag{3.10}$$

while

$$g^T \Delta S^h > 0 \tag{3.11}$$

Here g is the gradient $\left\{ \frac{\partial F}{\partial S_i} \right\}$ to the yield surface.

Within a load increment the relationship between force increment and plastic displacement is assumed to be linear. Since ΔS^h is the only component producing plastic flow the following relation yields:

$$\Delta S^h = k^h \Delta v^p \quad (3.12)$$

where k^h is a plastic moduli (hardening) matrix discussed in detail in section 3.5. The plastic displacement increment Δv^p is given by Eq (3.4).

3.4 Partial yielding and strain hardening model

The bounding surface concept /27/ formulated in force space is used to model strain hardening and partial yielding.

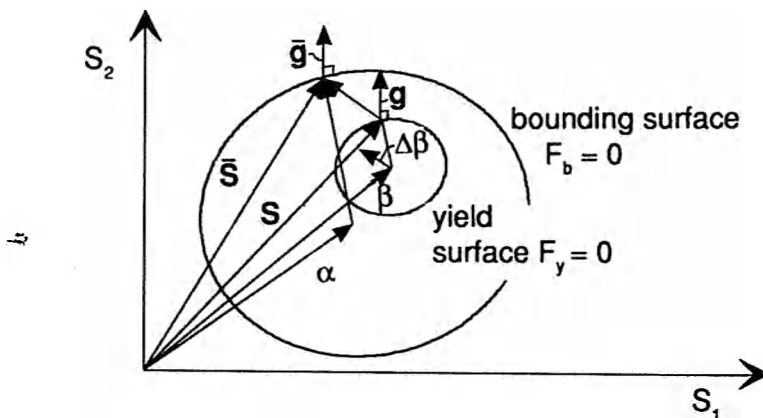


Figure 3.3 Schematic representation of yield and bounding surface

Consider the two surfaces in Figure 3.3 which are used to indicate the degree of plasticity for a cross-section. The actual state of stress resultants are marked with the position vector S .

Plastic Hinges

A yield surface is defined by the equation

$$F_y(s_i) = 0, \quad s_i = \frac{S_i - \beta_i}{\sigma_y w_i z_y} \quad \text{and } i = 1, 6 \quad (3.13)$$

where the extension parameter $0 < z_y < 1$.

When the force state S has reached the yield surface this corresponds to initial yielding in the cross section. Once the yield surface is reached, it starts to translate so that the stress resultants remain on the yield surface during subsequent loading. This translation is uniquely defined by the history of the position vector β , which marks the centre of the yield surface.

Associative plastic flow theory is applied in the way that the yield surface $F_y=0$ also serves as the plastic potential when calculating incremental plastic deformations Δv^P .

Further, in Figure 3.3 a bounding surface is defined which has the same shape as the yield surface. It is given by the equation.

$$F_b(s_i) = 0, \quad s_i = \frac{\bar{S}_i - \alpha_i}{\sigma_y w_i z_b} \quad \text{and } i = 1, 6 \quad (3.14)$$

where $z_b = 1$ is the bounding surface extension parameter. The bounding surface represents the outer limit for the translation of the yield surface. A point on the bounding surface denotes a fully plastic stress state. Plastic, kinematic hardening is modelled as a translation of the bounding surface in the stress resultant space, given by the history of the centre position vector α .

For a given force state S which have reached the yield surface, the conjugate point \bar{S} on the bounding surface is defined so that S and \bar{S} have unidirectional gradients g and \bar{g} as shown in Figure 3.3.

Figure 3.4 indicates the different location of stress points for different modes of deformation, and relates the multidimensional illustration in stress resultant space to a uniaxial strain curve.

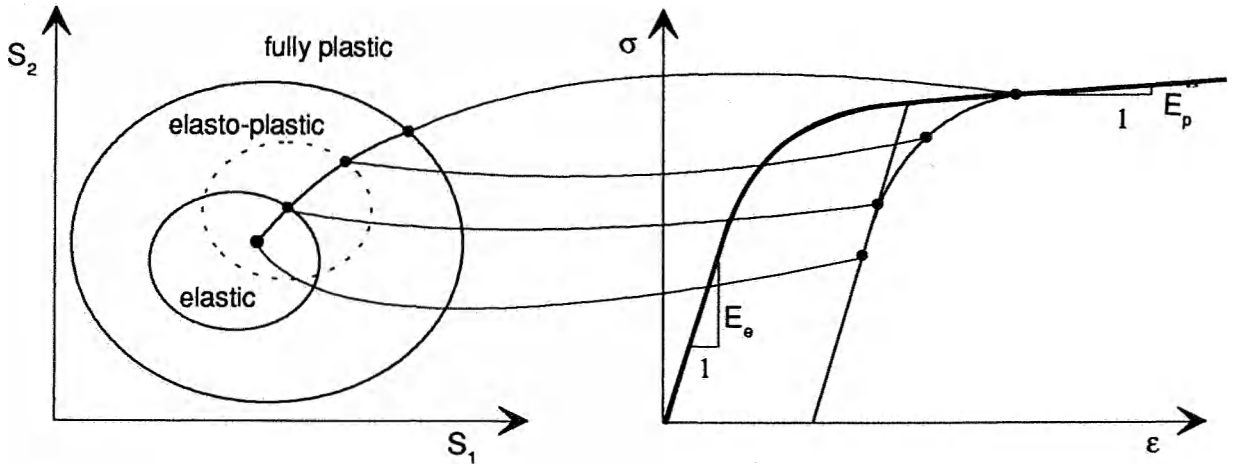


Figure 3.4 Analogy between multidimensional stress-space and uniaxial stress-strain curve.

For the adopted kinematic hardening rule no general rule exists for the motion of the yield surface. Prager /28/ and Ziegler /29/ have both proposed surface translation rules. Both these rules may violate the bounding surface concept in the sense that intersections of the yield and bounding surface may occur.

For the present formulation, the approach proposed by Mroz /30/ is adopted. In this model in which the violation of the bounding surface concept is avoided, the yield surface translates parallel to the vector connecting the stress resultant point and the conjugate point on the bounding surface, i e.

$$\Delta\beta = \mu(\bar{S} - S) \tag{3.15}$$

where μ is a scalar. The condition of equal gradient for \bar{S} and S leads to the requirement

$$\bar{S} - \alpha = z(\bar{S} - \beta) \tag{3.16}$$

where z defines the surface size ratio $z = z_b/z_y$.

Combining Equations (3.15) and (3.16) there comes out

Plastic Hinges

$$\Delta\beta = \mu(z(\mathbf{s}-\beta) - (\mathbf{s}-\alpha)) \quad (3.17)$$

The scalar μ is eliminated by introducing the consistency criterion stating that the force point is to remain on the translating yield surface, or:

$$\Delta F_y = \frac{\partial F}{\partial S_i} \Delta S_i + \frac{\partial F}{\partial \beta_i} \Delta \beta_i + \Delta \bar{F} = 0 \quad (3.18)$$

where $\Delta \bar{F}$ represents any deviation from the yield surface.

Utilizing the fact that

$$\frac{\partial F}{\partial \beta_i} = - \frac{\partial F}{\partial S_i} \quad (3.19)$$

Equation (3.18) can be written as

$$\Delta F_y = \mathbf{g}^T (\Delta \mathbf{S} - \Delta \beta) + \Delta \bar{F} = 0 \quad (3.20)$$

Combining Equations (3.15), (3.17) and (3.18) the incremental yield surface translation can be written on the the form:

$$\Delta \beta = (z(\mathbf{s}-\beta) - (\mathbf{s}-\alpha)) \frac{\mathbf{g}^T \Delta \mathbf{S} + \Delta \bar{F}}{\mathbf{g}^T (z(\mathbf{s}-\beta) - (\mathbf{s}-\alpha))} \quad (3.21)$$

which reduces to

$$\Delta \beta = \Delta \alpha = \frac{(\mathbf{s}-\beta)(\mathbf{g}^T \Delta \mathbf{S} + \Delta \bar{F})}{\mathbf{g}^T (\mathbf{s}-\beta)} \quad (3.22)$$

when the yield and bounding surface moves in contact.

Consistent with the formulation of the hardening increment $\Delta \mathbf{S}^h$ given in Equation (3.12), the incremental bounding surface translation should be along the hardening vector:

$$\Delta \alpha = \Delta \mathbf{S}^h = \mathbf{k}^h \cdot \Delta \mathbf{v}^p \quad (3.23)$$

rather than according to Eq 3.22.

Plastic Hinges

By translating the bounding surface according to Eq. (3.23) the movement is zero until the force state S reaches the yield surface ($F_y=0$) and becomes equal to the fully plastic rate when S reaches the bounding surface ($F_b=0$).

An unfortunate consequence of using Eq. (3.22) for updating the translation of the yield surface when the two surfaces move in contact is that the contact point remains fixed. It is better to let the contact point follow the present force point on the bounding surface. This is obtained by updating the centre point of the yield according to

$$\beta = \frac{(z-1)S + \alpha}{z} \quad (3.24)$$

In conclusion, the bounding surface offsets are always predicted by Eq. (3.12), the yield surface offsets by Eq. (3.21) if the yield surface does not contact the bounding surface and by Eq. (3.24) if the yield surface contacts the bounding surface.

In connection to cyclic analysis the shift to cyclic material parametric implies a shift of the yield surface offset which is given by:

$$\beta_c = \frac{(Z_{yc}/Z_{ym}-1) S + \beta_m}{Z_{yc}/Z_{ym}} \quad (3.24b)$$

where subscripts m and c denote monotonic and cyclic material parameters respectively.

3.5 The hardening matrix

The hardening matrix k^h contains the plastic moduli at a plastic hinge and is for the present formulation diagonal. For a three-dimensional beam k^h is given by:

$$k^h = \text{diagonal } \{k_{11}^h, k_{22}^h, \dots, k_{66}^h\} \quad (3.29)$$

Plastic Hinges

where the subscript corresponds to each degree-of-freedom. In the following k^h is briefly outlined.

It is assumed that the hardening in the fully plastic state for each load component S_i is proportional to the relative plastic displacement v_{ip}/v_i^p :

$$\frac{S_i^h}{S_{ip}} = c \frac{v_i^p}{v_{ip}} \quad (3.30)$$

where

- S_{ip} - plastic capacity for force component i
- v_{ip} - elastic displacement corresponding to S_{ip}
- S_i^h - hardening force component i
- v_i^p - plastic displacement associated to S_i^h

Eq 3.30 rearranged yields:

$$S_i^h = c_i \frac{S_{ip}}{v_{ip}} v_i^p \quad (3.31)$$

which dictates that the plastic modulus should be taken as a fraction of the elastic stiffness. Thus the plastic stiffness \bar{k}_{ii}^h in the axial direction is given by:

$$\bar{k}_{11}^h = c_1 \frac{EA}{l} \quad (3.32a)$$

where EA/l is the elements elastic stiffness and c_1 is a nondimensional plastic modulus.

Similarly it is found that the plastic stiffnesses for shear and torsional deformation for a beam element with length l is given by respectively:

$$\bar{k}_{22}^h = c_2 \cdot 12 \frac{EI_z}{l^3} \quad (3.32b)$$

$$\bar{k}_{33}^h = c_3 \cdot 12 \frac{EI_y}{l^3} \quad (3.32c)$$

Plastic Hinges

$$\bar{k}_{44}^h = c_4 \frac{EI_x}{l^3} \quad (3.32d)$$

where I_x is the torsional moment of inertia and I_y and I_z are moments of inertia about local element y and z axis respectively.

If all loads are applied at the nodes, the curvature along the member is a function of the member ends. By use of the virtual work principle the following plastic bending moduli are derived:

$$\bar{k}_{55}^h = c_5 \left(\frac{EI_y}{l} \right) \frac{6}{\left(2 - \frac{S_{5j}}{S_{5pi}} \right)} \quad (3.32e)$$

$$\bar{k}_{66}^h = c_6 \left(\frac{EI_z}{l} \right) \frac{6}{\left(2 - \frac{S_{6j}}{S_{6pi}} \right)} \quad (3.32f)$$

where S_{5j} and S_{6j} are the bending moments at node j and S_{5pi} and S_{6pi} are the plastic bending capacities at node i . The bending moment at the opposite node j in Eqs (3.32e) and (3.32f) accounts for the affect of curvature variations along the element on the yield hinge.

When the stress resultants are on the yield surface but have not reached the bounding surface, the plastic moduli have to be adjusted. For a one degree of freedom system the following relation holds:

$$\Delta v = \Delta \tilde{v}^e + \Delta v^p = \Delta S \left(\frac{1}{k^e} + \frac{1}{k^p} \right) \quad (3.25)$$

and

$$\frac{1}{k} = \frac{1}{k^e} + \frac{1}{k^p} \quad (3.26)$$

where k^e and k^p denote the elastic tangential stiffness and plastic stiffness, respectively. Obviously, the total stiffness k should be equal to k^e when the stress state just reaches the yield surface, ie k^p should be infinite in this case. For increasing stresses it should decrease smoothly towards the fully plastic modulus.

For this purpose, a distance parameter δ is needed. This is taken as the distance between the current point on the yield surface and the conjugate point on the bounding surface as illustrated in Figure 3.5.

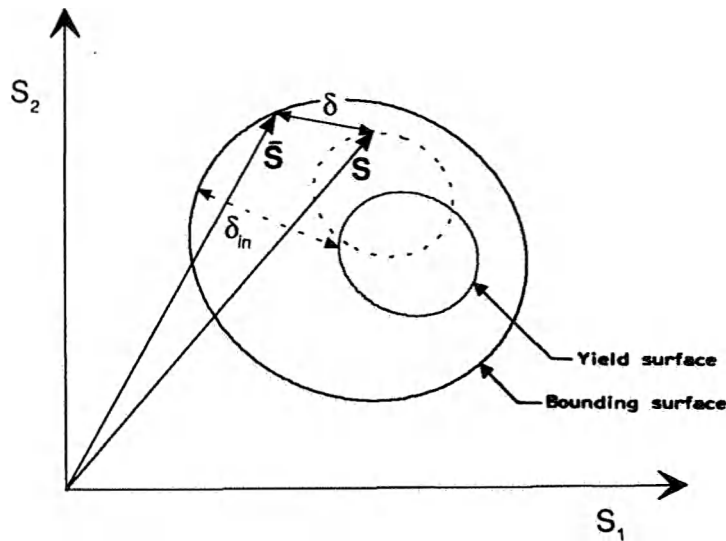


Figure 3.5 The distance parameter δ

The distance parameter δ is defined by:

$$\delta = [(\bar{s}_i - s_i)(\bar{s}_i - s_i)]^{1/2}, \quad i = 1, 6$$

$$= \left\{ \left[z \frac{(\bar{S}_i - \beta_i)}{S_{pi}} - \frac{(S_i - \alpha_i)}{S_{pi}} \right] \left[z \frac{(\bar{S}_i - \beta_i)}{S_{pi}} - \frac{(S_i - \beta_i)}{S_{pi}} \right] \right\}^{1/2} \quad (3.27)$$

where s_i is the nondimensional force vector and $z = \frac{z_b}{z_y}$ is the scalar factor relating the yield surface and bounding surface sizes.

S_{pi} is the plastic capacity of force component number i .

The distance at first yield is denoted δ_{in} . The desired properties of the hardening moduli are obtained by using the following relationship.

$$k_{ii}^h = k_{ii}^e \left(c_i + a_i \frac{\delta}{\delta_{in} - \delta} \right) \quad (3.28)$$

Plastic Hinges

where a_i is a parameter to be determined empirically, such that the transition performance is adequate. Thus, k_{ij}^h starts from infinity when $\delta = \delta_{in}$ and approaches the fully plastic hardening modulus \bar{k}_{ij}^h when $\delta \rightarrow 0$.

3.6 Plastic Potentials for Beams

3.6.1 Interaction Surface for Thin-Walled Tube

In the case of a fully plastic stress over a thin-walled cross section the interaction between axial stress and shear stress is normally neglected and the general expression (3.1) turns into

$$F(N, M_x, M_y, M_z, \beta_i, z) = 0 \quad (3.33)$$

$$(1 - m_x^2)^{1/2} \cdot \cos\left(\frac{\pi}{2} \cdot \frac{n}{(1 - m_x^2)^{1/2}}\right) - (m_y^2 + m_z^2)^{1/2} = 0$$

where n , m_x , m_y and m_z are nondimensional parameters defined by

$$n = \frac{N - \beta_1}{N_p z}, \quad m_x = \frac{M_x - \beta_4}{M_{px} \cdot z}, \quad m_y = \frac{M_y - \beta_5}{M_{py} \cdot z} \quad \text{and} \quad m_z = \frac{M_z - \beta_6}{M_{pz} \cdot z} \quad (3.34)$$

where N_p , M_{py} , M_{pz} and M_{px} are the plastic capacities for axial force, bending moment and torsional moment, respectively. z is the surface extension parameter and β_i are the surface offsets in force space. The formula does not account for local wall failure of the tube.

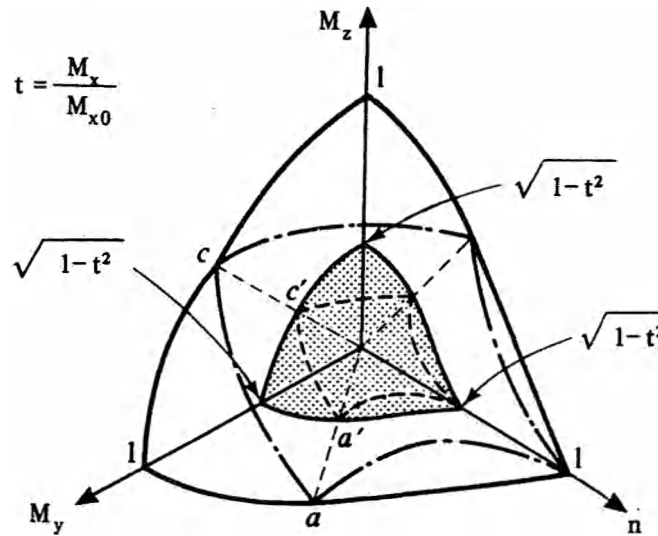


Figure 3.6 Family of lower bound interaction surfaces when $\beta_i=0$ and $z =1.0$

Fig. 3.6 gives a graph of the interaction surface in the force space. A similar expression for plastic capacity is also often being used for box type profiles.

3.6.2 Interaction Surface for Symmetric I-Profiles

For modelling deck structures I-profiles should be included. Exact interaction formulas for this type of cross section require several positions of the neutral axis to be considered, and the expressions obtained are complex to implement in a program. Therefore, empirical formulas are used.

A general form of the interaction formula was developed by Chen and Atsuta /20/. A draw back with this method is that the yield surface is multi-faceted. This poses the problem of identifying the active facet and to determine the correct gradient of the surface at facet intersections.

Alternatively a single continuous equation is proposed in Ref. /21/.

$$F = 1.15n^2 + m_y^2 + m_z^2 + 3.67n^2m_y^2 + 3.0n^6m_z^2 + 4.65m_y^4m_z^2 + q_y^8 + q_z^8 - 1 = 0 \quad (3.35)$$

where

Plastic Hinges

$$q_y = \frac{Q_y - \beta_2}{Q_{py} \cdot z'} \quad q_z = \frac{Q_y - \beta_3}{Q_{py} \cdot z} \quad (3.36)$$

and n , m_y and m_z are defined according to Eq(3.34).

Equation (3.35) was derived by a combination of trial and curve fitting. A comparison with the two-facet model proposed by Chen and Atsuta is shown in Figure 3.7.

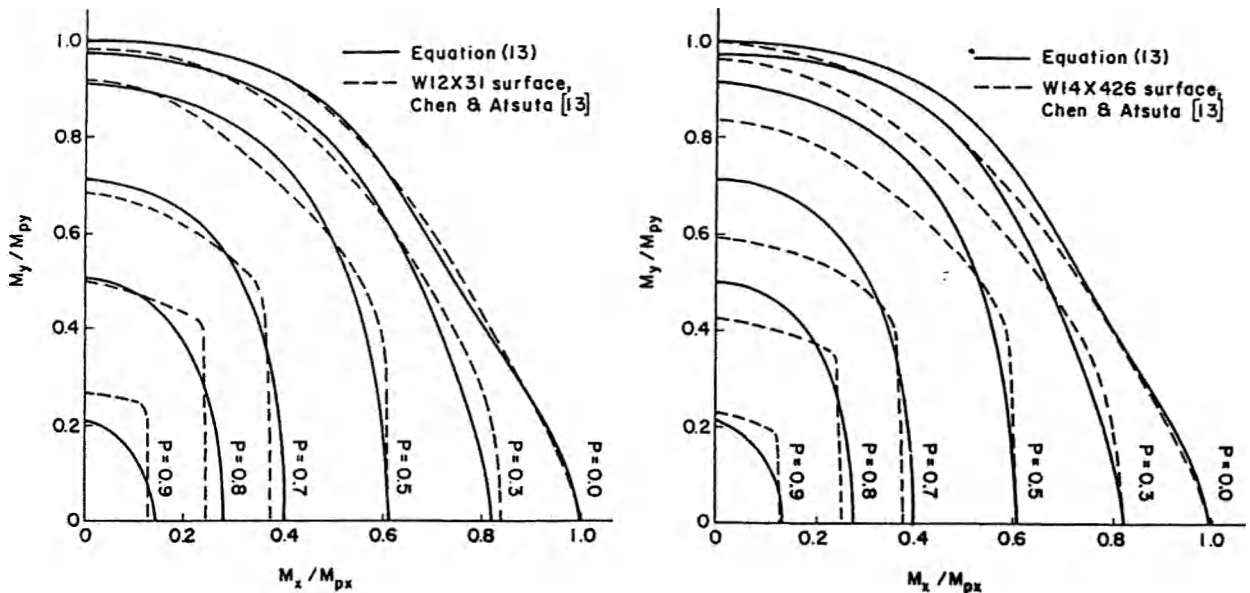


Figure 3.7 Comparison between present surface and the two-facet surface.

For deep girders the plastic shear capacities should be based upon a thorough evaluation of the post-critical behaviour of the web accounting for possible tension field effects.

3.6.3 Interaction Surface for Box Sections

Exact interaction formulas for box type cross-sections are difficult to obtain. Instead, approximate expressions are derived numerically.

The interaction between axial force and bending moment is adequately described by the following relationship

$$m + n_{\alpha} = 1 \quad (3.37)$$

Plastic Hinges

where m and n are nondimensional stress resultants (see eq. 3.34) and α is a parameter depending on the ratio between the web area, A_w , and total cross-sectional area, A . A reasonable fit with interaction curves given in Ref. /22/ is obtained with

$$\alpha = 1.8 \frac{A_w}{A} + 0.64, \quad \alpha \in (1.1, 2.0) \quad (3.38)$$

For biaxial bending the following interaction is adopted

$$\left(\frac{\beta_y}{m_y} + \frac{\beta_z}{m_z} \right) \frac{1}{\beta} = 1 \quad (3.39)$$

where β_y , β_z , are determined by curve fitting. For quadratic cross-sections $\beta_y = \beta_z = 1.75$ give satisfactory results. β is selected so as to give as much as possible linear behaviour of the interaction function with respect to axial force and bending. A reasonable value is $\beta = 3$.

In case of shear and torsion the effective yield stress of the web and the flanges are reduced according to the formula

$$\sigma_{F, q} = \sigma_F (1 - (q^2 + m_x^2))^{1/2} \quad (3.40)$$

and

$$q = \frac{Q}{Q_p} \quad (3.41)$$

where Q_p is the plastic capacity for the shear force, and m_x is defined in Eq. (3.34).

Accordingly, the effective plastic capacities for axial force and bending are modified due to shear and torsion as follows,

$$N_{P, q}/N_P = \frac{A_y}{A} (1 - (q_y^2 + m_x^2))^{1/2} + \frac{A_z}{A} (1 - (q_z^2 + m_x^2))^{1/2} \quad (3.42)$$

Plastic Hinges

$$M_{yP,q}/M_{yP} = \frac{A_z/A}{2-A_z/A} (1-(q_z^2+m_x^2))^{1/2} + \frac{2A_y/A}{2-A_z/A} (1-(q_y^2+m_x^2))^{1/2} \quad (3.43)$$

$$M_{zP,q}/M_{zP} = \frac{A_y/A}{2-A_y/A} (1-(q_y^2+m_x^2))^{1/2} + \frac{2A_z/A}{2-A_y/A} (1-(q_z^2+m_x^2))^{1/2} \quad (3.44)$$

The final interaction function now reads

$$F = \left\{ \left(\frac{M_y/M_{yP,q}}{1 - \left(\frac{N}{N_{P,q}} \right)} \right)^{\beta_y} + \left(\frac{M_z/M_{zP,q}}{1 - \left(\frac{N}{N_{P,q}} \right)} \right)^{\beta_z} \right\}^{\frac{1}{\beta}} - 1 = 0 \quad (3.45)$$

This expression is not convenient from a numerical point of view due to multiple occurrences of potential singularities in the denominators.

By rearranging Eq. (3.45) the following expression is found more suitable for computer implementation.

$$F = (A \cdot \bar{m}_y^{\beta_y} + B \bar{m}_z^{\beta_z})^{\frac{1}{\beta}} - (A B \beta_y \beta_z)^{\frac{1}{\beta}} = 0 \quad (3.46)$$

$$A = \frac{M_{zP,q}}{M_P} \left\{ \left(\frac{N_{P,q}}{N_P} \right)^{\alpha_z} - n^{\alpha_z} \right\} \quad (3.47)$$

$$B = \frac{M_{yP,q}}{M_P} \left\{ \left(\frac{N_{P,q}}{N_P} \right)^{\alpha_y} - n^{\alpha_y} \right\} \quad (3.48)$$

$$\bar{m}_y = \left(\frac{N_{P,q}}{N_P} \right)^{\alpha_y} m_y \quad (3.49)$$

$$\bar{m}_z = \left(\frac{N_{P,q}}{N_P} \right)^{\alpha_z} m_z \quad (3.50)$$

4 IMPLEMENTATION OF THE IDEALIZED STRUCTURAL UNIT METHOD

4.1 General Description

The present discretization technique, called the Idealized Structural Unit Method, is based on the physical analogy that one numerical element is used for each real structure element. The main objective is of course to minimize computer costs. Further, it is clear that this type of discretization is more oriented against conventional design philosophy since typical elements in the numerical model correspond to components to be checked in conventional design.

However, compared to conventional finite element models based upon updated Lagrangian formulation of so-called corotational formulation the idealized structural unit method implies a coarse element representation in the sense that each element between real nodal points is modelling by one numerical element. Due to this relative coarse discretization it is necessary to take in geometric nonlinearities on local element level in order to pick up local collapse modes.

The present version of the program USFOS differs in the way of handling large displacements on local element level and global level. On element level large deflection is incorporated by additional second order strain terms while the global effects are taken in by updating nodal point coordinates. Thus, a total Lagrangian formulation is implemented on element level. However, the program does not imply a complete total Lagrangian formulation since the element reference axes are updated throughout deformation.

4.2 Coordinate Systems

The present section describes the global reference systems and the local element coordinate axes. The geometric transformations in establishing global load-displacement relations are also explained.

4.2.1 Spatial Coordinates

A right-handed cartesian system X, Y, Z is being used for referenc system for nodal displacements. The corresponding translation components are denoted r_x, r_y, r_z and the rotations ϕ_x, ϕ_y, ϕ_z .

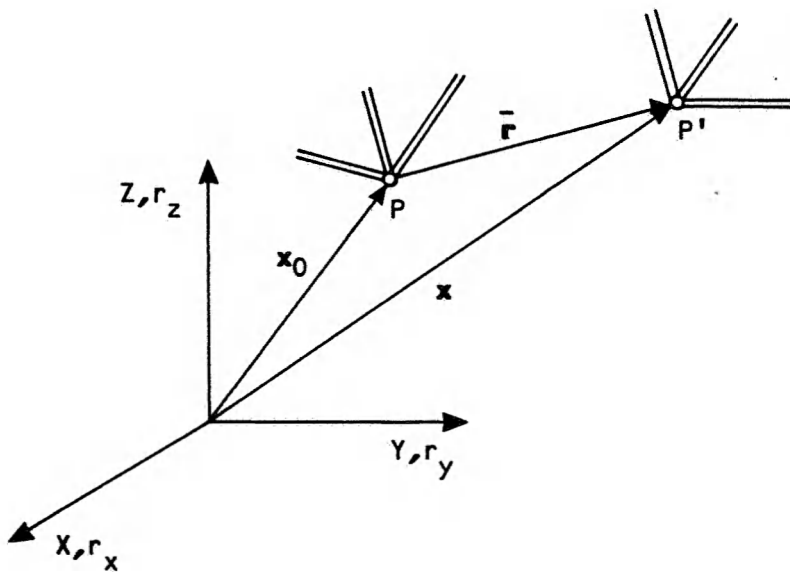


Figure 4.1 Spatial coordinates system

Fig. 4.1 shows a nodal point P in undeformed configuration and the position P' in deformed state. The displacement vector is

$$\bar{r} = \begin{bmatrix} r_x \\ r_y \\ r_z \end{bmatrix} \tag{4.1}$$

Implementation of Idealized Structural Unit Method

Denoting by X_0 the position vector of P in underformed configuration the deformed position vector reads

$$X = X_0 + \bar{r} \quad (4.2)$$

The global vector r in Eq. (4.1) with translation parameters only indicates together with Eq. (4.2) that rotations are not considered when updating the geometry of the structure. It is demonstrated later that the only way rotations $\varphi_x, \varphi_y, \varphi_z$ come in is on incremental form as degrees-of-freedom in the load-displacement relationship. The notation \bar{r} is being used in Eq. (4.1) in order to make a distinction from the vector r of nodal parameters used on incremental form in the solution algorithm.

$$r = [r_x, r_y, r_z, \varphi_x, \varphi_y, \varphi_z]^T \quad (4.3)$$

The spatial coordinates are being used as reference system for the global load-displacement equations on incremental form. This means that possible incremental element loads and displacements are referred to system X, Y, Z in the final stiffness expressions for the total structure. Thus, after having calculated incremental stiffness and element loads in a local element coordinate system, the element relations undergo geometric transformation into the spatial system before establishing interelement continuity.

The spatial coordinate system comes out with two functions

- a) To serve as a reference system for the position of nodal points and thereby a reference system for global frame geometry.
- b) To be a reference system for global load-displacement relations. Interelement continuity is established in the spatial system. This means in practice that element stiffnesses are transformed into the spatial system before adding together.

4.2.2 Local Element System

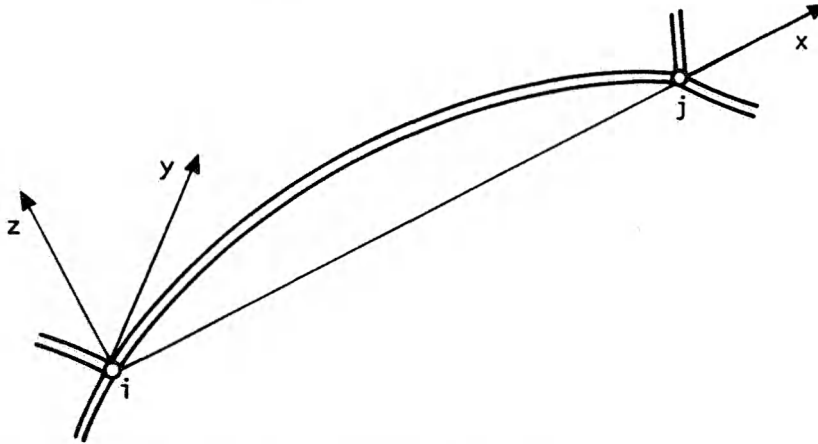


Figure 4.2 Local element coordinate system

Fig. 4.2 indicates a beam element at some stage of deformation. The end points of the element are numbered i and j , respectively. The direction cosines of the x -axis as referred to the spatial system become

$$\cos (x, X) = \frac{X_j - X_i}{l} \quad (4.4)$$

$$\cos (x, Y) = \frac{Y_j - Y_i}{l} \quad (4.5)$$

$$\cos (x, Z) = \frac{Z_j - Z_i}{l} \quad (4.6)$$

where the element length is given as

$$l = ((X_j - X_i)^2 + (Y_j - Y_i)^2 + (Z_j - Z_i)^2)^{1/2} \quad (4.7)$$

In order to fix the local xy -plane a vector \mathbf{y} is defined. This vector can be defined by specifying two points in space or two nodal points. The dot product

$$\alpha = \mathbf{i}_x \cdot \mathbf{y} \quad (4.8)$$

is evaluated where \mathbf{i}_x now is the unit vector along x .

$$\mathbf{i}_x = [\cos(x, X), \cos(x, Y), \cos(x, Z)]^T \quad (4.9)$$

The unit vector i_y in the local y -direction is now found from

$$i_y = \frac{y' - \alpha i_x}{|y' - \alpha i_x|} \quad (4.10)$$

Finally, the local z -direction is defined by the unit vector

$$i_z = i_x \times i_y \quad (4.11)$$

The above choice of vector y' should be taken under the consideration of possible predefined reference axes of bending, e.g. for I- and H-type of profiles.

4.2.3 Geometric Transformations

The transformations between local and global reference systems are in the following described for elements with eccentric coupling to nodal points, see Fig. 4.3.

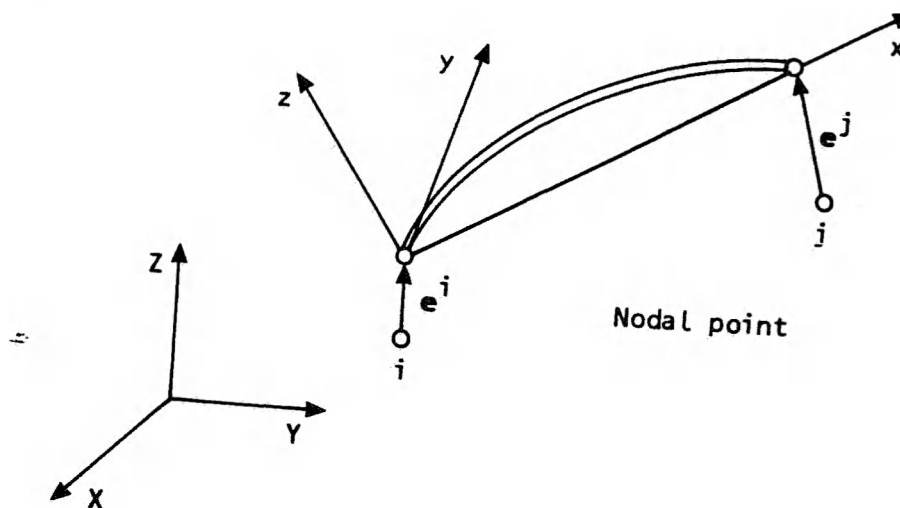


Figure 4.3 Beam element with node eccentricity in spatial system

The set of two by six parameters for each element is shown in Fig. 4.4. This is

Implementation of Idealized Structural Unit Method

the general beam element in three dimensions with three translational parameters and three rotational parameters at each node.

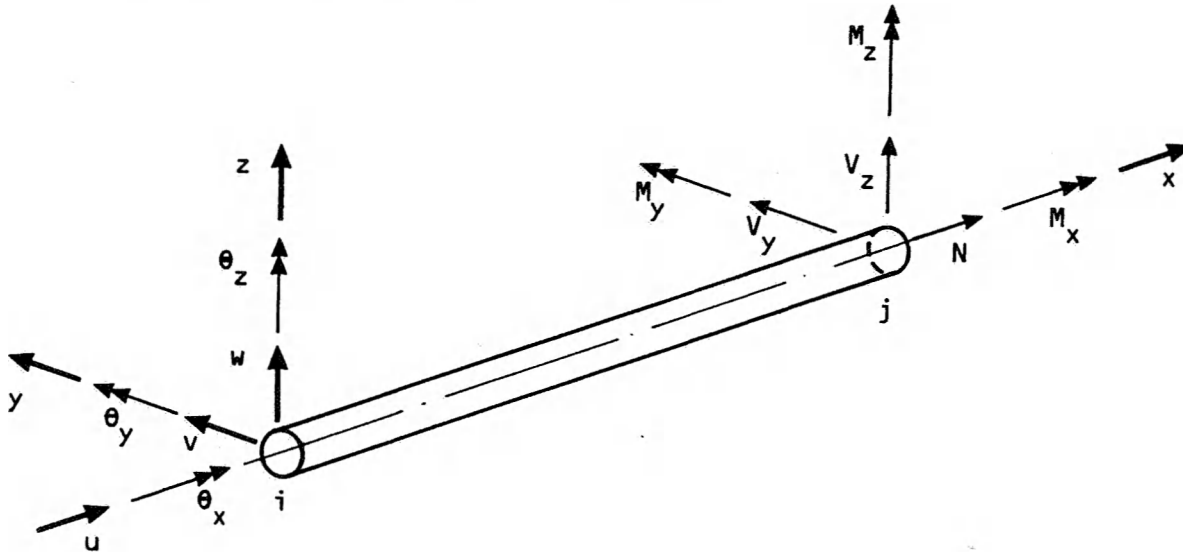


Figure 4.4 Three-dimensional beam element

The displacement parameters are indicated at end i of the element and the corresponding forces as node j.

Referring to Fig. 4.3 the geometric transformation is twofold. First, the parameters at the ends of the element are transformed into global axes and second, account is made for eccentric nodes.

The transformation between local and global axes is given by

$$\begin{bmatrix} u \\ v \\ w \end{bmatrix} = \begin{bmatrix} \cos(x,X) & \cos(x,Y) & \cos(x,Z) \\ \cos(y,X) & \cos(y,Y) & \cos(y,Z) \\ \cos(z,X) & \cos(z,Y) & \cos(z,Z) \end{bmatrix} \begin{bmatrix} r_X \\ r_Y \\ r_Z \end{bmatrix} \quad (4.12)$$

or

$$\mathbf{u} = \mathbf{G}\bar{\mathbf{r}} \quad (4.13)$$

The transformation for the six parameters at each node becomes

Implementation of Idealized Structural Unit Method

$$\begin{bmatrix} u \\ v \\ w \\ \theta_x \\ \theta_y \\ \theta_z \end{bmatrix} = \begin{bmatrix} & & & & & \\ & G & & & & \\ & & & & & \\ \hline & & & & & \\ & & & G & & \\ & & & & & \end{bmatrix} = \begin{bmatrix} r_X \\ r_Y \\ r_Z \\ \phi_X \\ \phi_Y \\ \phi_Z \end{bmatrix} \quad (4.14)$$

Denoting by k the element stiffness matrix in local system the global matrix reads

$$\bar{K} = T^T k T \quad (4.15)$$

where

$$T = \begin{bmatrix} G & G & | & G & G \end{bmatrix} \quad (4.16)$$

This stiffness is now referred to the element ends.

In the process of equilibrium correction it is also required to transform equilibrium element forces into global system. Denoting by S the equilibrium forces in local system the corresponding global components S_{eq} are found from

$$\bar{R}_{eq} = T^T S_{eq} \quad (4.17)$$

There now remains to account for possible node eccentricities.

According to Fig. 4.3 the eccentricity vectors e^i and e^j are defined as the vectors from nodal point to beam end. The components in global system are denoted by e_X, e_Y, e_Z . At each end of the element the following relation is valid

Implementation of Idealized Structural Unit Method

$$\begin{bmatrix} r_X \\ r_Y \\ r_Z \\ \varphi_X \\ \varphi_Y \\ \varphi_Z \end{bmatrix} = \begin{bmatrix} 1 & & & 0 & e_X & -e_Y \\ & 1 & & -e_Z & 0 & e_X \\ & & 1 & e_X & -e & 0 \\ \hline & & & 1 & & \\ & & & & 1 & \\ & & & & & 1 \end{bmatrix} \begin{bmatrix} r_X \\ r_Y \\ r_Z \\ \varphi_X \\ \varphi_Y \\ \varphi_Z \end{bmatrix} \quad (4.18)$$

element
node
end

or

$$r_{\text{element end}} = E r_{\text{node}} \quad (4.19)$$

The stiffness transformation now reads

$$K = L^T \bar{K} L = L^T T^T k T L \quad (4.20)$$

where

K is the 12·12 element stiffness matrix in global system with eccentricities included.

$L = [E^i E^j]$ is the transformation matrix due to eccentricity. The components of the eccentricity vectors are referred to global system from node to element end.

T is the matrix of direction cosines between local and global systems.

k is the element stiffness matrix in local system with no eccentricity at ends.

The transformation of internal equilibrium forces becomes

$$R_{\text{eq}} = L^T T^T S_{\text{eq}} \quad (4.21)$$

where

R is the global 12·1 element vector of equilibrium forces with eccentricities eq included.

S is the local 12·1 element vector of equilibrium forces with no eccentricity eq

The above transformations have to be carried out for each element before introducing the interelement continuity requirements.

4.3 Incremental Stiffness for Elastic Beam

The present section concerns the formulation of incremental stiffness for the three-dimensional beam element indicated in Fig. 4.4. The pure elastic element is first considered discussing alternative interpolation functions for the displacements. Modifications for plasticity are introduced by combining elastic stiffnesses with plastic properties described in Chapter 3.

4.3.1 Variational Formulation

The basis for deriving incremental stiffness for the beam element is given in Section 2.3.2 and most of the present discussion is devoted to choice of interpolation functions. The general description of displacement interpolation is given in Eq. (2.18) where

$u(x)$ is axial displacement of points on reference axis x .

$v(x)$ is deflection in y -direction of points along the beam.

$w(x)$ is deflection in z -direction of points along the beam.

It is assumed that the local x -axis goes through the centre of gravity of the beam cross section.

Implementation of Idealized Structural Unit Method

The incremental form of the first variation in potential energy can now be written according to Eq. (2.21)

$$\begin{aligned}
\delta\Delta U = & \delta\mathbf{u}^T \int_0^1 EA\varphi_{u,x}\varphi_{u,x}^T dx \Delta\mathbf{u} \\
& + \delta\mathbf{v}^T \int_0^1 EI_z (\varphi_{v,xx}\varphi_{v,xx}^T - \frac{N}{EI_z} \varphi_{v,x}\varphi_{v,x}^T) dx \Delta\mathbf{v} \\
& + \delta\mathbf{w}^T \int_0^1 EI_y (\varphi_{w,xx}\varphi_{w,xx}^T - \frac{N}{EI_y} \varphi_{w,x}\varphi_{w,x}^T) dx \Delta\mathbf{w} \\
& + \delta\mathbf{v}^T \int_0^1 EA\varphi_{v,x^v,x}\varphi_{u,x}^T dx \Delta\mathbf{u} \\
& + \delta\mathbf{u}^T \int_0^1 EA\varphi_{u,x^v,x}\varphi_{v,x}^T dx \Delta\mathbf{v} \\
& + \delta\mathbf{w}^T \int_0^1 EA\varphi_{w,x^w,x}\varphi_{u,x}^T dx \Delta\mathbf{u} \\
& + \delta\mathbf{u}^T \int_0^1 EA\varphi_{u,x^w,x}\varphi_{w,x}^T dx \Delta\mathbf{w} \\
& + \delta\mathbf{v}^T \int_0^1 EA\varphi_{v,x^v^2,x}\varphi_{v,x}^T dx \Delta\mathbf{v} \\
& + \delta\mathbf{w}^T \int_0^1 EA\varphi_{w,x^w^2,x}\varphi_{w,x}^T dx \Delta\mathbf{w} \\
& + \delta\mathbf{w}^T \int_0^1 EA\varphi_{w,x^w,x^v}\varphi_{v,x}^T dx \Delta\mathbf{v} \\
& + \delta\mathbf{v}^T \int_0^1 EA\varphi_{v,x^v,x^w}\varphi_{w,x}^T dx \Delta\mathbf{w}
\end{aligned} \tag{4.22}$$

Arranging the parameters of the element in the order \mathbf{u} , \mathbf{v} , \mathbf{w} the stiffness matrix may be ordered correspondingly.

Implementation of Idealized Structural Unit Method

$$\mathbf{k} = \begin{bmatrix} \mathbf{k}_{uu} & \mathbf{k}_{uv} & \mathbf{k}_{uw} \\ \mathbf{k}_{vu} & \mathbf{k}_{vv} & \mathbf{k}_{vw} \\ \mathbf{k}_{wu} & \mathbf{k}_{wv} & \mathbf{k}_{ww} \end{bmatrix} \quad (4.23)$$

The following expressions for the submatrices emerge from Eq. (4.22)

$$\mathbf{k}_{uu} = \int_0^1 EA \varphi_{u,x} \varphi_{u,x}^T dx \quad (4.24)$$

$$\mathbf{k}_{vv}^I = \int_0^1 EI_z (\varphi_{v,xx}^T \varphi_{v,xx} - \frac{N}{EI_z} \varphi_{v,x} \varphi_{v,x}^T) dx \quad (4.25)$$

$$\mathbf{k}_{ww}^{II} = \int_0^1 EI_y (\varphi_{w,xx}^T \varphi_{w,xx} - \frac{N}{EI_y} \varphi_{w,x} \varphi_{w,x}^T) dx \quad (4.26)$$

These are the diagonal submatrices also present in the secant stiffness matrix arising from Eq. (2.19). The subsequent terms comes from large rotations and are nonlinear geometric contributions.

$$\mathbf{k}_{vu} = \int_0^1 EA \varphi_{v,x} \varphi_{u,x}^T dx = \mathbf{k}_{uv}^T \quad (4.27)$$

$$\mathbf{k}_{wu} = \int_0^1 EA \varphi_{w,x} \varphi_{u,x}^T dx = \mathbf{k}_{uw}^T \quad (4.28)$$

These two are coupling matrices between axial and lateral deformation and linear in rotation.

Finally, the diagonal submatrices for deflection \mathbf{k}_{vv} and \mathbf{k}_{ww} get additional contributions that are of second order in rotation

$$\mathbf{k}_{vv}^{II} = \int_0^1 EA \varphi_{v,x}^2 \varphi_{v,x}^T dx \quad (4.29)$$

Implementation of Idealized Structural Unit Method

$$k_{ww}^{II} = \int_0^l EA \phi_{w,x}^2 \phi_{w,x}^T dx \quad (4.30)$$

while coupling matrices between the two directions of deflections come out of the two last integrals of Eq. (4.22)

$$k_{wv} = \int_0^l EA \phi_{w,x} \phi_{v,x}^T dx = k_{vw}^T \quad (4.31)$$

Eqs. (4.24 - 4.31) preserve symmetry in the final incremental stiffness matrix. The contributions from Eqs. (4.27 - 4.31) give the corrections of element stiffness matrix due to large deflections over the element. In an updated or corotational formulation these extra terms are normally neglected and only the linear secant submatrices in Eqs. (4.24 - 4.26) are normally used. Several numerical elements are then needed over one real beam element.

It should be emphasized that the above derivations do not include torsion. Torsion stiffness is directly put into the stiffness matrix in USFOS.

4.3.2 Interpolation Functions satisfying the Differential Equations

Two alternative choices of interpolation functions are incorporated in USFOS. The original version of the program is based upon functions $\phi_v(x)$ and $\phi_w(x)$ that satisfy the differential equations for a beam with axial force N (positive in compression) and no lateral load

$$v_{,xxxx} + \frac{N}{EI_z} v_{,xx} = 0 \quad (4.32)$$

$$w_{,xxxx} + \frac{N}{EI_z} w_{,xx} = 0 \quad (4.33)$$

In the following only deflection v in y -direction is considered. The deflection w in z -direction can be treated in a similar manner. However, Eqs. (4.32 - 4.33) become more complicated when deflection occurs in y - and z -direction simultaneously. This is discussed later in this section.

Implementation of Idealized Structural Unit Method

Introducing now the notation

$$k^2 = \frac{N}{EI} \quad N \text{ positive for compression} \quad (4.34)$$

gives for N in compression the following solution of Eq. (4.32)

$$v(x) = A_1 \cdot \cos kx + A_2 \cdot \sin kx + A_3 \cdot \frac{x}{l} + A_4 \quad (4.35)$$

and for N in tension

$$v(x) = A_1 \cdot e^{kx} + A_2 \cdot e^{-kx} + A_3 \cdot \frac{x}{l} + A_4 \quad (4.36)$$

or equivalent

$$v(x) = A_1 \cdot \cosh kx + A_2 \cdot \sinh kx + A_3 \cdot \frac{x}{l} + A_4 \quad (4.37)$$

The parameters $A_1 - A_4$ are treated as generalized displacements. Denoting by \mathbf{q}_v the vector

$$\mathbf{q}_v = [A_1 \ A_2 \ A_3 \ A_4]^T \quad (4.38)$$

the interpolation functions are collected in the vector

$$\Phi_{qv}(x) = [\cos k_y x, \sin k_y x, \frac{x}{l}, 1]^T \quad (4.39)$$

for N in compression, and

$$\Phi_{qv}(x) = [e^{k_y x}, e^{-k_y x}, \frac{x}{l}, 1]^T \quad (4.40)$$

for N in tension. For both cases the interpolation of deflection v is written

$$v(x) = \Phi_{qv}^T(x) \mathbf{q}_v \quad (4.41)$$

Similar expressions can be set for deflection w

$$\mathbf{q}_w = [B_1 \ B_2 \ B_3 \ B_4]^T \quad (4.42)$$

$$\Phi_{qw}(x) = [\cos k_z x, \sin k_z x, \frac{x}{l}, 1]^T \quad (4.43)$$

for N in compression, and

Implementation of Idealized Structural Unit Method

$$\Phi_{qw}(x) = [e^{k_z x}, e^{-k_z x}, \frac{x}{l}, 1]^T \quad (4.44)$$

for N in tension. The interpolation of w becomes

$$w(x) = \Phi_{qw}^T(x) \mathbf{q}_w \quad (4.45)$$

The interpolation of axial displacement $u(x)$ was originally linear. However, with the strain expression in Eq. (2.6) self-straining may easily occur since by rigid body rotation the constant term $u_{,x}$ does not match the higher order contributions in $v_{,x}^2$ and $w_{,x}^2$. The same problem has been discussed by Søreide /16/ for the finite element technique based on total Lagrangian Formulation.

Higher order variation of $u(x)$ is chosen similar to the interpolations of deflections, namely

$$u(x) = \Phi_{qu}^T(x) \mathbf{q}_u \quad (4.46)$$

with

$$\mathbf{q}_u = [C_1 \ C_2 \ C_3 \ C_4]^T \quad (4.47)$$

For N in compression the interpolation read

$$\Phi_{qu}(x) = [\cos kx, \sin kx, \frac{x}{l}, 1]^T \quad (4.48)$$

and for N in tension

$$\Phi_{qu}(x) = [e^{kx}, e^{-kx}, \frac{x}{l}, 1]^T \quad (4.49)$$

$$k = (k_y^2 + k_z^2 - k_y k_z)^{1/2} \quad (4.50)$$

It is seen that the parameters A, B and C are associated with rigid body motion only and have no stiffness influence. Therefore, the typical submatrices are of dimension 3·3 in generalized displacements.

Referring to Fig. 4.4 the relations between generalized displacements and real displacements are as follows

Implementation of Idealized Structural Unit Method

Deflection v: $\mathbf{T}_A \mathbf{q}_v = \mathbf{v}$ (4.51)

or for N in compression

$$\begin{bmatrix} 1 & 0 & 0 & 1 \\ 0 & k_y & \frac{1}{l} & 0 \\ c & s & 1 & 1 \\ -k_y \cdot s & k_y \cdot c & \frac{1}{l} & 0 \end{bmatrix} \begin{bmatrix} A_1 \\ A_2 \\ A_3 \\ A_4 \end{bmatrix} = \begin{bmatrix} v_1 \\ \theta_{z1} \\ v_2 \\ \theta_{z2} \end{bmatrix} \quad (4.52)$$

$c = \text{cos}k_y \cdot l$; $s = \text{sin}k_y \cdot l$

and for N in tension

$$\begin{bmatrix} 1 & 1 & 0 & 1 \\ k_y & -k_y & \frac{1}{l} & 0 \\ e^{k_y \cdot l} & e^{-k_y \cdot l} & 1 & 1 \\ k_y e^{k_y \cdot l} & -k_y e^{-k_y \cdot l} & \frac{1}{l} & 0 \end{bmatrix} \begin{bmatrix} A_1 \\ A_2 \\ A_3 \\ A_4 \end{bmatrix} = \begin{bmatrix} v_1 \\ \theta_{z1} \\ v_2 \\ \theta_{z2} \end{bmatrix} \quad (4.53)$$

Deflection w: $\mathbf{T}_B \mathbf{q}_w = \mathbf{w}$

or for N in compression

$$\begin{bmatrix} 1 & 0 & 0 & 1 \\ 0 & -k_z & -\frac{1}{l} & 0 \\ c & s & 1 & 1 \\ k_z \cdot s & -k_z \cdot c & -\frac{1}{l} & 0 \end{bmatrix} \begin{bmatrix} B_1 \\ B_2 \\ B_3 \\ B_4 \end{bmatrix} = \begin{bmatrix} w_1 \\ \theta_{y1} \\ w_2 \\ \theta_{y2} \end{bmatrix} \quad (4.54)$$

$c = \text{cos}k_z \cdot l$; $s = \text{sin}k_z \cdot l$

Implementation of Idealized Structural Unit Method

and for N in tension

$$\begin{bmatrix} 1 & 1 & 0 & 1 \\ -k_z & k_z & -\frac{1}{l} & 0 \\ k_z \cdot l & -k_z \cdot l & 1 & 1 \\ -k_z e^{k_z \cdot l} & k_z e^{-k_z \cdot l} & -\frac{1}{l} & 0 \end{bmatrix} \begin{bmatrix} B_1 \\ B_2 \\ B_3 \\ B_4 \end{bmatrix} = \begin{bmatrix} w_1 \\ \theta_{Y^1} \\ w_2 \\ \theta_{Y^2} \end{bmatrix} \quad (4.55)$$

The axial interpolation undergoes static condensation into two parameters u_1 and u_2 at element ends. The first step in this procedure is to keep C_1 and C_2 still as generalized displacements and to introduce u_1 and u_2 instead of C_3 and C_4 in the following way

$$\begin{bmatrix} 1 & 0 & 0 & 0 \\ 0 & 1 & 0 & 0 \\ 1 & 0 & 0 & 1 \\ c & s & 1 & 1 \end{bmatrix} \begin{bmatrix} C_1 \\ C_2 \\ C_3 \\ C_4 \end{bmatrix} = \begin{bmatrix} C_1 \\ C_2 \\ u_1 \\ u_2 \end{bmatrix} \quad (4.56)$$

$$c = \cos kl \quad s = \sin kl$$

or

$$\mathbf{T} \mathbf{q} = \mathbf{u} \quad (4.57)$$

$$\begin{matrix} \mathbf{c} & \mathbf{u} & \mathbf{c} \end{matrix}$$

where \mathbf{u} denotes the uncondensed axial displacement vector.

Further details on stiffness evaluation are given in Section 4.3.4.

Implementation of Idealized Structural Unit Method

4.3.3 Third Order Polynomials as Interpolation Functions

The computer program also includes the conventional third order polynomials for deflection

$$\begin{bmatrix} v \\ \theta_z \end{bmatrix} = \Phi_{qw}^T \mathbf{T} - \Phi_{q0}^T \mathbf{T} = \begin{bmatrix} \frac{x}{l} \\ 1 \end{bmatrix} \quad (4.58)$$

which now are equal for compression and tension

Eq. (4.51) turns into

$$\begin{bmatrix} 0 & 0 & 0 & 1 \\ 0 & 0 & \frac{1}{l} & 0 \\ 1 & 1 & 1 & 1 \\ \frac{3}{l} & \frac{2}{l} & \frac{1}{l} & 0 \end{bmatrix} \begin{bmatrix} A_1 \\ A_2 \\ A_3 \\ A_4 \end{bmatrix} = \begin{bmatrix} v_1 \\ \theta_{z^1} \\ v_2 \\ \theta_{z^2} \end{bmatrix} \quad (4.59)$$

and Eq. (4.53) reads

$$\begin{bmatrix} 0 & 0 & 0 & 0 \\ 0 & 0 & -\frac{1}{l} & 0 \\ 1 & 1 & 1 & 1 \\ \frac{3}{l} & -\frac{2}{l} & -\frac{1}{l} & 0 \end{bmatrix} \begin{bmatrix} B_1 \\ B_2 \\ B_3 \\ B_4 \end{bmatrix} = \begin{bmatrix} w_1 \\ \theta_{y^1} \\ w_2 \\ \theta_{y^2} \end{bmatrix} \quad (4.60)$$

The generalized axial coordinates in terms of nodal parameters u_1 and u_2 given by Eq. (4.57) become

$$\begin{bmatrix} 1 & 0 & 0 & 0 \\ 0 & 1 & 0 & 0 \\ 0 & 0 & 0 & 1 \\ 1 & 1 & 1 & 1 \end{bmatrix} \begin{bmatrix} C_1 \\ C_2 \\ C_3 \\ C_4 \end{bmatrix} = \begin{bmatrix} C_1 \\ C_2 \\ u_1 \\ u_2 \end{bmatrix} \quad (4.61)$$

4.3.4 Final Stiffness Matrix

It is easily verified that the three rigid body parameters A_4 , B_4 and C_4 do not enter into the stiffness expressions (4.22). The 9x9 element matrix of Eq. (4.23) can be evaluated in generalized coordinates

$$\mathbf{k}_q = \begin{bmatrix} \mathbf{k}_{ququ} & \mathbf{k}_{quqv} & \mathbf{k}_{quqw} \\ \mathbf{k}_{qvqu} & \mathbf{k}_{qvqv} & \mathbf{k}_{qvqw} \\ \mathbf{k}_{qwqu} & \mathbf{k}_{qwqv} & \mathbf{k}_{qwqw} \end{bmatrix} \tag{4.62}$$

with all submatrices of dimensions (3·3).

The transformation into parameters u_c implies the following operations on submatrices in Eq. (4.62)

$$\mathbf{k}_{ucuc} = (\mathbf{T}_c^{-1}) \mathbf{k}_{ququ} (\mathbf{T}_c^{-1}) \tag{4.63}$$

$$\mathbf{k}_{ucqv} = (\mathbf{T}_c^{-1}) \mathbf{k}_{quqv} \tag{4.64}$$

$$\mathbf{k}_{ucqw} = (\mathbf{T}_c^{-1}) \mathbf{k}_{quqw} \tag{4.65}$$

The 4·4 matrix \mathbf{k}_{ucuc} is divided into 2·2 submatrices connected to parameters C_1 , C_2 and u_1 , u_2 .

$$\mathbf{k}_{ucuc} = \begin{bmatrix} \mathbf{k}_{cc} & \mathbf{0} \\ \mathbf{0} & \mathbf{k}_{uu} \end{bmatrix} \tag{4.66}$$

Further the matrix \mathbf{k}_{ucqv} is horizontally split

Implementation of Idealized Structural Unit Method

$$\mathbf{k}_{ucqv} = \begin{bmatrix} \mathbf{k}_{cqv} \\ \mathbf{k}_{uqv} \end{bmatrix} \quad (4.67)$$

and correspondingly

$$\mathbf{k}_{ucqw} = \begin{bmatrix} \mathbf{k}_{cqw} \\ \mathbf{k}_{uqw} \end{bmatrix} \quad (2.4) \quad (4.68)$$

The axial mixed vector of Eqs. (4.56, 4.61) is subdivided

$$\begin{bmatrix} C_1 \\ C_2 \\ \hline u_1 \\ u_2 \end{bmatrix} = \begin{bmatrix} \mathbf{c} \\ \mathbf{u} \end{bmatrix} \quad (4.69)$$

The incremental virtual work associated with generalized parameters C_1, C_2 gets the form

$$\delta \mathbf{c}^T \Delta \mathbf{S}_c = \delta \mathbf{c}^T \{ \mathbf{k}_{cc} \Delta \mathbf{c} + \mathbf{k}_{cqv} \Delta \mathbf{q}_v + \mathbf{k}_{cqw} \Delta \mathbf{q}_w \} \quad (4.70)$$

Having u_1, u_2 as the final parameters in axial displacement the work associated with $\delta \mathbf{c}$ should vanish. This results in the well known procedure for static condensation.

$$\Delta \mathbf{c} = - \mathbf{k}_{cc}^{-1} \{ \mathbf{k}_{cqv} \Delta \mathbf{q}_v + \mathbf{k}_{cqw} \Delta \mathbf{q}_w \} \quad (4.71)$$

where $\mathbf{k}_{cu} = \mathbf{0}$ is incorporated

Implementation of Idealized Structural Unit Method

The incremental virtual work associated with \mathbf{q}_v is now

$$\begin{aligned} \delta \mathbf{q}_v^T \Delta \mathbf{S}_{qv} &= \delta \mathbf{q}_v^T \{ \mathbf{k}_{cq}^T \Delta \mathbf{c} + \mathbf{k}_{uqv}^T \Delta \mathbf{u} \\ &\quad + \mathbf{k}_{qvqv} \Delta \mathbf{q}_v + \mathbf{k}_{qvqw} \Delta \mathbf{q}_w \} \end{aligned} \quad (4.72)$$

Combining Eqs. (4.71, 4.72) gives

$$\begin{aligned} \delta \mathbf{q}_v^T \Delta \mathbf{S}_{qv} &= \delta \mathbf{q}_v^T \{ \mathbf{k}_{uqv}^T \Delta \mathbf{u} + (\mathbf{k}_{qvqv} - \mathbf{k}_{cq}^T \mathbf{k}_{cc}^{-1} \mathbf{k}_{cq}) \Delta \mathbf{q}_v \\ &\quad + (\mathbf{k}_{qvqw} - \mathbf{k}_{cq}^T \mathbf{k}_{cc}^{-1} \mathbf{k}_{cqw}) \Delta \mathbf{q}_w \} \end{aligned} \quad (4.73)$$

hence leading to the modified submatrices

$$\bar{\mathbf{k}}_{qvqv} = \mathbf{k}_{qvqv} - \mathbf{k}_{cq}^T \mathbf{k}_{cc}^{-1} \mathbf{k}_{cq} \quad (4.74)$$

$$\bar{\mathbf{k}}_{qvqw} = \mathbf{k}_{qvqw} - \mathbf{k}_{cq}^T \mathbf{k}_{cc}^{-1} \mathbf{k}_{cqw} \quad (4.75)$$

A similar evaluation of $\delta \mathbf{q}_w^T \Delta \mathbf{S}_{qw}$ leads to

$$\bar{\mathbf{k}}_{qwqw} = \mathbf{k}_{qwqw} - \mathbf{k}_{cqw}^T \mathbf{k}_{cc}^{-1} \mathbf{k}_{cqw} \quad (4.76)$$

$$\bar{\mathbf{k}}_{qwqv} = \mathbf{k}_{qwqv} - \mathbf{k}_{cqw}^T \mathbf{k}_{cc}^{-1} \mathbf{k}_{cqv} = \bar{\mathbf{k}}_{qvqw}^T \quad (4.77)$$

The final transitions from generalized coordinates \mathbf{q}_v and \mathbf{q}_w into nodal displacement parameters \mathbf{v} and \mathbf{w} out as

$$\mathbf{k}_{uv} = \mathbf{k}_{uqv} (\mathbf{T}_A^{-1}) \quad (4.78)$$

$$\mathbf{k}_{vv} = (\mathbf{T}_A^{-1})^T \bar{\mathbf{k}}_{qvqv} (\mathbf{T}_A^{-1}) \quad (4.79)$$

$$\mathbf{k}_{uw} = \mathbf{k}_{uqw} (\mathbf{T}_B^{-1}) \quad (4.80)$$

Implementation of Idealized Structural Unit Method

$$\mathbf{k}_{vw} = (\mathbf{T}_A^{-1})^T \bar{\mathbf{k}}_{qvqw} (\mathbf{T}_B^{-1}) \quad (4.81)$$

$$\mathbf{k}_{ww} = (\mathbf{T}_B^{-1})^T \mathbf{k}_{qwqw} (\mathbf{T}_B^{-1}) \quad (4.82)$$

Before organizing the incremental stiffness matrix node-wise the above sub-matrices are defined out of

$$\begin{bmatrix} \Delta \mathbf{S}_u \\ \Delta \mathbf{S}_v \\ \Delta \mathbf{S}_w \\ (10 \cdot 1) \end{bmatrix} = \begin{bmatrix} \mathbf{k}_{uu} & \mathbf{k}_{uv} & \mathbf{k}_{uw} \\ (2 \cdot 2) & (2 \cdot 4) & (2 \cdot 4) \\ \mathbf{k}_{vu} & \mathbf{k}_{vv} & \mathbf{k}_{vw} \\ (4 \cdot 2) & (4 \cdot 4) & (4 \cdot 4) \\ \mathbf{k}_{wu} & \mathbf{k}_{wv} & \mathbf{k}_{ww} \\ (4 \cdot 2) & (4 \cdot 4) & (4 \cdot 4) \end{bmatrix} \begin{bmatrix} \Delta u \\ \Delta v \\ \Delta w \\ (10 \cdot 1) \end{bmatrix} \quad (4.83)$$

For the full three-dimensional beam element the torsional rigidity associated with θ_1 and θ_2 has to be included. The St. Venant elastic rigidity GI_t/K is put on main diagonal and $-GI_t/K$ on coupling terms.

The final transformation into node-by-node order is a simple reorganization of Eq. (4.83) and is not given in detail here.

4.4 Modifications for Plastic Hinges

The present section concerns the modification of elastic stiffness matrix due to plastification. As explained in Chapter 3 plastification is supposed to be concentrated at hinges. The present version of USFOS considers three alternative locations of these plastic hinges for each element, namely at the element ends and at midspan.

4.4.1 Plastic Hinge at Element Ends

First, some comments are given on the calculation of elastic and plastic deformations in the vicinity of a plastic hinge

Figure 4.5 Rotations at beam end

Fig. 4.5 shows a beam end coupled to a node with an assumed plastic hinge at the beam end. The node rotation is θ . Due to concentrated rotation at the plastic hinge a discontinuity occurs in beam rotations across the hinge and the following relation comes out

$$\theta_{\text{node}} = \theta_{\text{hinge}} + \theta_{\text{elastic}} \quad (4.84)$$

It is clear that when introducing interelement continuity θ_{node} should be the characteristic parameter at the beam end and not θ_{elastic} .

Similar considerations can also be made for the other displacement parameters. Thus, by using the notation

$$\mathbf{v}_i^T = [u \ v \ w \ \theta_x \ \theta_y \ \theta_z] \quad i = 1, 2 \quad (4.85)$$

and

$$\mathbf{v}^T = [\mathbf{v}_1^T \ \mathbf{v}_2^T] \quad (4.86)$$

The elastic and plastic rotations are separated in the way

$$\mathbf{v} = \mathbf{v}^e + \mathbf{v}^p \quad (4.87)$$

where indices e and p denotes elastic and plastic (hinge) parameters, respectively.

Implementing the system of Eqs. (4.85 - 86) also for beam end forces

Implementation of Idealized Structural Unit Method

$$\frac{\partial F}{\partial \mathbf{S}_i} \Delta \mathbf{S}_i^t + \frac{\partial F}{\partial \mathbf{S}_{p_i}} \Delta \mathbf{S}_{p_i} = 0 \quad (4.94a)$$

Inserting Equation (3.8) gives:

$$\mathbf{g}_i^T (\Delta \mathbf{S}_i - \Delta \mathbf{S}_i^h + \frac{\partial \mathbf{S}}{\partial \mathbf{S}_p} \Delta \mathbf{S}_p) \quad (4.94b)$$

Substituting Equation (3.12) into (4.94) gives

$$\mathbf{g}_i^T (\Delta \mathbf{S}_i - \mathbf{k}_{ii}^h \Delta \mathbf{v}_i^p - \mathbf{C}_{p_i} \Delta \mathbf{v}_i^p) = 0, \quad i = 1, 2$$

Combining Eqs. (4.93-94) leads to the following equations for $\Delta \lambda_1$ and $\Delta \lambda_2$.

$$\begin{bmatrix} \mathbf{g}_1^T (\mathbf{k}_{11} + \mathbf{k}_{11}^h + \mathbf{C}_{11}) \mathbf{g}_1 & \mathbf{g}_1^T \mathbf{k}_{12} \mathbf{g}_2 \\ \mathbf{g}_2^T \mathbf{k}_{21} \mathbf{g}_1 & \mathbf{g}_2^T (\mathbf{k}_{22} + \mathbf{k}_{22}^h + \mathbf{C}_{22}) \mathbf{g}_2 \end{bmatrix} \begin{bmatrix} \Delta \lambda_1 \\ \Delta \lambda_2 \end{bmatrix} = \begin{bmatrix} \mathbf{g}_1^T \mathbf{k}_{11} & \mathbf{g}_1^T \mathbf{k}_{12} \\ \mathbf{g}_2^T \mathbf{k}_{21} & \mathbf{g}_2^T \mathbf{k}_{22} \end{bmatrix} \begin{bmatrix} \Delta \mathbf{v}_1 \\ \Delta \mathbf{v}_2 \end{bmatrix} + \begin{bmatrix} \mathbf{g}_1^T \Delta \bar{\mathbf{S}}_1 \\ \mathbf{g}_2^T \Delta \bar{\mathbf{S}}_2 \end{bmatrix} \quad (4.95)$$

(2·2) (2·12)

Here \mathbf{k}_{11}^h and \mathbf{k}_{22}^h are the hardening matrices associated with beam element end 1 and end 2 respectively. From section 3.6 it is also evident that $\mathbf{k}_{12}^h = \mathbf{k}_{21}^h = 0$

The solution for $\Delta \lambda_1$ and $\Delta \lambda_2$ can be written

$$\begin{bmatrix} \Delta \lambda_1 \\ \Delta \lambda_2 \end{bmatrix} = \begin{bmatrix} \mathbf{h}_{11}^T & \mathbf{h}_{12}^T \\ \mathbf{h}_{21}^T & \mathbf{h}_{22}^T \end{bmatrix} \begin{bmatrix} \Delta \mathbf{v}_1 \\ \Delta \mathbf{v}_2 \end{bmatrix} + \begin{bmatrix} \mathbf{p}_{11}^T & \mathbf{p}_{12}^T \\ \mathbf{p}_{21}^T & \mathbf{p}_{22}^T \end{bmatrix} \begin{bmatrix} \Delta \bar{\mathbf{S}}_1 \\ \Delta \bar{\mathbf{S}}_2 \end{bmatrix} \quad (4.96)$$

where

$$\mathbf{h}_{11}^T = \frac{1}{\det} \{ (\mathbf{g}_2^T (\mathbf{k}_{22} + \mathbf{k}_{22}^h + \mathbf{C}_{22}) \mathbf{g}_2) \mathbf{g}_1^T \mathbf{k}_{11} - (\mathbf{g}_1^T \mathbf{k}_{12} \mathbf{g}_2) \mathbf{g}_2^T \mathbf{k}_{21} \} \quad (4.97)$$

$$\mathbf{h}_{12}^T = \frac{1}{\det} \{ (\mathbf{g}_2^T (\mathbf{k}_{22} + \mathbf{k}_{22}^h + \mathbf{C}_{22}) \mathbf{g}_2) \mathbf{g}_1^T \mathbf{k}_{12} - (\mathbf{g}_1^T \mathbf{k}_{12} \mathbf{g}_2) \mathbf{g}_2^T \mathbf{k}_{22} \} \quad (4.98)$$

$$\mathbf{h}_{21}^T = \frac{1}{\det} \{ (\mathbf{g}_1^T (\mathbf{k}_{11} + \mathbf{k}_{11}^h + \mathbf{C}_{11}) \mathbf{g}_1) \mathbf{g}_2^T \mathbf{k}_{21} - (\mathbf{g}_2^T \mathbf{k}_{21} \mathbf{g}_1) \mathbf{g}_1^T \mathbf{k}_{11} \} \quad (4.99)$$

Implementation of Idealized Structural Unit Method

$$\mathbf{h}_{22}^T = \frac{1}{\det} \{ (\mathbf{g}_1^T (\mathbf{k}_{11} + \mathbf{k}_{11}^h + \mathbf{C}_{11}) \mathbf{g}_1) \mathbf{g}_2^T \mathbf{k}_{22} - (\mathbf{g}_2^T \mathbf{k}_{21} \mathbf{g}_1) \mathbf{g}_1^T \mathbf{k}_{12} \} \quad (4.100)$$

$$\mathbf{p}_{11}^T = \frac{1}{\det} (\mathbf{g}_2^T (\mathbf{k}_{22} + \mathbf{k}_{22}^h + \mathbf{C}_{22}) \mathbf{g}_2) \mathbf{g}_1^T \quad (4.101)$$

$$\mathbf{p}_{12}^T = \frac{1}{\det} (-\mathbf{g}_1^T \mathbf{k}_{12} \mathbf{g}_2) \mathbf{g}_2^T \quad (4.102)$$

$$\mathbf{p}_{21}^T = \frac{1}{\det} (-\mathbf{g}_2^T \mathbf{k}_{21} \mathbf{g}_1) \mathbf{g}_1^T \quad (4.103)$$

$$\mathbf{p}_{22}^T = \frac{1}{\det} (\mathbf{g}_1^T (\mathbf{k}_{11} + \mathbf{k}_{11}^h + \mathbf{C}_{11}) \mathbf{g}_1) \mathbf{g}_2^T \quad (4.104)$$

$$\det = (\mathbf{g}_1^T (\mathbf{k}_{11} + \mathbf{k}_{11}^h + \mathbf{C}_{11}) \mathbf{g}_1) (\mathbf{g}_2^T (\mathbf{k}_{22} + \mathbf{k}_{22}^h + \mathbf{C}_{22}) \mathbf{g}_2) - (\mathbf{g}_1^T \mathbf{k}_{12} \mathbf{g}_2)^2 \quad (4.105)$$

For the case which not includes material hardening $\mathbf{k}_{11}^h = \mathbf{k}_{22}^h = \mathbf{0}$ and Eqs. (4.95) - (4.105) are simplified accordingly.

The quantities in paranthesis () come out to be scalars. Each of the sub-vectors \mathbf{h}_{ij} and \mathbf{p}_{ij} has dimension 6·1. It is seen that there is a contribution to the plastic increment from both the displacement increment as well as from the consistent nodal force increment.

The elasto-plastic stiffness of the element is now obtained by substituting Eq. (4.96) into Eq. (4.93). The result is

$$\begin{bmatrix} \Delta \mathbf{S}_1 \\ \Delta \mathbf{S}_2 \end{bmatrix} = \begin{bmatrix} \mathbf{k}_{11}^{ep} & \mathbf{k}_{12}^{ep} \\ \mathbf{k}_{21}^{ep} & \mathbf{k}_{22}^{ep} \end{bmatrix} \begin{bmatrix} \Delta \mathbf{v}_1 \\ \Delta \mathbf{v}_2 \end{bmatrix} + \begin{bmatrix} \mathbf{p}_{11}^{ep} & \mathbf{p}_{12}^{ep} \\ \mathbf{p}_{21}^{ep} & \mathbf{p}_{22}^{ep} \end{bmatrix} \begin{bmatrix} \Delta \bar{\mathbf{S}}_1 \\ \Delta \bar{\mathbf{S}}_2 \end{bmatrix} \quad (4.106)$$

where Eq. (4.106) now gives the incremental elasto-plastic stiffness for the beam element. The elasto-plastic submatrices \mathbf{k}_{ij}^{ep} come out as

Implementation of Idealized Structural Unit Method

$$k_{ij}^{ep} = k_{ij} - k_{ik} g_k h_{kj}^T ; \quad (4.107)$$

$$p_{ij}^{ep} = \delta_{ij} - k_{ik} g_k p_{kj}^T \quad i, j, k = 1, 2 \quad (4.108)$$

In Eqs. (4.107-108) Einsteins summation convention is adopted and thus k is the dummy summation index.

In the case of plastification only at one end of the element the above expressions are simplified. Denoting by index i ($i = 1$ or 2) the end that is plastified Eq. (4.94) is still valid and Eq. (4.95) reduces to

$$(g_i^T (k_{ii} + k_{ii}^h + C_{ii}) g_i) \Delta \lambda_i = [g_i^T k_{i1} \quad g_i^T k_{i2}] \begin{bmatrix} \Delta v_1 \\ \Delta v_2 \end{bmatrix} + g_i^T \Delta \bar{S}_i \quad (4.109)$$

Note: Not sum over index i .

Eqs. (4.97 - 105) are simplified to

$$h_{i1}^T = \frac{1}{\det} g_i^T k_{i1} \quad (\text{not sum}) \quad (4.110)$$

$$h_{i2}^T = \frac{1}{\det} g_i^T k_{i2} \quad (\text{not sum}) \quad (4.111)$$

$$p_i^T = \frac{1}{\det} g_i^T \quad (4.112)$$

$$\det = g_i^T (k_{ii} + k_{ii}^h + C_{ii}) g_i \quad (\text{not sum}) \quad (4.113)$$

other elements vanish.

It is easily verified by introducing Eqs. (4.97-105) into Eqs. (4.107-108) that symmetry of the stiffness matrix is preserved through the elasto-plastic modifications.

During a finite load increment the stress state in fact moves tangential to the

Implementation of Idealized Structural Unit Method

yield surface. The deviation from the true yield surface may be corrected for by introducing an equivalent load vector. Rearranging Eq. (4.94) the consistency condition may now be expressed

$$\mathbf{g}_i^T \Delta \mathbf{S}_i^t + \Delta \bar{F}_i = 0 \quad (i = 1, 2, \text{ not sum over } i) \quad (4.114)$$

where $\Delta \bar{F}_i$ represents the deviation from the yield surface at end i .

Introducing Eq. (4.114) into Eqs. (4.93) there comes out a contribution to the plastic increments.

$$\begin{bmatrix} \Delta \lambda_1^* \\ \Delta \lambda_2^* \end{bmatrix} = \begin{bmatrix} t_{11} & t_{12} \\ t_{21} & t_{22} \end{bmatrix} \begin{bmatrix} \Delta \bar{F}_1 \\ \Delta \bar{F}_2 \end{bmatrix} \quad (4.115)$$

where

$$t_{11} = \frac{1}{\det} (\mathbf{g}_2^T (\mathbf{k}_{22} + \mathbf{k}_{22}^h + \mathbf{C}_{22}) \mathbf{g}_{22}) \quad (4.116)$$

$$t_{21} = \frac{1}{\det} (-\mathbf{g}_1^T \mathbf{k}_{12} \mathbf{g}_2) \quad (4.117)$$

$$t_{21} = \frac{1}{\det} (-\mathbf{g}_2^T \mathbf{k}_{21} \mathbf{g}_1) \quad (4.118)$$

$$t_{22} = \frac{1}{\det} (\mathbf{g}_1^T (\mathbf{k}_{11} + \mathbf{k}_{11}^h + \mathbf{C}_{11}) \mathbf{g}_1) \quad (4.119)$$

The equivalent model force vector contribution becomes

$$\begin{bmatrix} \Delta \mathbf{S}^* \\ \Delta \mathbf{S}_2^* \end{bmatrix} = - \begin{bmatrix} t_{11}^{ep} & t_{12}^{ep} \\ t_{21}^{ep} & t_{22}^{ep} \end{bmatrix} \begin{bmatrix} \Delta \bar{F}_1 \\ \Delta \bar{F}_2 \end{bmatrix} \quad (4.120)$$

The elasto-plastic subvector t_{ij}^{ep} comes out as

$$t_{ij}^{ep} = -\mathbf{k}_{ik} \mathbf{g}_k t_{kj} \quad (4.121)$$

Implementation of Idealized Structural Unit Method

For plasticification at only one end a similar simplification is valid, namely

$$t_i = \frac{1}{\det} \Delta \lambda_i \quad i = 1, 2 \quad (4.122)$$

and the determinant given by eq. (4.113) other elements vanish.

Contrary to the consistent nodal force increment, the equivalent nodal force vector due to yield surface deviation has a distinct sign and magnitude. Hence, it should not be scaled or reversed, as for example during global unloading, but only be taken into account during equilibrium iteration.

4.4.2 Plastic Hinge at Element Midspan

The check for plastification is also performed at element midspan. If the plastic capacity is reached at midspan the member is divided into two new members, see Fig. 4.6.

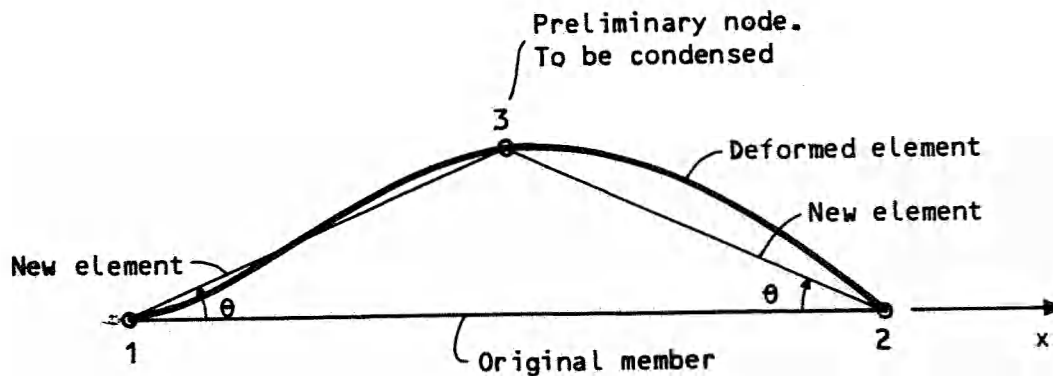


Fig. 4.6 Subdivision of beam element for plastic hinge at midspan

The orientations of the two new elements 1 - 3 and 3 - 2 are calculated on the basis of the updated local deformations of element 1 - 2. New local accumulated deformations are calculated for elements 1 - 3 and 3 - 2 as the difference between the deformed element 1 - 2 and the straight lines 1 - 3 and 3 - 2. This is practically performed by introducing accumulated end rotations for the two

Implementation of Idealized Structural Unit Method

new elements equal to the accumulated rotations for element 1 - 2 in points 1,3, 2 minus/plus rigid body rotations θ .

The elastic stiffnesses are found for elements 1 - 3 and 3 - 2 with local large-deflection effects included. A plastic hinge is introduced in one of the two new elements at node 3 and the stiffness matrix for this element is modified.

Finally, the stiffness matrices for the two elements are transformed into the original member system 1 - 2 and added. The extra node 3 is thereafter eliminated by static condensation.

By the above procedure the original member 1 - 2 is again the basic element to use further in the global frame analysis. The process of static condensation is only performed at element level and does not imply much computer costs.

4.5 Accumulation of Stress Resultants

The procedure for calculating internal stress resultants in the structure is of vital importance for the stability of the solution algorithm. It is essential that the calculation of stress resultants is consistent with the scheme for incremental stiffness. If not, false unloading during iteration may occur.

Special care must be shown when using the Livesly expressions for stiffness combined with the load-dependent shape functions of Section 4.3.2. The change of shape functions during incrementation is here an extra source of problems.

The incremental elasto-plastic force-displacement relation for an element is given by Eq. (4.83). The basis for this expression is the elastic element stiffness in Eq. (4.22). As pointed out in Section 2.3.1 the incremental stiffness represents a linearized version in the way that higher order terms of Δv_x and Δw_x are neglected. For the elastic axial strain increment the correct expression reads

$$\Delta \epsilon_x = \Delta u_x + v_x \cdot \Delta v_x + w_x \cdot \Delta w_x + \frac{1}{2} \Delta v_x^2 + \frac{1}{2} \Delta w_x^2 \quad (4.123)$$

Implementation of Idealized Structural Unit Method

The last two terms are neglected by the linearized incremental stiffness. However, when calculating change in stress resultant N the complete expression (4.123) should be included.

The notation consistent now means that for one element, within one cycle of loading the terms of Eq. (4.83) are the same for calculating incremental stiffness at the start of the cycle and for calculating stress resultant increments at the end of the cycle. This means that for each element the local stiffness matrix may be stored and then updated with the next cycle.

The inclusion of the nonlinear incremental rotations in $\Delta \epsilon_x$ may be considered as a tension correction of the effective axial deformation. In the case where the element undergoes increment in compression during a step the two last terms in Eq. (4.123) reduce the compressive $\Delta \epsilon_x$ due to additional deflection flexibility. For tension increment $\Delta \epsilon_x$ the two terms give extra membrane stiffness. The general effect of these terms is therefore to give a stiffer element for tension and softer element for compression.

The elasto-plastic incremental load-displacement relation on local element level given by Eq. (4.83) is now used for calculating load increments. The modification for nonlinear strain terms is incorporated by substituting the axial displacement Δu_1 by

$$\Delta u_1^* = \Delta u_1 - \frac{1}{2} \left\{ \int (\Delta v_x^2 + \Delta w_x^2) dx \right\} \quad (4.124)$$

Generally, with coupling terms in the stiffness matrix this gives corrections in incremental axial force, shear forces and moments.

It should be emphasized that in order to perform the modification (4.124) back-substitution via Eqs. (4.96 - 91) is necessary so as to obtain the pure elastic deformations. This backsubstitution has to be carried out in any case before the generation of new incremental stiffness since v_x and w_x for the elastic element must be updated according to Eq. (4.22).

After calculating stress resultant increments by Eqs. (4.83, 4.124) these are added to the previous values and a new cycle is performed.

An alternative scheme for calculating internal forces, is to use the elastic secant stiffness in Eqs. (2.17, 19), so that

$$\Delta \mathbf{S} = \mathbf{k}_{\text{sec}} \cdot \mathbf{V}_{\text{elas}} \quad (4.125)$$

where \mathbf{k}_{sec} is the elastic stiffness matrix, containing geometric contributions, and \mathbf{V}_{elas} is the vector of total elastic, nodal displacements.

This formulation has been implemented in USFOS and proved to perform well.

5 SOLUTION ALGORITHM

The present chapter gives a review of the basic numerical techniques implemented in USFOS for solving the nonlinear equation. Special attention is given to reliable techniques for collapse and buckling problems.

Two instability phenomena that are frequently encountered in nonlinear structural problems are limit points and bifurcation points. They are illustrated in Figure 5.1.

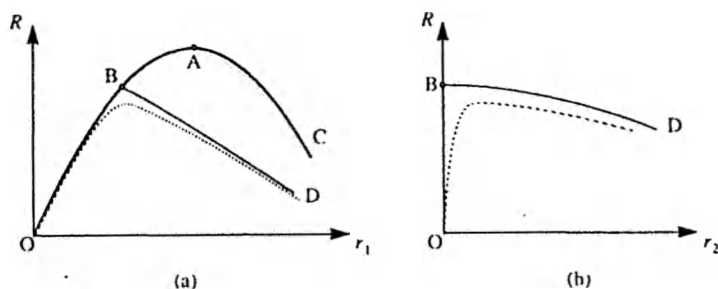


Figure 5.1: Load-deflection curve with a limit point A and a bifurcation point B.

In an incremental-iterative solution strategy the traversal of a limit point is characterized by a continuous decrease (increase) of stiffness until a local maximum (minimum) of the load is obtained. The mode of deformation is stable in the sense that the deformation components grow monotonously. At the limit point A the following relations hold true:

$$S_p = 0$$

$$\det (K_I) = 0$$

$$K_I \Phi = 0$$

$$\Phi^T R \neq 0$$

(5.1)

Solution Algorithm

Here K_I denotes the tangent stiffness matrix,

Φ is the eigenvectors of the tangent stiffness matrix

and R is the increment in the external load vector.

The current stiffness parameter S_p is for a typical load step number i defined by :

$$S_p^i = \frac{\Delta x^{1T} \Delta R^1}{\Delta x^{iT} \Delta R^i} \frac{|\Delta R^i|^2}{|\Delta R^1|^2}$$

and has the initial value 1.0 at step number 1. This makes S_p to be a normalized measure of the tangential stiffness along the deformation path.

A point where the load displacement curve branches into two or more solution paths is called a bifurcation point. This is indicated by point B in Fig 5.1. Beyond the bifurcation point the solution may follow any of the branches. Switching over to the correct path, being the path with the lower energy, implies often a change in the deformation pattern, so that all deformation components do not grow monotonously. This is characterized as a snap-back (spring-back) type of deformation.

At the bifurcation point the following conditions apply

$$S_p \neq 0$$

$$\det (K_I) = 0$$

$$K_I \Phi = 0$$

$$\Phi^T R = 0$$

(5.2)

A bifurcation point may be turned into the a limit point by introducing components of the correct bifurcation path as small imperfections to the system. These imperfections will cause the structure to deform along the dashed line in Fig 5.1 and the behaviour resembles that of a limit point.

The traversing of a bifurcation point is especially challenging from a numerical

point of view. The prebuckling deformations may lack sufficient components to allow switching to the correct path. Sometimes the solution alternates between two branches. The correct path is not known apriori and can not be introduced as initial imperfections unless a complete reanalysis is performed once a bifurcation point is detected.

Very often standard procedures for equilibrium iterations fail to converge at limit - and bifurcation points. However, self adaptive solution schemes such as arc length methods have proved to cope well with such problems. Due to its simplicity the method with iterations on the normal plane is preferred.

5.1 Step-by Step Method

The two sources of nonlinearity, namely material plastification and large deflections, have been implemented in the incremental load/displacement relation. Thus, it is natural to go for a step-by-step technique.

The incremental stiffness is expressed by the following relation

$$\mathbf{K}_I^{i-1} \Delta \mathbf{r}^i = \Delta \mathbf{R}^i \quad (5.3)$$

where index "i" denotes step number. \mathbf{K}_I is the incremental global stiffness and $\Delta \mathbf{R}$ and $\Delta \mathbf{r}$ incremental loads and displacements, respectively.

The total load after step number i is accumulated from the previous steps in the way:

$$\mathbf{R}^i = \mathbf{R}^{i-1} + \Delta \mathbf{R}^i \quad (5.4)$$

and similarly the displacements

$$\mathbf{r}^i = \mathbf{r}^{i-1} + \Delta \mathbf{r}^i \quad (5.5)$$

It should be emphasized again that the incremental matrix \mathbf{K}_I generally is a function of the current configuration of the structure, and for elasto-plastic

problems, the entire deformation history.

The program applies the simple Euler-Cauchy incrementation method, see also Fig. 5.2. The major deficiency by this technique is the risk for drift off from the exact solution path. Corrections for this uncertainty is taken care of by including equilibrium corrections in the load vector at every step, see Fig. 5.3.

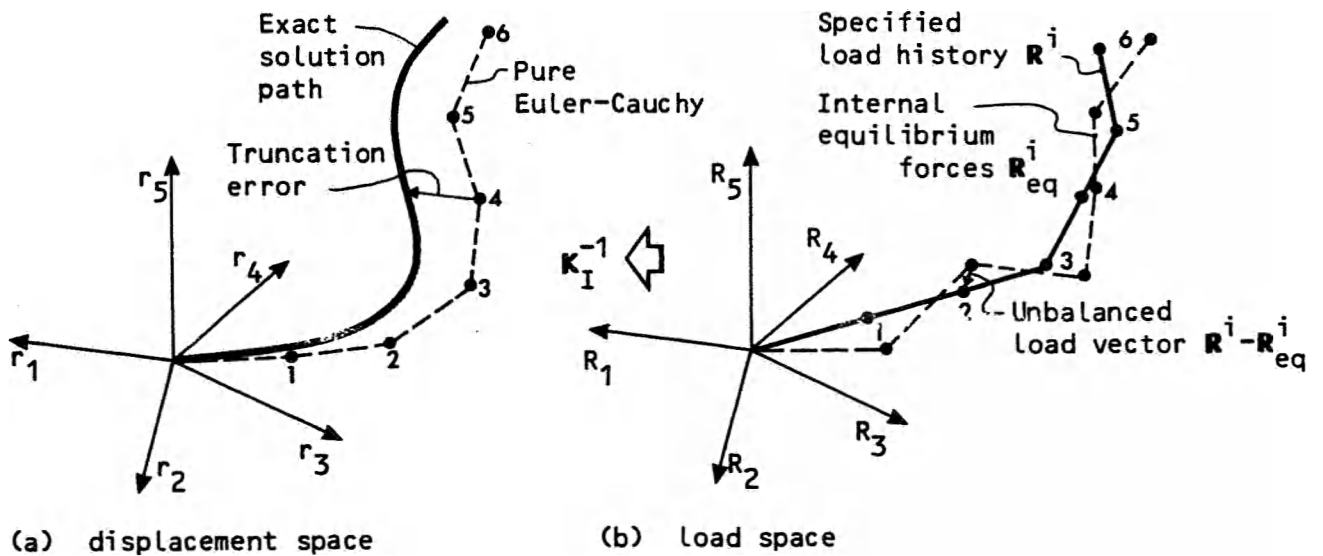


Figure 5.2 Displacement and load histories by Euler-Cauchy incrementation

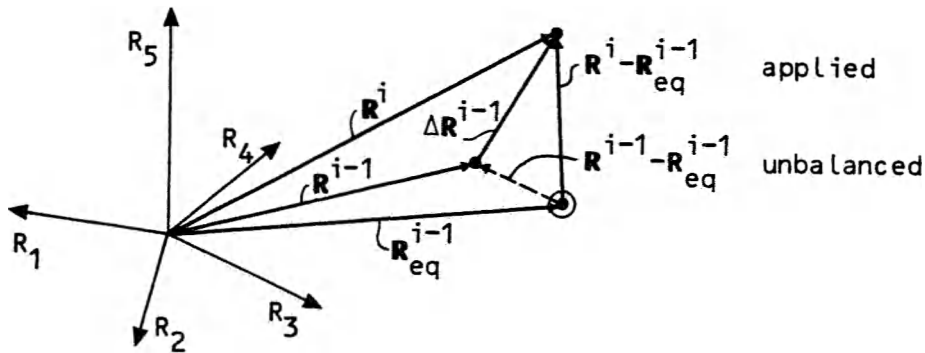


Figure 5.3 Load increment no. 1 with equilibrium correction

Fig. 5.2 indicates the pure Euler-Cauchy incrementation technique in multidimensional displacement and stress space. The external load is specified by load steps in Fig. 5.2b (Solid line) and the corresponding exact displacement curve is the solid curve in Fig. 5.2a.

The Euler-Cauchy solution is illustrated by the dotted line in the displacement space (Fig. 5.2a) indicating a truncation error (drift-off) related to the exact path.

The history of the global vector of internal equilibrium forces R_{eq}^i , corresponding to the approximated displacement solution is dotted in the load space of Fig. 5.2b. It is indicated that the vector of equilibrium forces may show a highly nonregular variation during displacement history.

Fig. 5.3 illustrates the process of Euler-Cauchy incrementation combined with equilibrium correction. Let R^{i-1} be specified external loads after step no. $i-1$. The current increment no. i of external loads goes from R^{i-1} to R^i . At level no. $i-1$ comparison is made between external loads and internal equilibrium forces in global system, R_{eq}^{i-1} . The unbalance $R^{i-1} - R_{eq}^{i-1}$ is added as a correction to the specified increment in external loads so that the load increment given in the program is $R^i - R_{eq}^{i-1}$.

It is easy to implement the above modification for equilibrium correction in USFOS since R_{eq} is available from the stress state. The extra computer time at each load level is moderate.

5.2 Equilibrium Iteration

A further extension of the process of equilibrium correction is to introduce equilibrium iterations on the unbalanced load vector $R - R_{eq}$ at each level of specified external loads. For pure Newton-Raphson iteration the iteration cycle j at load level i is given by

$$K_I^{i,j-1} \Delta r^{i,j} = \Delta R^{i,j} \quad (5.6)$$

where $\Delta R^{i,j}$ is the unbalanced load vector

$$\Delta R^{i,j} = R^i - R_{eq}^{i,j-1} \quad (5.7)$$

The qualities of Newton-Raphson iteration as applied to highly sensitive structure problems are discussed in Ref. /17/.

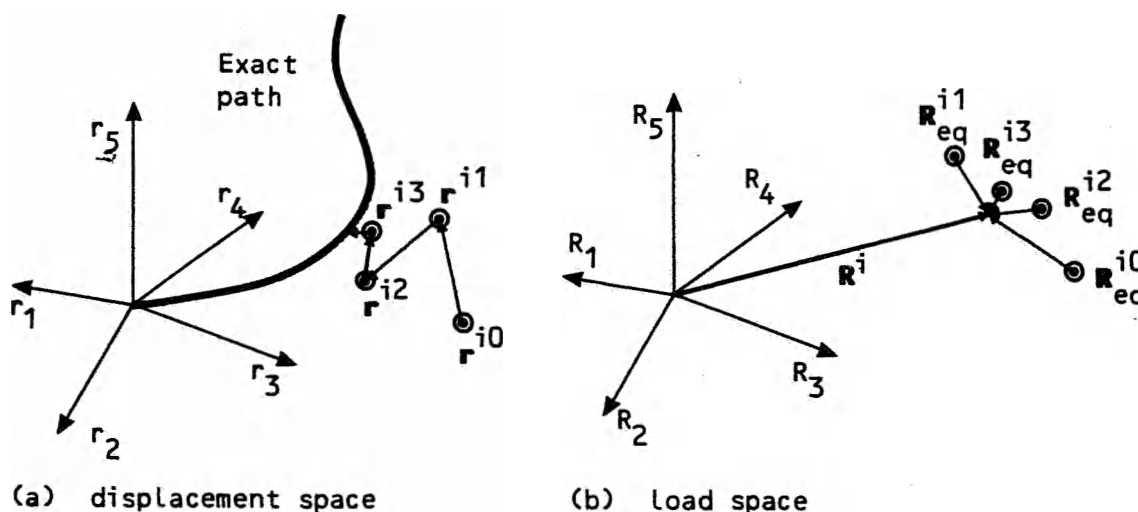


Figure 5.4 Newton-Raphson iteration in displacement and load space

Solution Algorithm

The process of equilibrium iteration is illustrated in Fig. 5.4 where it is indicated how the equilibrium configurations are updated through the process. As shown in Fig. 5.4.b the level of external specified load R^1 is kept constant during iteration. Again, the non-consequent direction of the corrective load vector $R^i - R_{eq}^{i,j}$ is indicated.

The pure Newton-Raphson iteration requires an updated tangent stiffness $K_I^{i,j}$ for each iteration cycle. For many problems computer costs are saved by a so-called modified Newton-Raphson procedure where the stiffness is kept constant over a number of cycles. The simplest version is for all iteration cycles within a load step to keep the stiffness from the first cycle where the specified load step is applied.

5.3 Arch length control

In the arch length method the increment size is calculated from a prescribed arc length in the load-displacement space defined as

$$\Delta l = \sqrt{(\Delta r^{i,0})^T \Delta r^{i,0} + (\Delta R^{i,0})^T \Delta R^{i,0}} \quad (5.8)$$

where $\Delta r^{i,0}$ is the displacement increment corresponding to the initial increment of the external load $\Delta R^{i,0}$.

In the iterative phase the solution is forced to travel in a plane normal to the increment vector as illustrated in Fig 5.5.

5

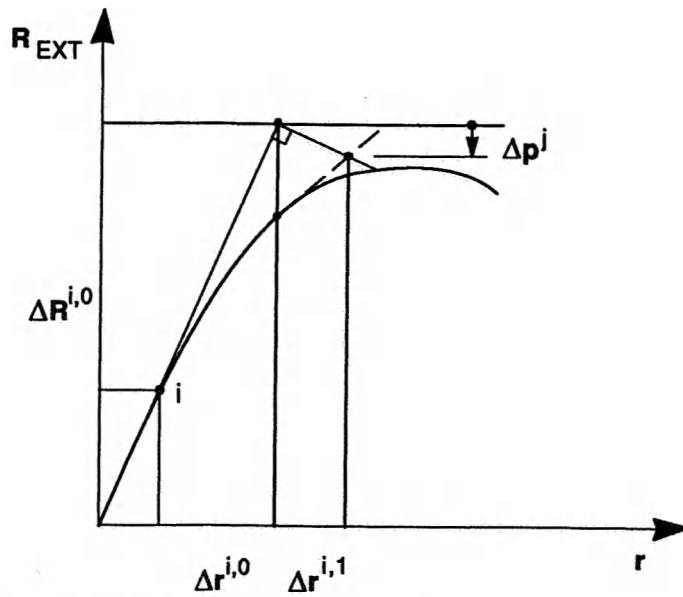


Figure 5.5: Iteration on a normal plate.

This is facilitated by imposing the condition

$$(\Delta \mathbf{r}^{i,0})^T \Delta \mathbf{r}^{i,j} + (\Delta \mathbf{R}^{i,0})^T \Delta \mathbf{R}^{i,j} = 0 \quad (5.9)$$

where $\Delta \mathbf{R}^{i,j}$ and $\Delta \mathbf{r}^{i,j}$ are the change in the external load and displacements during iteration step j , respectively.

The iterative change in displacements consists of two contributions, one due to unbalanced forces \mathbf{R}_{unbal} and one due to a change in the increment of the external load during iteration number j ;

$$\Delta \mathbf{r}^{i,j} = \Delta p \Delta \mathbf{r}^{i,0} \quad (5.10)$$

Thus the resulting iterative change of displacements becomes

$$\Delta \mathbf{r}^{i,j} = \Delta \mathbf{r}_{unbal}^{i,j} + \Delta p^j \Delta \mathbf{r}_{ext}^{i,j} \quad (5.11)$$

where

$$\Delta \mathbf{r}_{ext}^{i,j} = (\mathbf{K}_I^{i,j})^{-1} \Delta \mathbf{R}^{i,0} \quad (5.12)$$

$$\Delta \mathbf{r}_{unbal}^{i,j} = (\mathbf{K}_I^{i,j})^{-1} \Delta \mathbf{R}_{unbal}^{i,j} \quad (5.13)$$

Combining equations (5.9) and (5.11) there is obtained

$$\Delta p^j = - \frac{(\Delta \mathbf{r}^{i,j})^T \Delta \mathbf{r}_{\text{unbal}}^{i,j}}{(\Delta \mathbf{r}^{i,0})^T \Delta \mathbf{r}^{i,0} + (\Delta \mathbf{R}^{i,0})^T \Delta \mathbf{R}^{i,0}} \quad (5.14)$$

Because the displacements and loads are given in different scales, the terms in Eq (5.14) are scaled against the increments in displacements and load in the first load step, i.e.

$$\Delta p^j = - \frac{\frac{(\Delta \mathbf{r}^{i,j})^T \Delta \mathbf{r}_{\text{unbal}}^{i,j}}{(\Delta \mathbf{r}^{1,0})^T \Delta \mathbf{r}^{1,0}}}{\frac{(\Delta \mathbf{r}^{i,0})^T \Delta \mathbf{r}^{i,0}}{(\Delta \mathbf{r}^{1,0})^T \Delta \mathbf{r}^{1,0}} + \frac{(\Delta \mathbf{R}^{i,0})^T \Delta \mathbf{R}^{i,0}}{(\Delta \mathbf{r}^{1,0})^T \Delta \mathbf{R}^{1,0}}} \quad (5.15)$$

It is seen that the procedure implies that each iteration is solved in two steps. The first step is as before the contribution from the unbalanced forces, given by Eq (5.13) and the second step is the contribution from a change in the external load vector given by Eqs (5.9), (5.12) and (5.15). Thus, the difference from the conventional iterative procedure describes in Section 5.2 is that the external forces no longer remains fixed during iteration.

Under certain circumstances the iteration process may fail to converge when passing limit - or bifurcation points. This is illustrated in Fig 5.6.

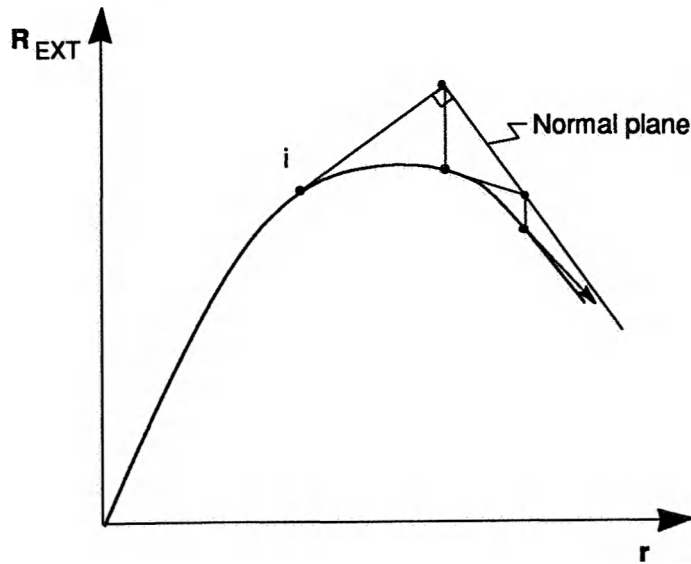


Figure 5.6 Iteration failure.

In such situations the following procedure is adopted:

The current stiffness parameter (with reference to the reference load pattern) and the determinant of the stiffness matrix are calculated at each iteration step. If either of them becomes singular or change sign the iterations are terminated. The sign of the iterative change in external load and associated displacements (second term in Eq (5.11) are reversed. In the next step the iterations are resumed as usual. This is illustrated in Fig 5.7. For further details, see USFOS Users Manual section 4.2.3.

→

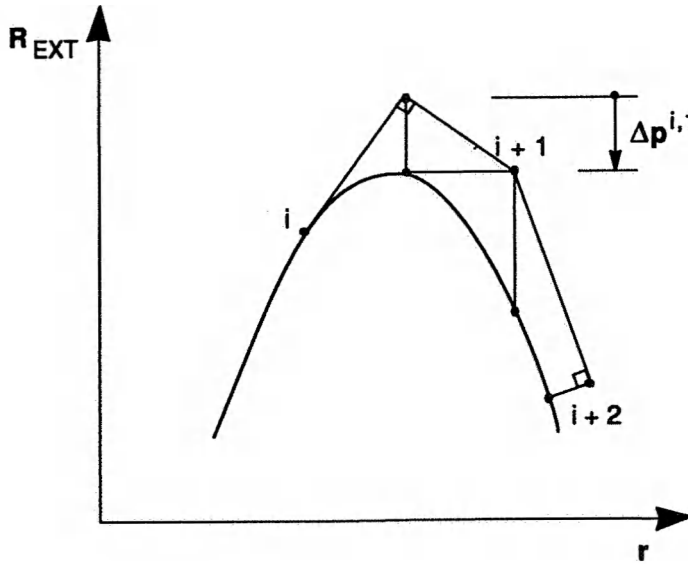


Figure 5.7 Iterations beyond critical points.

5.4 Convergence Criterion

In order to adequately terminate the equilibrium iterations some convergence criterium must be incorporated. Principally, two groups are available, namely displacement criteria and force criteria. These are based on rate of displacement and equilibrium force change respectively. Due to the arbitrary variation of the equilibrium force vector some type of displacement norm is usually recommended.

The two alternative criteria may be written as:

$$\left[\frac{\Delta \mathbf{r}^{i,j}}{\Delta \mathbf{r}^{i,0}} \right] = \left[\frac{\Delta \mathbf{R}^{i,j}}{\Delta \mathbf{R}^{i,0}} \right] \quad (5.16)$$

where $\Delta \mathbf{R}^{i,j}$ and $\Delta \mathbf{r}^{i,j}$ are the load and displacement vectors of iteration j of step i and $\Delta \mathbf{R}^{i,0}$ and $\Delta \mathbf{r}^{i,0}$ are the load and displacement increments for step number i .

For the program USFOS, the displacement norm is preferred and the convergence criterion for terminating the iteration process is written as:

$$\delta r_{it} = \varepsilon_{it} \quad (5.17)$$

where ε_{it} is a presented limit, normally in the range $1.0 \cdot 10^{-4}$ to $1.0 \cdot 10^{-3}$.

In order to terminate the iteration for non-converging or slowly-converging systems a maximum number of iteration cycles per load step is imposed.

5.5 Increment Scaling

It is indicated by the above description of numerical procedure that the truncation error may bring the solution far from the true path. Special care must be taken when abrupt changes occur in the structure system, e.g. by the creation of plastic hinges. It may be difficult to reach the true solution by equilibrium iterations for cases where the specified load increments are too large. In order to guarantee for this problem a procedure for increment scaling is implemented. This is organized in the way that when plastification is detected during an increment, the size of the increment is scaled down so as to just reach the failure surface at the point of plastification.

By this technique a safer process of load incrementation is obtained since abrupt changes in structure stiffness are taken into the step-by-step scheme as early as possible.

→

5.6 Bifurcation Analysis

When the condition in Eq (5.2) is fulfilled, i.e. the incremental matrix becomes singular while the current stiffness parameter is nonvanishing, bifurcation is taking place. To enhance the numerical stability of the solution, a perturbation in the form of the assumed correct buckling mode is injected.

In practice it is difficult and timeconsuming to find the exact point of singu-

larity. Hence, the bifurcation analysis is carried out once the determinant changes sign while the change in current stiffness parameter may be larger than a prescribed level.

The eigenvalues and eigenvectors of the tangent stiffness matrix are defined by

$$\mathbf{K}_I \Phi_j = \omega_j \Phi_j \quad (5.18)$$

in which ω_j is the eigenvalue and Φ_j is the eigenvector.

The eigenvalue calculation is carried out by means of a standard routine for subspace iteration.

An eigenvector corresponding to a negative eigenvalue represents a possible bifurcation branch.

Two alternatives exist for buckling mode injection. The eigenvector may be added to the total displacement vector or it may be handled as an additional external load. The latter approach is chosen in the present formulation and for an intermediate load step the incremental equations read:

$$\mathbf{K}_I \Delta \mathbf{r}^{i,0} = c \Phi_j \quad (5.19)$$

where c is a scaling factor.

Unfortunately, the eigenvectors carry no information about the sign. It is also noted that the eigenvector is orthogonal with respect to the load vector for proportional loading so that the incremental work of the external load vanishes. In general this is not the case for nonproportional loading.

A possible way of calculating the signs is to impose the condition that the angle between the eigenvector and the total displacements should be minimum or

$$\mathbf{r}^T \Phi_j > 0 \quad (5.20)$$

A possible approach is to consider the bifurcation load as a new load case and perform the bifurcation separately (analogous to simulation of fracture). In the present formulation the bifurcation load is considered as a separate load case which the user has to include manually during a restart analysis. The procedure for generating bifurcation load data as well as control of the subsequent restart analysis, is described in Section 4.7 of the USFOS Users Manual.

6. MODELLING OF DENTED TUBULAR MEMBERS

6.1 Introduction

This section deals with modelling the structural properties of dented and distorted tubular members. Such damages are typically due to impacts from supply vessels and dropped objects.

For an accurate simulation of the behaviour of the damaged element a nonlinear, shell element modelling of the dented section would be required. However, it is very difficult to perform such analyses properly and they are often time-consuming and costly. For this reason various simplified techniques have been developed. Some methods are based upon the conventional finite element technique where the dent is accounted for by using empirical reduction factors for yield strength and material stiffness /23/. Other methods use the stress resultants directly. By idealizing the dent geometry and stress distribution, analytical integration over the dented cross-section is made feasible /24/.

The work described in Ref. /24/ has resulted in a computer program DENTA for residual strength assessment of damaged tubular members. It combines numerical/analytical techniques with empirical relationships. It has been verified by comparisons to a large number of experiments (108) with scale models of damaged tubulars. On the whole, the same technique is also used in USFOS although some of the details have been omitted.

→

6.2 Idealization of Dented Tube

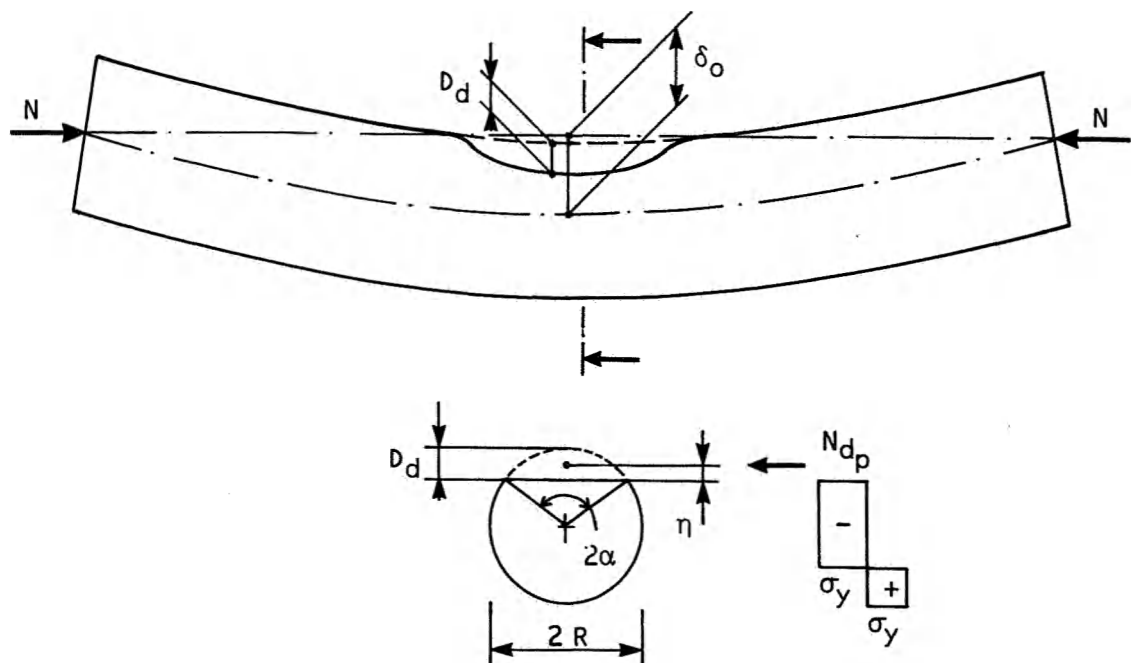
Two damage modes are considered, namely

- lateral distortion of tube axis; the cross-section remains intact
- local denting/ovalization of the cross-section

Lateral distortion of the cross-section can be considered as an initial imperfection. This has been considered in Section 2.4 and is not described further in the present section. It should be observed, however, that the procedure in

Section 2.4 is based upon an initial stress free deflection. If residual stresses are to be included, the damage process itself must be simulated.

As shown in Figure 6.1 the dent is assumed to extend over a finite length of the beam with two adjacent undamaged sections. Further, the dented section is idealized so as to consist of two parts; the dented part of the cross-section and the undamaged part.



Figur 6.1 Idealized model of dented element

The derivations are based upon the following assumptions

- i) The length of the dented section is small compared to member length. Hence, the effect of the dent on the elastic element stiffness is neglected, both with respect to reduced flexural rigidity and eccentricity in the dented region. These effects are considered to be of minor importance compared to the reduction in plastic capacity and possible lateral distortion of member axis.

- ii) The dent influences the plastic cross-sectional capacities of the cross-section. The eccentricity of the neutral axis caused by the dent is accounted for.
- iii) The dent may occur either at midspan or at beam ends.

These assumptions are very convenient with respect to implementation of the dented element model. Most of the revisions can be isolated in a separate module related to determination of plastic cross-sectional capacities. The location of the dent at midspan or at beam ends is somewhat restrictive. On the other hand, calculations show that the results are rather insensitive to moderate changes in dent location relative to beam midspan.

6.3 Plastic Potential for Dented Section

The fully plastic stress distribution for the damaged section is shown in Figure 6.1, assuming the dent in compression. By integration the following axial force-bending moment interaction emerges

$$F = \frac{M}{M_0} - \cos\left\{\frac{\pi}{2} \frac{N-N_{dp}}{N_0} + \frac{\alpha}{2}\right\} + \frac{1}{2} \sin\alpha - \frac{\pi}{2} \frac{N-N_{dp}}{N_0} \sin\alpha = 0 \quad (6.1)$$

where

N_0, M_0 = plastic capacities in pure compression and bending, respectively

$$\eta = R\{\sin\alpha/\alpha - \cos\alpha\}$$

$$\alpha = \arccos\left(1 - \frac{D_d}{R}\right)$$

$$N_{dp} = C_{dp} \sigma_y D \alpha \left\{ (4\eta^2 + t^2)^{\frac{1}{2}} - 2\eta \right\}$$

$$C_{dp} = 80 \cdot t/D$$

N_{dp} signifies the plastic capacity of the dented, flat section. It is assumed to remain constant in the post-collapse region. It is derived from single flat, bent plate analogy. C_{dp} is an empirical correction factor. It accounts for restraining effect from the undamaged part of the shell for D/t ratios less than 80. For $D/t > 80$ it reduces the strength, in order to account for second order bending effects for very high wall slenderness.

By setting the dent depth $D_d = 0$ it is seen that equation 6.1 condenses to the ordinary plastic interaction relation for undamaged tube.

In the post-collapse range the dent starts to grow. On the basis of significant experimental evidence it is found that the current dent depth, D_{dg} can be considered to be a function of the nominal geometry and the axial force level relative to the ultimate axial force. By regression analysis the following expression is obtained

$$D_{dg} = D_d + G_1 f_{g_1}(N, N_u, N_0) + G_2 f_{g_2}(N, N_u, N_0) \quad (6.2)$$

where

D_d = dent depth at the onset of plasticity

$$G_1 = 2.54 \cdot 10^{-3} D/t + 5.093 \cdot 10^{-5} (D/t)^2 - 3.465 \cdot 10^{-7} (D/t)^3 \geq 0$$

$$G_2 = 3.056(\sigma_y/E)(D/t) + 8.024G_1 - 29.24G_1^2 + 34.12G_1^3 - 0.8525 \geq 0$$

$$f_{g_1} = D \left[(1 - N/N_0)^{2.8} - (1 - N_u/N_0) \left(1 - \frac{N}{N_0}\right)^{1.8} \right]$$

$$f_{g_2} = 0.25D \left(1 - \frac{N}{N_u}\right) \sin\left(\frac{\pi}{2} \frac{N_u - N}{N_u}\right)$$

where

N_u = ultimate axial force in the member; it remains constant in the post-collapse region

In calculation of the gradient to the yield surface the partial derivative of dent depth with respect to axial force is required. It is found practical to perform this numerically due to the complexity of equation 6.2.

6.4 Extension to 3 dimensions

The fully plastic interaction relationships become significantly more complex under general 3-dimensional loading. As indicated in Figure 6.3 the plastic neutral axis is generally not parallel to the resulting bending moment due to the cross-sectional unsymmetry caused by the damage. A major task in the subsequent derivations is to determine the inclination of the neutral axis with respect to the y-axis for a specified direction of the resulting bending moment

(specified by the inclination θ). Depending on the stress distribution, 12 different cases need to be considered, in order to establish the complete interaction relationship, which generally takes the form /25/

$$\Gamma = \left(\left(\frac{M_Y}{M_{Y_0}} \right)^2 + \left(\frac{M_Z}{M_{Z_0}} \right)^2 \right)^{\frac{1}{2}} - (A^2 + B^2)^{\frac{1}{2}} = 0 \quad (6.3)$$

The following quantities are defined

$$\theta = \arctan \frac{M_Z}{M_Y}, \quad 0 \leq \theta \leq \pi \quad (6.4)$$

$$\tau = \arctan \frac{B}{A}, \quad -\frac{\pi}{2} \leq \tau \leq \frac{\pi}{2} \quad (6.5)$$

$$\varphi = \theta - \tau$$

A and B are calculated as follows

$$\text{Case I: } 0 \leq \varphi \leq \alpha \quad \pi - \alpha \leq \varphi \leq \pi$$

$$\text{a) } 0 \leq \gamma \leq \pi - (\alpha + \varphi), \quad M_Y \geq 0$$

$$\gamma = \frac{1}{2} \left(\pi - \left(1 - \frac{\sigma_{dp}}{\sigma_Y} \right) \alpha - \pi \frac{N}{N_0} \right)$$

$$A = \sin \gamma - \frac{1}{2} \left(1 - \frac{\sigma_{dp}}{\sigma_Y} \right) \sin \alpha \cos \varphi$$

$$B = \frac{1}{2} \left(1 - \frac{\sigma_{dp}}{\sigma_Y} \right) \sin \alpha \sin \varphi$$

$$\text{b) } \pi - (\alpha + \varphi) \leq \gamma \leq \pi - (\alpha - \varphi), \quad M_Y \geq 0$$

$$\gamma = \frac{\pi \left(1 + \frac{\sigma_{dp}}{\sigma_Y} \right) + (\varphi - \alpha) \left(1 - \frac{\sigma_{dp}}{\sigma_Y} \right) - 2\pi \frac{N}{N_0}}{3 + \frac{\sigma_{dp}}{\sigma_Y}}$$

$$A = \frac{1}{4} \left[\left(3 + \frac{\sigma_{dp}}{\sigma_y} \right) \sin \gamma - \left(1 - \frac{\sigma_{dp}}{\sigma_y} \right) \sin(\alpha - \varphi) \right]$$

$$B = \frac{1}{4} \left(1 - \frac{\sigma_{dp}}{\sigma_y} \right) (\cos(\alpha - \varphi) + \cos \gamma)$$

c) $\pi - (\alpha - \varphi) \leq \gamma \leq \pi, \quad M_y > 0$

$$\gamma = -\pi \frac{\left(\frac{N}{N_0} - \frac{\sigma_{dp}}{\sigma_y} \right)}{1 + \frac{\sigma_{dp}}{\sigma_y}}$$

$$A = \frac{1}{2} \left(1 + \frac{\sigma_{dp}}{\sigma_y} \right) \sin \gamma$$

$$B = 0$$

d) $0 \leq \gamma \leq \pi - (\alpha + \varphi) \quad M_y \leq 0$

$$\gamma = \frac{\pi}{2} \left(1 + \frac{N}{N_0} \right)$$

$$A = -\sin \gamma$$

$$B = 0$$

e) $\pi - (\alpha - \varphi) \leq \pi - (\alpha - \varphi) \quad M_y \leq 0$

$$\gamma = \frac{\pi \left(1 + \frac{\sigma_{dp}}{\sigma_y} \right) + (\alpha - \varphi) \left(1 - \frac{\sigma_{dp}}{\sigma_y} \right) + 2\pi \frac{N}{N_0}}{3 + \frac{\sigma_{dp}}{\sigma_y}}$$

$$A = -\frac{1}{4} \left[\left(3 + \frac{\sigma_{dp}}{\sigma_y} \right) \sin \gamma + \left(1 - \frac{\sigma_{dp}}{\sigma_y} \right) \sin(\alpha + \varphi) \right]$$

$$B = -\frac{1}{4} \left(1 - \frac{\sigma_{dp}}{\sigma_y} \right) (\cos(\alpha + \varphi) + \cos \gamma)$$

$$f) \quad \pi - (\alpha + \varphi) \leq \gamma \leq \pi, \quad M_y \leq 0$$

$$\gamma = \frac{\alpha \left(1 - \frac{\sigma_{dp}}{\sigma_y}\right) + \pi \left(\frac{\sigma_{dp}}{\sigma_y} + \frac{N}{N_0}\right)}{1 + \frac{\sigma_{dp}}{\sigma_y}}$$

$$A = -\frac{1}{2} \left[\left(1 - \frac{\sigma_{dp}}{\sigma_y}\right) \sin \alpha \cos \varphi - \left(1 + \frac{\sigma_{dp}}{\sigma_y}\right) \sin \gamma \right]$$

$$B = \frac{1}{2} \left(1 - \frac{\sigma_{dp}}{\sigma_y}\right) \sin \alpha \sin \gamma$$

Case II $\alpha \leq \varphi \leq \pi - \alpha$

$$a) \quad 0 \leq \gamma \leq \pi - (\alpha + \varphi), \quad M_z \geq 0$$

γ, A, B as case 1a.

$$b) \quad \pi - (\alpha + \beta) \leq \gamma \leq \pi - (\varphi - \alpha), \quad M_z \geq 0$$

γ, A, B as case 1b

$$c) \quad \pi - (\varphi - \alpha) \leq \gamma \leq \pi, \quad M_z \geq 0$$

$$\gamma = \frac{\pi}{2} \left(1 - \frac{N}{N_0}\right)$$

$$A = \sin \gamma$$

$$B = 0$$

$$d) \quad 0 \leq \gamma \leq \pi - (\alpha + \varphi), \quad M_z \leq 0$$

γ, B, A as case 1d

$$e) \quad \pi - (\alpha + \varphi) \leq \gamma \leq \pi - (\varphi - \alpha) \quad M_z \leq 0$$

γ, B, A as case 1e

$$f) \quad \pi - (\varphi - \alpha) \leq \gamma \leq \pi, \quad M_z \leq 0$$

$$\gamma = \frac{1}{2} \left[\pi \left(1 + \frac{N}{N_0} \right) + \left(1 - \frac{\sigma_{dp}}{\sigma_y} \right) \alpha \right]$$

$$A = -\sin \gamma + \frac{1}{2} \left(1 - \frac{\sigma_{dp}}{\sigma_y} \right) \sin \alpha \cos \varphi$$

$$B = \frac{1}{2} \left(1 - \frac{\sigma_{dp}}{\sigma_y} \right) \sin \alpha \sin \varphi$$

It is seen that τ depends on A and B , which themselves are functions of τ . This problem is solved by an iterative procedure where τ is updated once γ, A and B have been calculated. The process converges normally rapidly.

7. TEMPERATURE EFFECTS

7.1 Introduction

The structural resistance to thermal loading consists of two aspects

- heat transfer analysis
- structural response analysis

The first element concerns calculation of the unsteady conductive, convective and radiative heat transfer and is not dealt with in USFOS. Rather, it is considered to be known and given as input to USFOS.

The second element concerns assessment of the critical temperature with respect to progressive collapse and the time to reach this state for a given temperature field history. Only these aspects will be considered.

The structural response is mainly affected through the following thermal and mechanical properties

- thermal expansion
- the elastic modulus
- the yield strength
- creep

The effect of creep is not included in the present model.

7.2 Beam Element Formulation

7.2.1 Basic assumptions

The temperature distribution assumed is illustrated in Figure 7.1. The temperature is assumed constant in the axial direction but varies over element cross-section according to

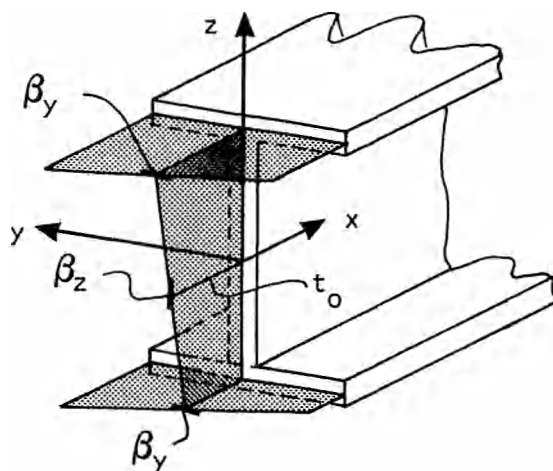


Figure 7.1 Temperature distribution.

$$t = t_0 + \beta_y y + \beta_z z \quad (7.1)$$

where t_0 is the temperature at some reference temperature axis. The temperature gradients in y - and z -direction are defined by

$$\beta_y = \frac{\partial t}{\partial y} = \frac{t_{yu} - t_{yl}}{h_y} \quad (7.2)$$

and

$$\beta_z = \frac{\partial t}{\partial z} = \frac{t_{zu} - t_{zl}}{h_z} \quad (7.3)$$

where

t_{yu}, t_{zu} = temperature at upper face of cross-section (positive y - and z -axis)

t_{yl}, t_{zl} = temperature at lower face of cross-section (negative y - and z -axis)

h_y, h_z = height of cross-section in y - and z -direction, respectively

The stress-strain relationship for a point with coordinates (y, z) relative to

the temperature reference axis is given by

$$\sigma_x = E_s(t_0, Y, z) \{ \epsilon_x - \alpha(t_0, Y, z) \cdot t(t_0, Y, z) \} \quad (7.4)$$

E_s = current (secant) elastic modulus
 α = coefficient of thermal expansion

In the following it is assumed that E_s and α is constant over the cross-section based upon an average temperature. The expansion coefficient is only moderately dependent on the temperature and is therefore also assumed constant.

7.2.2 Equilibrium equations

On the above assumptions it is convenient to let the temperature coordinate system coincide with the local element coordinate system. The potential energy for the heat affected element takes the form

$$\begin{aligned} U = & \frac{1}{2} \int_0^l E_s A (u_{,x} + \frac{1}{2} v_{,x}^2 + \frac{1}{2} w_{,x}^2 - \alpha t_0)^2 dx \\ & + \frac{1}{2} \int_0^l E_s I_z (v_{,xx} + \alpha \beta_y)^2 dx \\ & + \frac{1}{2} \int_0^l E_s I_z (w_{,xx} + \alpha \beta_z)^2 dx \end{aligned} \quad (7.5)$$

The first variation of strain energy comes out to be

$$\begin{aligned} \delta U = & \int_0^l EA u_{,x} \delta u_{,x} dx \\ & + \int_0^l E_s I_z (v_{,xx} \delta v_{,xx} - \frac{N}{E_s I_z} v_{,x} \delta v_{,x}) dx \\ & + \int_0^l E_s I_z (w_{,xx} \delta w_{,xx} - \frac{N}{E_s I_z} w_{,x} \delta w_{,x}) dx \end{aligned}$$

Temperature Effects

$$\begin{aligned}
& - \int_0^1 (N + E_s A u_{,x}) \delta u_{,x} dx \\
& + \int_0^1 E_s I_z \alpha \beta_z \delta v_{,xx} dx + \int_0^K E_s I_y \alpha \beta_y \delta w_{,xx} dx
\end{aligned} \tag{7.6}$$

where

$$N = -E_s A \left\{ u_{,x} + \frac{1}{2} v_{,x}^2 + \frac{1}{2} w_{,x}^2 - \alpha t_0 \right\} \tag{7.7}$$

The first terms in Eq. (7.4) are recognized as the conventional equilibrium condition (Eq. (2.17)) expressed in total displacements and current secant elastic modulus E_s .

The last two terms represents the forces corresponding to the increase of curvature due to the temperature gradient.

7.2.3 Incremental equations

The variation on incremental form is expressed by

$$\begin{aligned}
\delta(U + \Delta U) = & \int_0^1 (E_s + \Delta E_s) A \left\{ u_{,x} + \Delta u_{,x} + \frac{1}{2} (v_{,x} + \Delta v_{,x})^2 \right. \\
& \left. - \frac{1}{2} (w_{,x} + \Delta w_{,x})^2 - \alpha (t_0 + \Delta t_0) \right\} \{ \delta u_{,x} + (v_{,x} + \Delta v_{,x}) \delta v_{,x} \\
& - (w_{,x} + \Delta w_{,x}) \delta w_{,x} \} dx
\end{aligned} \tag{7.8}$$

$$\begin{aligned}
& \int_0^1 (E_s + \Delta E_s) I_z (v_{,xx} + \Delta v_{,xx} + \alpha \beta_y + \alpha \Delta \beta_y) \delta v_{,xx} dx \\
& \int_0^1 (E_s + \Delta E_s) I_y (w_{,xx} + \Delta w_{,xx} + \alpha \beta_z + \alpha \Delta \beta_z) \delta w_{,xx} dx
\end{aligned} \tag{7.8}$$

Incorporating δu from Eq. (7.6) gives

$$\begin{aligned}
 \delta \Delta U &= \delta(U + \Delta U) - \delta U \\
 &= \int_0^1 E_s A \Delta u_{,x} \delta u_{,x} dx \\
 &+ \int_0^1 E_s I_z (v_{,xx} \delta v_{,xx} - \frac{N}{E_s I_z} \Delta v_{,x} \delta v_{,x}) dx \\
 &+ \int_0^1 E_s I_y (w_{,xx} \delta w_{,xx} - \frac{N}{E_s I_z} \Delta w_{,x} \delta w_{,x}) dx \\
 &+ \text{remaining nonlinear terms in Eq. (2.21)} \\
 &+ \int_0^1 E_s I_z \alpha \Delta \beta_y \delta v_{,xx} dx + \int_0^1 E_s I_y \alpha \Delta \beta_z \delta w_{,xx} dx \\
 &- \int_0^1 E_s A \alpha \Delta t_0 (\delta u_{,x} + v_{,x} \sigma v_{,x} + w_{,x} \delta w_{,x}) \\
 &= \int_0^1 \Delta N \delta u_{,x} dx \\
 &+ \int_0^1 \Delta E_s I_z (v_{,xx} + \alpha \beta_y) \delta v_{,xx} - \frac{\Delta N}{\Delta E_s I_z} v_{,x} \delta v_{,x} dx \\
 &+ \int_0^1 \Delta E_s I_y (w_{,xx} + \alpha \beta_z) \delta w_{,xx} - \frac{\Delta N}{\Delta E_s I_y} w_{,x} \delta w_{,x} dx \\
 &+ \text{higher order terms.}
 \end{aligned} \tag{7.9}$$

where

$$\Delta N = \Delta E_s A \left(u_{,x} + \frac{1}{2} v_{,x}^2 + \frac{1}{2} w_{,x}^2 - \alpha t_0 \right) \tag{7.10}$$

The incremental equations consist of three contributions:

I : Incremental stiffness for isothermal deformation, identical to Eq. 2.21

II : Load increments in bending moments and axial force due to temperature increment. Nonlinear terms due to beam rotation contributes to the incremental axial temperature force.

III: Load increments due to change in elastic modulus.

By introducing the approximation

$$\frac{\Delta N}{\Delta E_s} \approx \frac{N}{E_s}$$

the modification in load is obtained by means of the secant stiffness matrix scaled by $\Delta E_s / E_s$ and multiplied by the total displacements.

7.2.4 Modification due to yield stress degradation

The reduction of yield stress at elevated temperatures causes a shrinkage of the yield surface. For members with plastic hinges this shrinkage will cause the stress resultants to depart from the yield surface. However, this effect can be accounted for, by including in the consistency criterion Eq. (4.111) an additional term, which represents the change of the yield surface due to the temperature increment:

$$\Delta F = \Delta F_{t=\text{constant}} + \Delta F_{\Delta t} = 0 \quad (7.11)$$

The second term takes the form

$$\Delta F_{\Delta t} = -\mathbf{g}^T \cdot \mathbf{S} \frac{\Delta \sigma_y}{\sigma_y} \quad (7.12)$$

\mathbf{g} is the vector of partial derivatives of the plastic potential with respect to each force component (Eq. (4.92)). \mathbf{S} is the vector of stress resultants as given by Eq. (4.89).

Comparing Eq. (7.12) to Eq. (4.103) it is seen that the change of yield stress can be considered to produce a contribution to the increment of the consistent nodal forces equal to

$$\Delta \bar{s} = -s \frac{\Delta \sigma}{\sigma_y} \quad (7.13)$$

6

7.3 Plate Element Formulation

Thermal Expansion

Thermal expansion effects are accounted for in a similar way as for the beam element by introducing equivalent incremental temperature forces.

A linear temperature distribution between the nodes are assumed as shown in Figure 7.2.

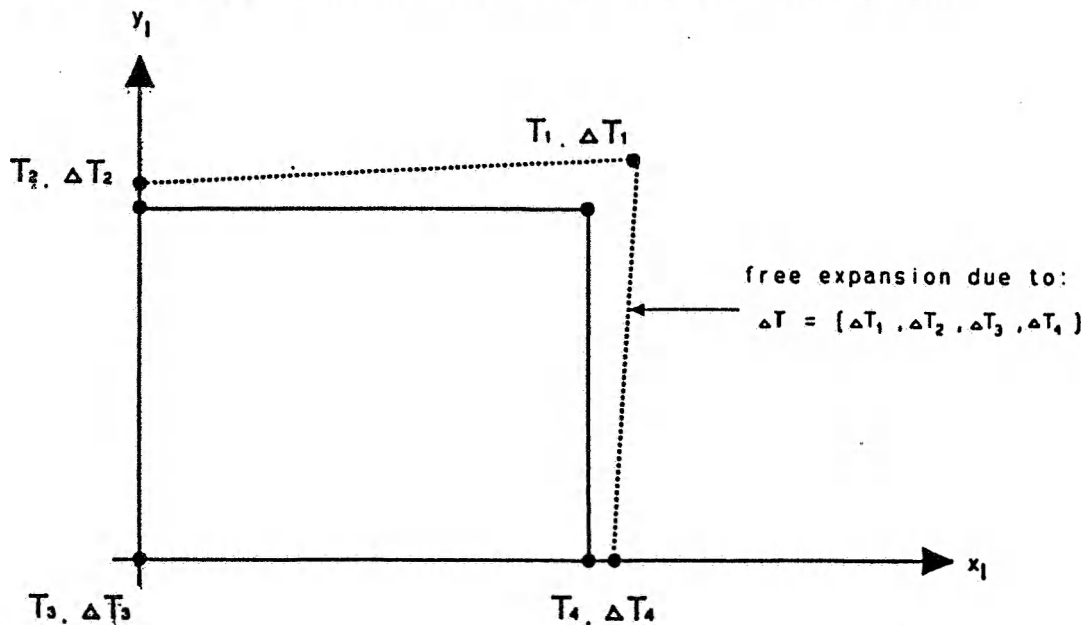


Figure 7.2

The objective is to develop the equivalent thermal nodal forces due to a temperature increment ΔT . First, the incremental initial strain matrix consistent with the temperature increase is written as:

$$\Delta \mathbf{e} = \begin{bmatrix} \Delta \epsilon_x \\ \Delta \epsilon_y \\ \Delta \gamma_{xy} \end{bmatrix} = c \begin{bmatrix} \Delta T_1 & \Delta T_2 & \Delta T_3 & \Delta T_4 \\ \Delta T_1 & \Delta T_2 & \Delta T_3 & \Delta T_4 \\ 0 & 0 & 0 & 0 \end{bmatrix} \quad 7.14$$

where the factor c is given by

- i) $c = \alpha$ for plane stress state
- ii) $c = (1 + \nu) \alpha$ for plane strain state

ν is the Poisson ratio and α the thermal expansion coefficient which here is assumed independent of the temperature.

Introducing the interpolation matrix of bilinear interpolation functions N , the incremental nodal initial strain vector is given by

$$\Delta e_o = \Delta e \cdot N \quad 7.15$$

The incremental equivalent nodal temperature force vector is then given by

$$\Delta S^T = \int_V P^T E \Delta e_o dV \quad 7.16$$

where the elasticity matrix for plane stress state is given by

$$E = \frac{E}{1 - \nu^2} \begin{bmatrix} 1 & \nu & 0 \\ \nu & 1 & 0 \\ 0 & 0 & \frac{1-\nu}{2} \end{bmatrix}$$

The elastic modulus should be calculated on basis of the average plate temperature when setting up the elasticity matrix E :

$$T = \frac{1}{4} \sum_{i=1}^4 T_i$$

$$P = T \begin{bmatrix} J^{-1} & 0 \\ 0 & J^{-1} \end{bmatrix} P_N \quad 7.17$$

where

$$T = \begin{bmatrix} 1 & 0 & 0 & 0 \\ 0 & 0 & 0 & 1 \\ 0 & 1 & 1 & 0 \end{bmatrix} \quad 7.18$$

and J^{-1} is the inverse of the Jacobian matrix and P_N contains the derivatives of the shape functions N_i with respect to the natural coordinates (x, y)

$$J = \begin{bmatrix} \frac{\partial x}{\partial \xi} & \frac{\partial y}{\partial \xi} \\ \frac{\partial x}{\partial \eta} & \frac{\partial y}{\partial \eta} \end{bmatrix} \quad 7.19$$

$$P_N = \begin{bmatrix} N_{1,\xi} & 0 & \dots & N_{6,\xi} & 0 \\ N_{1,\eta} & 0 & \dots & N_{6,\eta} & 0 \\ 0 & N_{1,\xi} & \dots & 0 & N_{6,\xi} \\ 0 & N_{1,\eta} & \dots & 0 & N_{6,\eta} \end{bmatrix}$$

Yield Stress Degradation

The yield stress temperature dependency is governed by the ECCS curve given in Figure 7.2.

Equivalent to the beam element formulation, the yield stress decrement caused by an temperature increment, is accounted for by introducing the load term ΔS^σ , see Figure 7.3.

$$\Delta S^\sigma = \frac{\Delta \sigma_y}{\sigma_y} S = \frac{\Delta \sigma_y}{\sigma_y} [S_i], \quad i = 1, 8 \tag{7.20}$$

where S is the plate element total internal restoring force vector, $\Delta \sigma_y$ is the yield stress decrement due to ΔT and σ_y is the yield stress at the current temperature which is taken as the element average temperature.

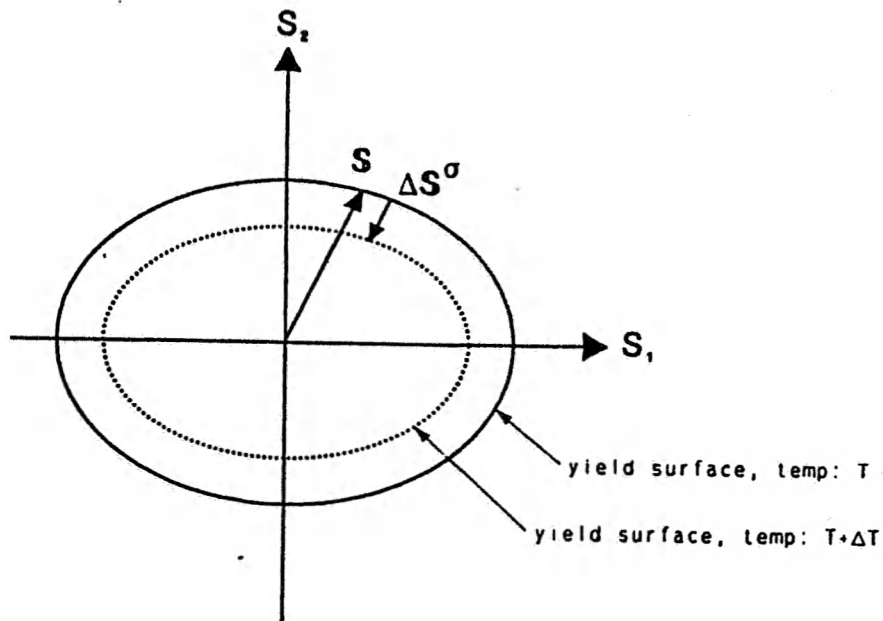


Figure 7.3

The equivalent load term given by (7.22) is only introduced when yielding has occurred.

Elastic Modulus Degradation

The elastic modulus temperature dependency is given by the ECCS curve shown in Figure 7.4.

The equivalent load term due to the change in the elastic modulus is, as for the beam element, approximated to:

$$\Delta S^E = \frac{\Delta E}{E} \cdot k^e (v - v^T)$$

where k^e is the elastic stiffness matrix, v the nodal total displacement vector and v^T the total nodal free temperature displacement vector.

7.4 Mechanical properties

7.4.1 Structural Steel

Experimental data of the degradation of elastic modulus and yield strength at elevated temperatures show a wide scatter.

The following approximate relationships, proposed by ECCS /26/, have been adopted

$$\frac{\sigma_y(t)}{\sigma_y(20)} = 1 + \frac{t}{767 \ln(t/1750)}, \quad 0 \leq t \leq 600^{\circ}\text{C} \quad (7.22)$$

$$\frac{E(t)}{E(20)} = 1 + 15.9 \cdot 10^{-5}t - 34.5 \cdot 10^{-7}t^2 + 11.8 \cdot 10^{-9}t^3 - 17.2 \cdot 10^{-12}t^4 \quad 0 \leq t \leq 600^{\circ}\text{C} \quad (7.23)$$

The relationships are also depicted in Figure 7.4.

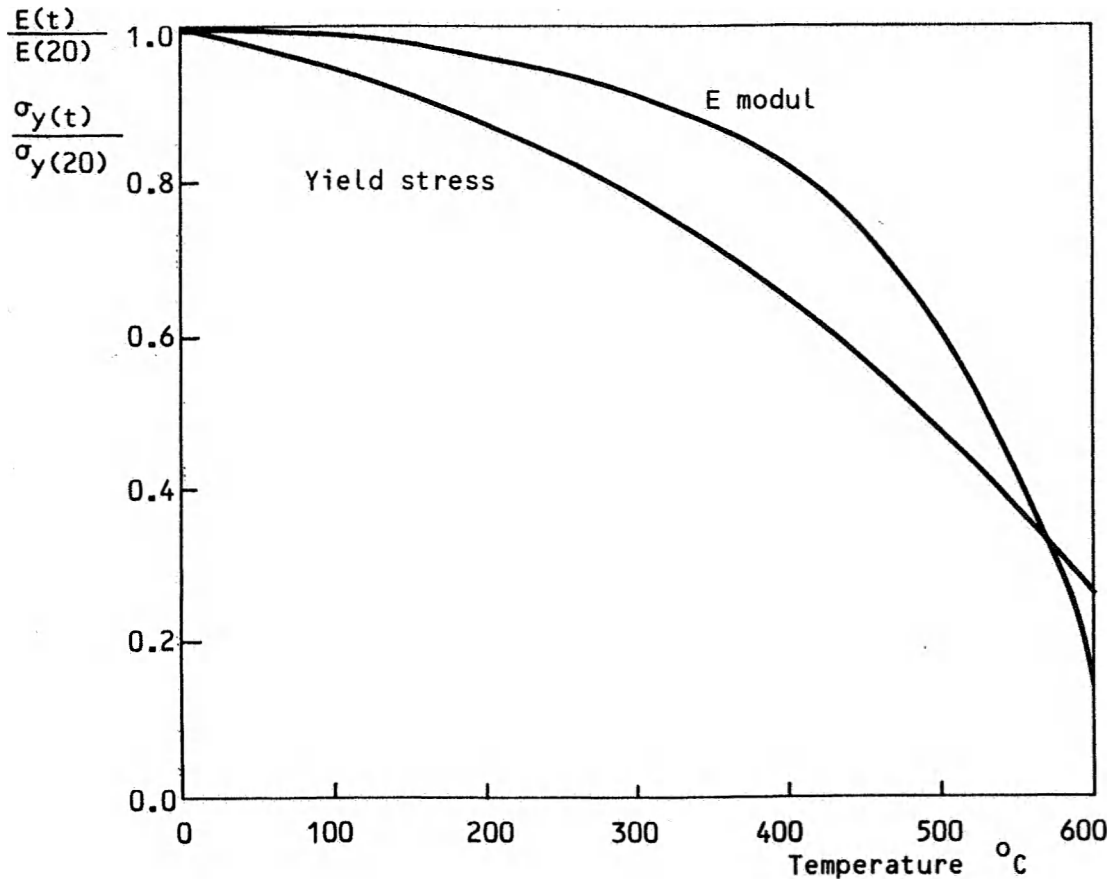


Figure 7.4 Temperature dependence of yield stress and elastic modulus according to ECCS.

The coefficient of linear expansion of steel shows a small variation with respect to temperature. However, in the present version of the program it is assumed constant.

8. LINEAR DEPENDENCY

8.1 INTRODUCTION

This section describes how linear dependent degrees of freedom (dofs) are implemented in USFOS. The method is useful in modelling structures where there, for some reason, are information available indicating that one dof can be expressed as a linear combination of other dofs. Such structures are for example jackets with internal piles in the legs. The pile is free to move axially within the leg, but constrained to follow its lateral displacements. Also, internal hinges can be modelled. It is a special case of the general, linear constraint equation defining a slave dof.

8.2 DERIVATION OF KINEMATIC CONSTRAINTS

Linear dependency is defined by one slave node and a master element. The user defines which degrees of freedom (dofs) to be subjected to kinematic constraints. The actual coupling coefficient is calculated by the program, based on the location of the slave node relative to the nodes of the master element. The coefficients are updated for each load increment.

Internal hinges are modelled by specifying two nodes at the hinge and then couple the degrees of freedom that are to be equal. In this case the slave dofs are only coupled to the master node located at the hinge.

Figure 8.1 shows the coordinate systems used to establish linear dependencies. The slave node is denoted by s and the "master" element length is l_m . The local coordinate system (x_m, y_m, z_m) of an element connected to nodes m_i, m_j constitutes the set of three orthogonal vectors.

Let \mathbf{x}_{m0}^s denote the position vector of s in the local coordinate system. The position vector in deformed configuration reads

$$\mathbf{x}_m^s = \mathbf{x}_{m0}^s + \mathbf{u}_m^s \quad (8.1)$$

Linear Dependency

where $\bar{\mathbf{u}}_m^s$ is the vector of pure translation displacements. The displacement vector in local coordinate system with all nodal parameters is defined by

$$\mathbf{u}_m^s = \{u_m^s, v_m^s, w_m^s, \phi_{xm}^s, \phi_{ym}^s, \phi_{zm}^s\}^T \quad (8.2)$$

A parameter β is defined such that

$$\beta = \frac{x_m^s}{K_m} \quad (8.3)$$

and is a measure of the relative position of the slave node in the local x-axis.

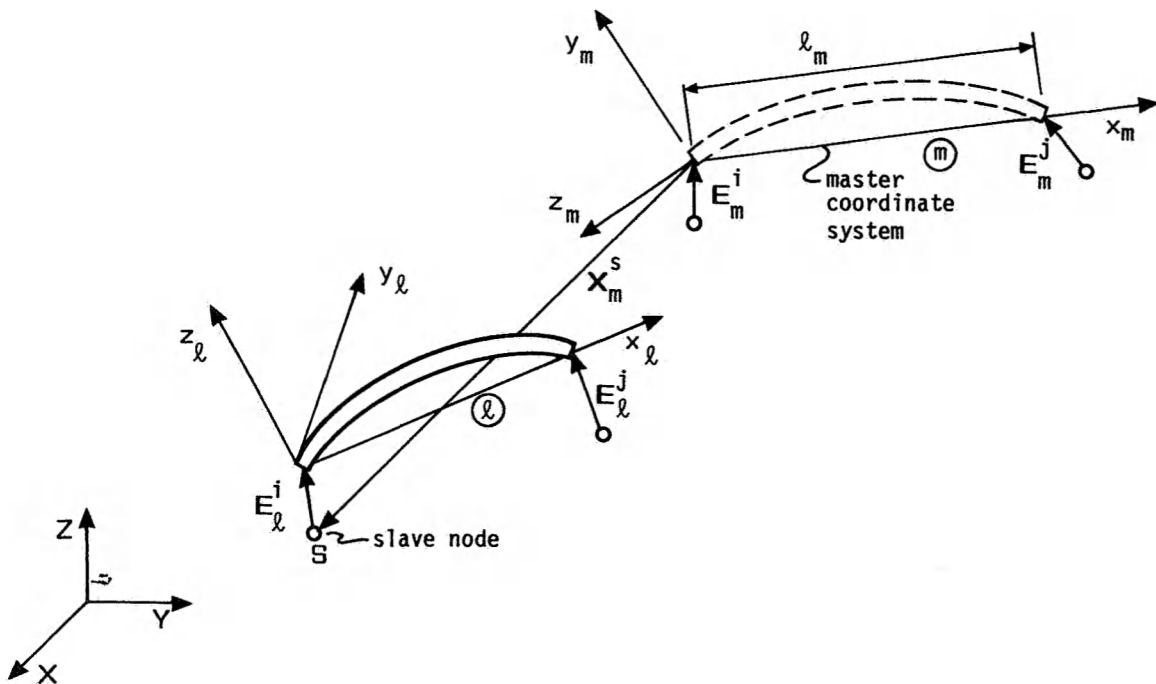


Figure 8.1. Coordinate systems for linear dependencies.

The following linear dependencies can be specified for the incremental displacements of the slave node.

Linear Dependency

$$\Delta u_m^s = [(1-\beta), \beta] \begin{bmatrix} \Delta u_m^i \\ \Delta u_m^j \end{bmatrix} \quad (8.4)$$

$$\Delta v_m^s = [(1-\beta), \beta] \begin{bmatrix} \Delta v_m^i \\ \Delta v_m^j \end{bmatrix} - [(1-\beta)z_m^s, \beta z_m^s] \begin{bmatrix} \Delta \varphi_{xm}^i \\ \Delta \varphi_{xm}^j \end{bmatrix} \quad (8.5)$$

$$\Delta w_m^s = [(1-\beta), \beta] \begin{bmatrix} \Delta w_m^i \\ \Delta w_m^j \end{bmatrix} + [(1-\beta)y_m^s, \beta y_m^s] \begin{bmatrix} \Delta \varphi_{xm}^i \\ \Delta \varphi_{xm}^j \end{bmatrix} \quad (8.6)$$

$$\Delta \varphi_{xm}^s = [(1-\beta), \beta] \begin{bmatrix} \Delta \varphi_{xm}^i \\ \Delta \varphi_{xm}^j \end{bmatrix} \quad (8.7)$$

$$\Delta \varphi_{ym}^s = [(1-\beta), \beta] \begin{bmatrix} \Delta \varphi_{ym}^i \\ \Delta \varphi_{ym}^j \end{bmatrix} \quad (8.8)$$

$$\Delta \varphi_{zm}^s = [(1-\beta), \beta] \begin{bmatrix} \Delta \varphi_{zm}^i \\ \Delta \varphi_{zm}^j \end{bmatrix} \quad (8.9)$$

It is emphasized that the slave node is forced to move relative to the planes of the local coordinate system of the master element. If the slave node is located significantly off the x-axis of the master element, torsion of the master element implies large lateral displacements of the slave node. For this reason, the coupling to torsion in eqs. (8.5) and (8.6) may be suppressed by the user.

Formally, let C represent the constraints imposed on the slave node such that

Linear Dependency

$$\Delta u_m^s = C \begin{bmatrix} \Delta u_m^i \\ \Delta u_m^j \end{bmatrix} \quad (8.10)$$

The corresponding relationship to the global degree of freedom is given by

$$\Delta u_m^g = C T_m L_m \begin{bmatrix} \Delta x_x^i \\ \Delta x_x^j \end{bmatrix} \quad (8.11)$$

where $T_m = [G_m \ G_m | G_m \ G_m]$ is the matrix of direction cosines between local and global systems for the "master" element and $L_m = [E_m^i, \ E_m^j]$ is the transformation matrix due to eccentricity.

For an element end connected to a slave node, the displacements in the local system must first be transformed to the special coordinate system, m. This is given by

$$\Delta u_m^s = \bar{T}_K \cdot \Delta u_K \quad \bar{T}_m^T \cdot \Delta u_m^s \quad (8.12)$$

where

$$\bar{T}_K = [G_K \ G_K] \quad \bar{T}_m = [G_m \ G_m]$$

The stiffness transformation for element K now reads

$$\bar{K}^K = T^{*T} K^K T^* \quad (8.13)$$

where

$$T^* = \begin{bmatrix} B, & \bar{T}_K E_K^j \end{bmatrix}$$

where

$$B = \bar{T}_K E_K^i \bar{T}_m^T C T_m L_m$$

Linear Dependency

The transformation is indeed only carried out for the degrees of freedom of the slave node which are actually subjected to constraints. The remaining degrees of freedom are treated as independent and are solved in the local coordinate system.

9 LOCAL FLEXIBILITY

9.1 Introduction

Most of the framed structures used in the offshore petroleum industry consist of tubular members.

It is common to idealize the structures to consist of beam elements only, and shell effects at the joints are neglected.

This "node flexibility" influences the behaviour of the structures, and the force patterns change.

Except simple analytical methods, superelement technique is the present tool to consider these effects. The tubular joints are then modelled using finite elements and each joint will represent one superelement.

At sections in sufficient distance from the joint, the tube properties are transferred to a beam by using a Navier transformation.

Beam elements are used between the tubular joints, and a realistic structural model is obtained.

However, this technique is time consuming and costly, both with respect to computer time and to the manhours to produce the required input for the finite element analysis program. The technique described has been used for monitoring a build structure.

In the following a technique for calculating a transition element between braces and chord is presented. The computer time consumption using this technique is less than 1/100 of what the superelement technique requires. In addition, no manual modelling is required. The transition element takes care of the shell properties of the joint, and makes an integrated shell/frame analysis possible. A complete shell analysis of each selected tubular joint is performed during the generating of the structure's system stiffness matrix. The shell analysis results in the stiffness properties of the actual tubular joint transition element.

9.2 BASIC

The technique is based on the solution of simply supported shells subjected to highly concentrated distributed loads. The loads are: Radial load, tangential load, moment about X- axis and moment about Y-axis.

Donnell simplifications of the differential equations for the circular cylindrical shell are made, and a Galerkin solution technique is used. Trigonometric series are suggested as displacement functions in the Y- and Z- directions. The displacement of the middle surface in the X-direction is put equal to zero all over, and will then exclude the global beam bending mode.

9.3 MODELLING OF A BRACE/CHORD CONNECTION

Before introducing any simplifications on a brace/chord modelling, it is necessary to look at the basic load-carrying behaviour of such a connection.

Fig. 1 defines a Y-joint, the angle of inclination, θ , and the global Z-axis.

The special case, $\theta = \pi/2$, defines the so called T-joint.

Fig. 2 shows a section through the T-joint and defines the circumferential angle, ϕ , in the leg.

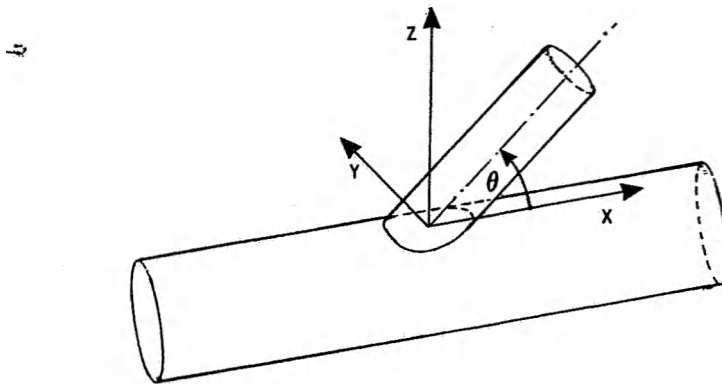


Figure 1 Y-joint

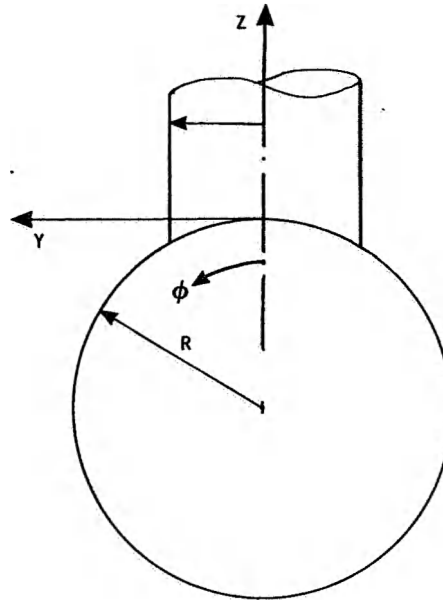


Figure 2 Section through T-joint

The loads have to be transferred from the braces, through the joint to the chord. The stiffness in the global Z-direction of the chord surface is a combination of radial and tangent stiffnesses.

At a point, $\phi=0$, only the radial stiffness contributes to the total stiffness in the global Z-direction. Moving along the arc perpendicular to the generatrix, contribution from tangent stiffness will increase. For $\phi = \pi/2$, only the tangent stiffness contributes to the total stiffness in the Z-direction. The tangent stiffness is assumed to be much larger than the radial stiffness.

The local stiffness against rotation about the intersection curve also contributes to the total stiffness. This rotation stiffness varies along the intersection curve. The resulting stiffness in global Z-direction will then vary along the intersection curve between brace and chord.

The following two assumptions are made:

- The stiffness of the brace wall in the global Z-direction is much larger than the stiffness of the chord surface in the same global direction. Thus, local deformations of the brace end in the Z-direction is disregarded.
- Stiffness properties of the brace ends are constant along the intersection curve.

As the brace diameter relative to the chord diameter, the so called β -ratio, increases towards 1.0 or alternatively, the angle θ reduces, these assumptions become less valid.

The two assumptions imply that the intersection curve between brace and chord does not change its shape. The intersection curve moves as a rigid body only. It is then possible to express the displacement in the global Z-direction along the intersection curve by the degrees of freedom in one reference point.

9.4 STIFFNESS MATRIX FOR DEGREES OF FREEDOM ON THE CHORD SHELL SURFACE

A more exact tubular frame modelling requires extra degrees of freedom on the chord shell surface.

A global chord surface node means a node that later will be used in the global frame modelling and defines a brace beam end.

The degrees of freedom in these global nodes, here called global degrees of freedom, will be included in the total system analysis.

Only three degrees of freedom per surface nodal point are expected to influence the behaviour of the frame.

These are:

- Translation in the direction of the Z-axis
- Rotation about the Y-axis
- Rotation about the X-axis

See fig. 1 for definition of the global coordinate system.

The three remaining degrees of freedom are assumed to be linearly dependent on the chord centre degrees of freedom.

Fig. 3 defines the global degrees of freedom on the chord shell surface. These are assumed to be independent of the chord center degrees of freedom.

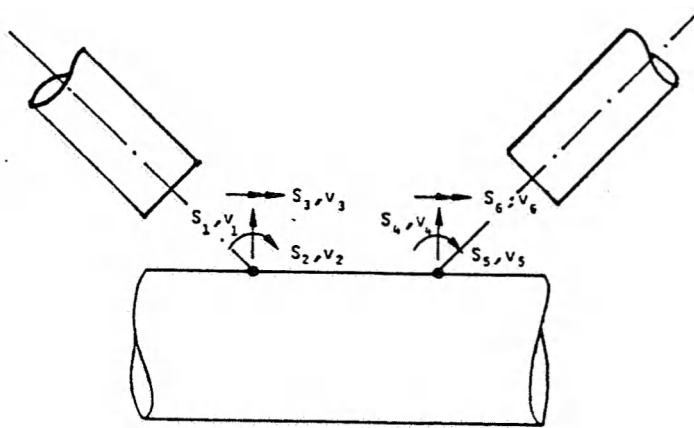


Figure 3 Independent chord surface degrees of freedom in a K-joint

Local degrees of freedom mean degrees of freedom on a brace/chord intersection curve that is used in the local shell analysis and will not be included in the total system analysis. The local degrees of freedom are eliminated, and the resultant properties of the brace/chord connection will be expressed by the global degrees of freedom.

Fig. 4 shows the global degrees of freedom on the chord shell surface and defines the local degrees of freedom along the intersection curve.

USFOS Theory Manual
Local Flexibility

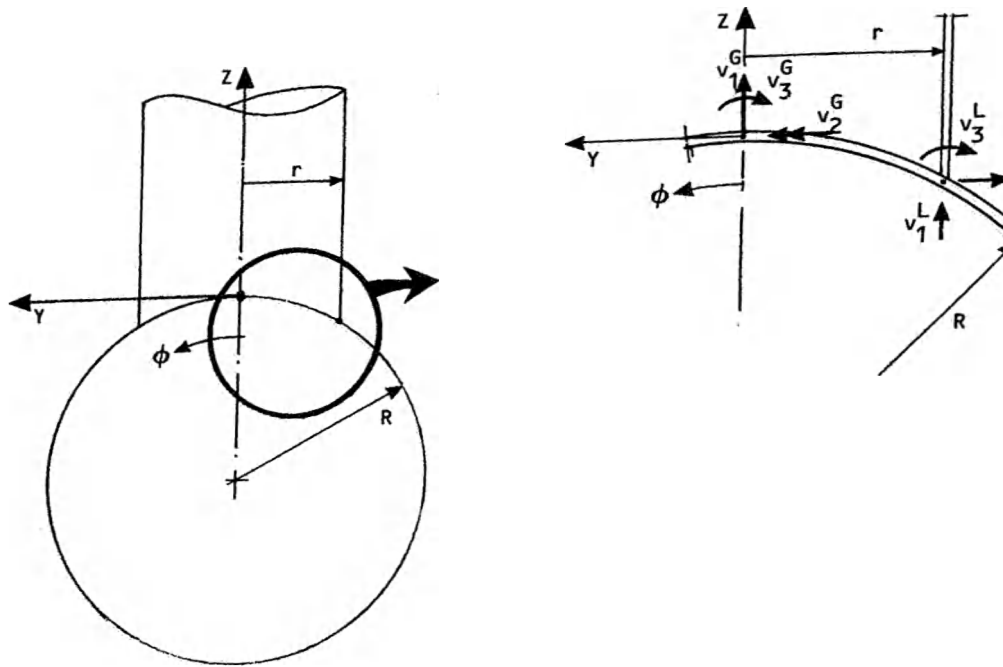


Figure 4 Local degrees of freedom along the brace/chord intersection curve and the global surface node degrees of freedom

The connection between the local and the global degrees of freedom will be expressed as follows:

The global chord surface node is assumed to be situated where the brace tube centre line meets the chord shell surface, see figs. 3 and 4.

Figures 5 - 7 describe the assumed rigid body displacement of the brace/chord intersection curve caused by axial load, in plane moment and out of plane moment in the free end of the brace.

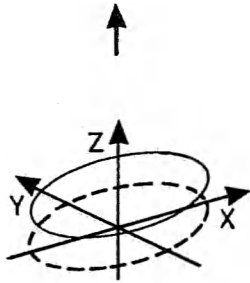


Figure 5 Translation
 of intersection curve
 compatible with a Z-
 translation of the global
 surface node

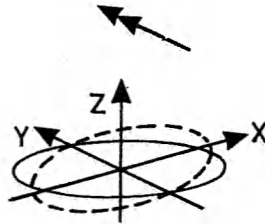


Figure 6 Rotation
 of intersection curve
 compatible with rotation
 of the global surface
 node about the Y-axis

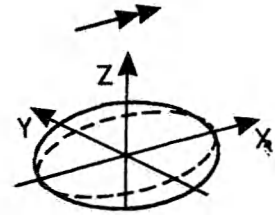


Figure 7 Rotation
 of intersection curve
 compatible with rotation
 of the global surface
 node about the Y-axis

The local Z-displacement is expressed by the global degrees of freedom by the following relation, see fig 4:

$$v_1^L = \begin{bmatrix} -X & R \sin \phi \end{bmatrix} \begin{bmatrix} v_1^G \\ v_2^G \\ v_3^G \end{bmatrix}$$

In practice, the compatibility conditions for the displacements in the Z-direction are satisfied at discrete points along the intersection curve only, see fig 8 The intersection curve may in general be of arbitrary shape.

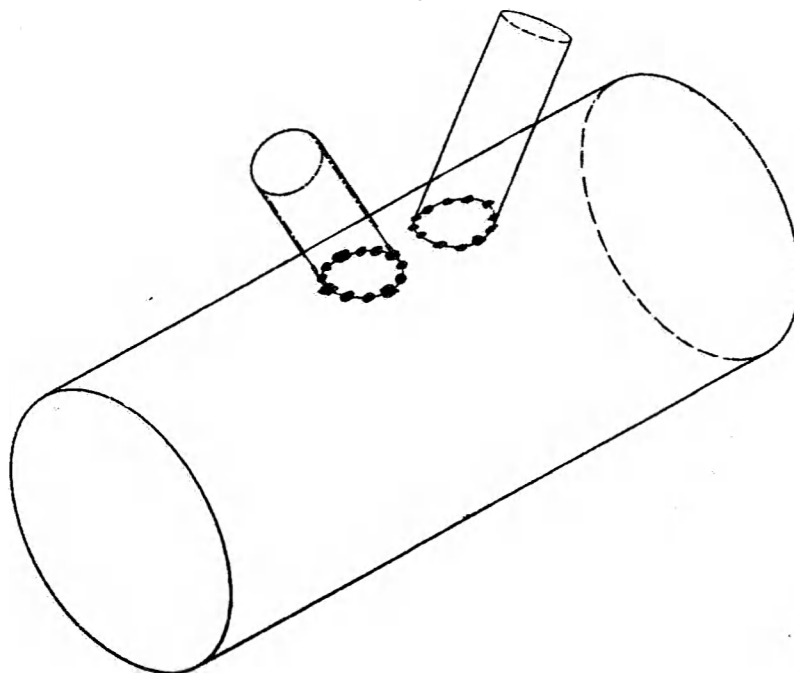


Figure 8 Simulation of a brace/chord connection

For a tubular joint, a varying number of internal shell surface nodes take care of the boundary conditions on the intersection curves.

The interaction between all internal degrees of freedom, expressed by a stiffness matrix, are established by inverting the corresponding flexibility matrix. The classical shell solutions described above are used for calculating the flexibility matrix.

The degrees of freedom at each internal surface node are:

- Radial displacement
- Tangent displacement
- Rotation about the tangent to the intersection curve

The linear dependencies between the degrees of freedom at the global surface nodes and the internal degrees of freedom at the intersection curves make it possible to eliminate the internal degrees of freedom. The properties of the intersection curves are then expressed by the degrees of freedom at the global

surface nodes only, resulting in the stiffness matrix for the so called "shell property element".

Figure 9 shows a K-joint and fig. 10 describes the suggested frame model that consider the shell effects at the joints.

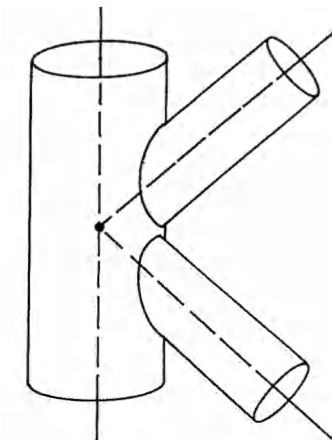


Figure 9 Real K-joint

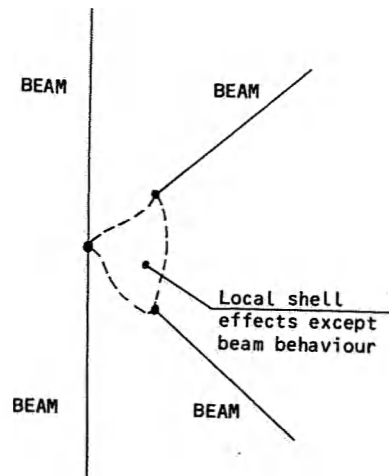


Figure 10 Suggested tubular frame model that consider the local shell behaviour.

The stresses in the chord caused by the four concentrated loads, radial load, tangential load, moment about the X-axis and moment about the Y-axis are calculated. The total stresses in the chord are obtained by superposition of contributions from the four load components at each internal node.

The intensity of the internal loads along the intersection curves are calculated by solving equations based on the above assumed rigid body behaviour of the intersection curves.

→

9.4 EXAMPLES

The behaviour of the method is illustrated by some numerical examples.

The above described boundary conditions between brace and chord curve are satisfied at discrete points at the intersection curve only. Figure 11 illustrates the effect on stiffness and stress when varying the number of internal nodes, NPOINT. In this example the d/D - ratio is 0.5.

Other d/D -ratios used in practical design give similar convergence.

The number of internal nodes is chosen equal to 24 in the following examples.

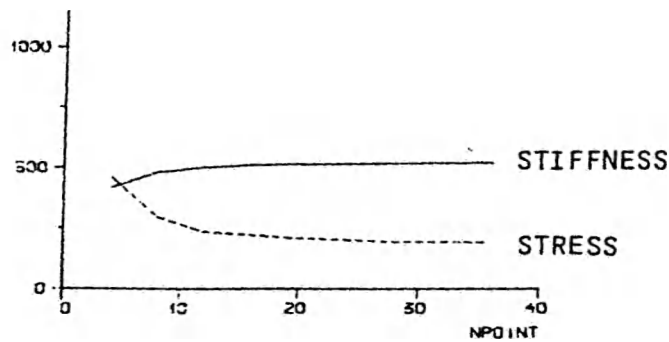


Figure 11 Stiffness and stress dependence on the number of internal nodes used to describe the brace/chord interaction

The resultant displacements in the chord at section $X = L/2$, due to loads in a simulated brace end are illustrated in the following. Figure 12 and 13 represent axial compressive force and out of plane moment, respectively.

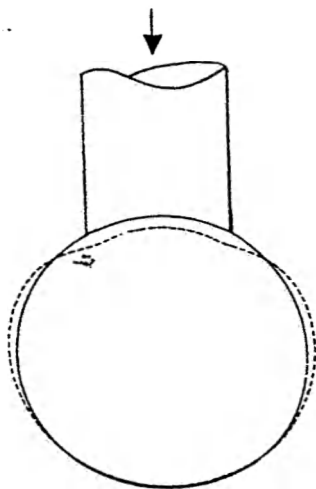


Figure 12 Displacement along the curve, $X = L/2$ due to axial compressive load in the simulated brace end
 $d/D = 0.5$

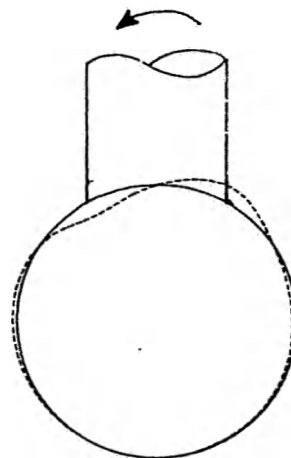


Figure 13 Displacement along the curve, $X = L/2$ due to out of plane moment in the simulated brace end
 $d/D = 0.5$

Local Flexibility

Figures 14 and 15 show the displacement field along the generatrix $\varphi = 0$ due to axial force and in-plane moment at the free end of the brace, respectively.

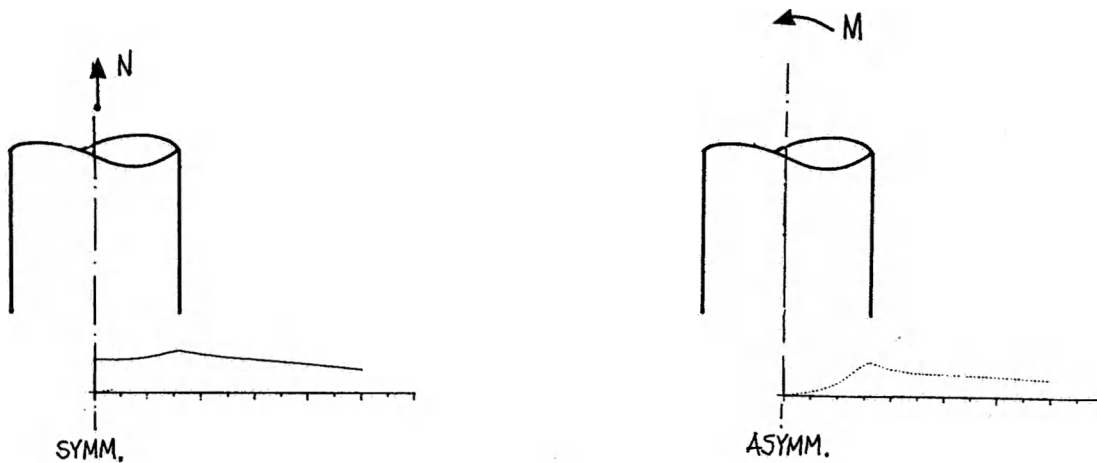


Figure 14 Displacement along the generatrix, $\varphi = 0$ due to axial force at the simulated brace end.
 $d/D = 0.5$

Figure 15 Displacement along the generatrix, $\varphi = 0$ due to in-plane moment at the simulated brace end.
 $d/D = 0.5$

The displacement fields have reasonable shapes.

Flexibility properties of 16 T-joints and 2 K-joints are compared with corresponding FEM-results obtained from the SESAM programme. The β -ratios are in the range 0.25 - 0.95, and there is good accordance between the results from the two techniques, (+/- 10-15%).

The resultant stresses in the chord due to loads at the free end of the brace are calculated for two T-joints with d/D -ratio = 0.25 and 0.65, respectively. The results from the above described technique and conventional FEM solutions are compared. Figure 16 gives the element mesh used.

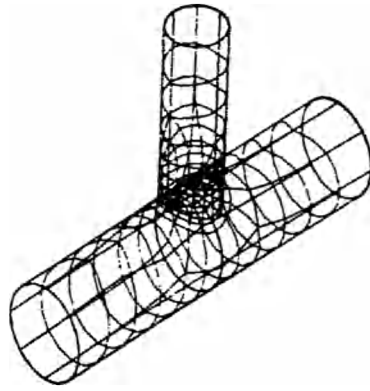


Figure 16 Element mesh used in the FEM analysis

The σ_{yy} -distributions along the intersection curve are shown in figs 17 and 18.

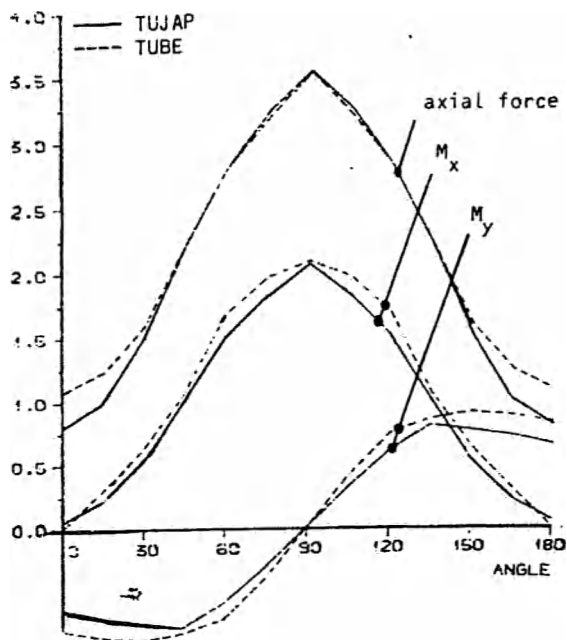


Figure 17 Stress distribution along intersection curve. $\beta = 0.25$

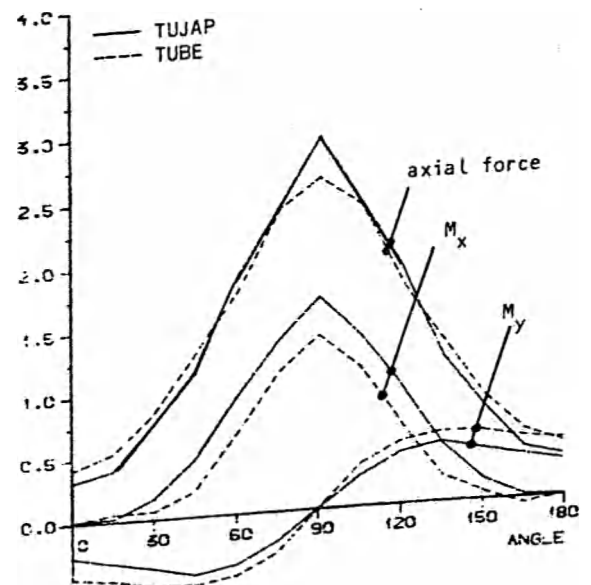


Figure 18 Stress distribution along intersection curve. $\beta = 0.65$

As indicated in the Figures 17 and 18, the stress distributions match very well.

Hot spot stresses calculated, using the above described technique, are compared with corresponding results from FEM - solutions for 16 different T-joints. The

results are in good agreement, within a range of +/- 10-15%.

Finally, an integrated shell/frame analysis of a deep water jacket is described, see Figure 19.

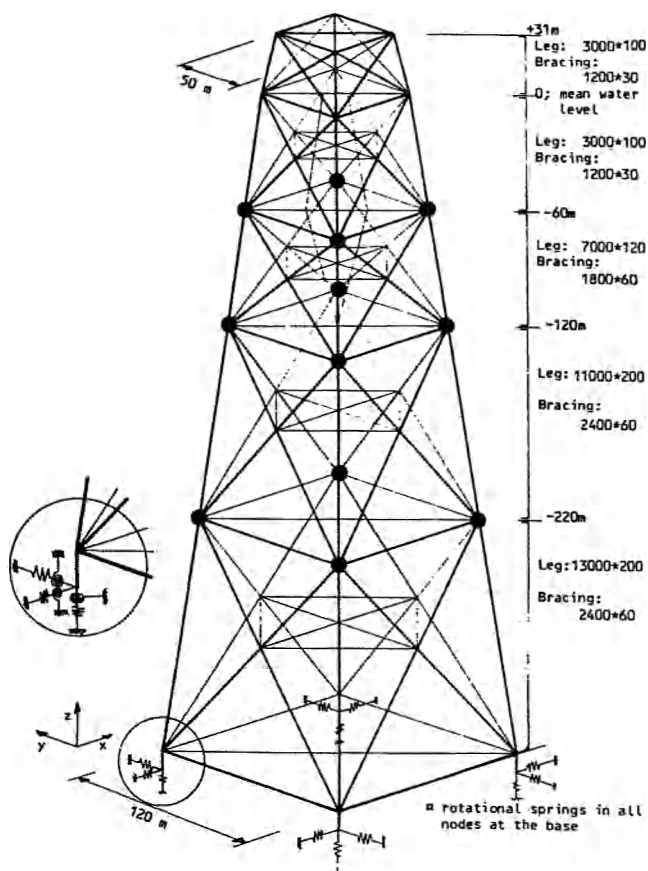


Figure 19 Element mesh of the jacket structure

The 12 marked joints in fig. 19 are modelled with, and for comparison, without use of the above described brace/chord transition element. In this special example 6 braces are connected to the joint, requiring 6 extra nodes per joint. The transition element consists of 7 nodes, one chord center node and 6 global surface nodes.

For the other joints, conventional rigid joint modelling is used.

Both quasistatic analyses and free vibration analyses are performed. The change in brace end forces due to the two different structural models are of interest in connection with the quasistatic analyses. Only the change in natural

frequencies are examined in connection with the free vibration analyses.

Wave data used in the quasistatic analyses are:

- Amplitude : 15.5 m
- Period : 20.0 s

The wave moves in positive X-direction. The water depth is 340.0 m.

The frame analysis, included shell analyses of the 12 selected nodes requires about 15.0 minutes CPU at a Norsk Data's ND 570 computer, (3.5mips).

Corresponding CPU time-consumption using the Superelement technique, is about 3 days. The difference in modelling time between the two methods is of the same order as the CPU time-consumption.

Different results are observed at both quasistatic and dynamic analyses.

The bending moments at the brace ends are primarily influenced by the node flexibility, (up to 400% increase). Figure 20 describes a typical behaviour of the bending moments during a wave periode, (step 1 to 13), for a brace end. The solid lines represent the conventional model, while dotted lines represent the model that includes "shell property elements".

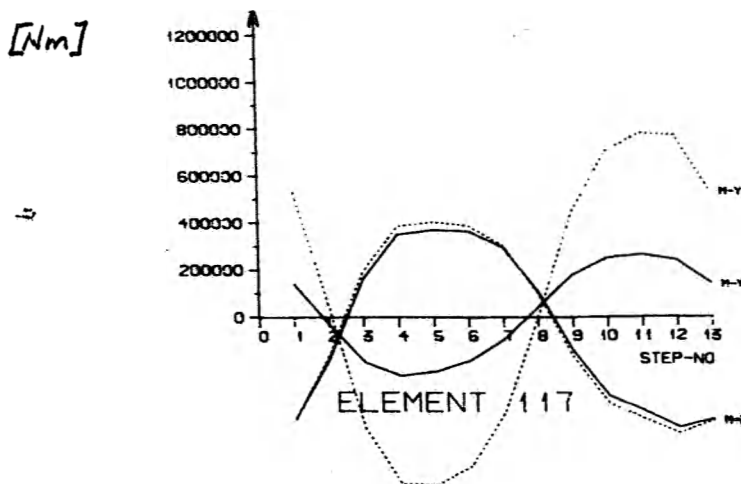


Figure 20 Bending moments at brace end situated 100m below surface

Similar differences in bending moments are observed at the other brace ends.

Local Flexibility

A comparison of maximum axial forces at the braces is made, and the use of the "shell property elements" results in only a few percentage reduction of the axial forces.

The global stiffness of the structure is less severely influenced by the use of "shell property elements", and the dynamic properties are practically unchanged.

9.5 CONCLUSION

The method described above is effective, and makes integrated shell/frame analyses possible.

The properties of the transition element, or the so called "shell property element", are compared with corresponding properties of Finite Element solutions, and there is good accordance for simple tubular joints.

The above described technique determines the hot spot stresses as well as the distribution in the chord with good accuracy, but needing less than 1/100 of the resources compared with Finite Element solutions.

b

10 FRACTURE CRITERIA

10.1 INTRODUCTION

Progressive collapse analysis by means of USFOS assumes implicitly perfectly ductile behaviour, i.e. rupture does not take place at any location. In practice the material endurance is limited, rupture may take place due to excessive straining possibly accelerated by local cracks. Hence, the capacity as predicted by USFOS may be overestimated.

An inherent problem with the plastic hinge concept used in USFOS is that no information is provided as to the strain level in the hinges. In fact, all strains are concentrated at one point of zero length, which means that the strains go towards infinity.

In order to develop a fracture criterion it is necessary to obtain a strain estimate. The purpose of the present study is to develop a simplified model, where the total strain is related to the plastic deformations in the yield hinge. The nominal strain is then compared with a critical strain derived from fracture mechanics principles (Level 3 method). If the critical strain is exceeded the member in question including its load effects should be removed in the subsequent analysis.

10.2 ROTATION IN ELASTO-PLASTIC REGION

10.2.1 Rectangular cross-section

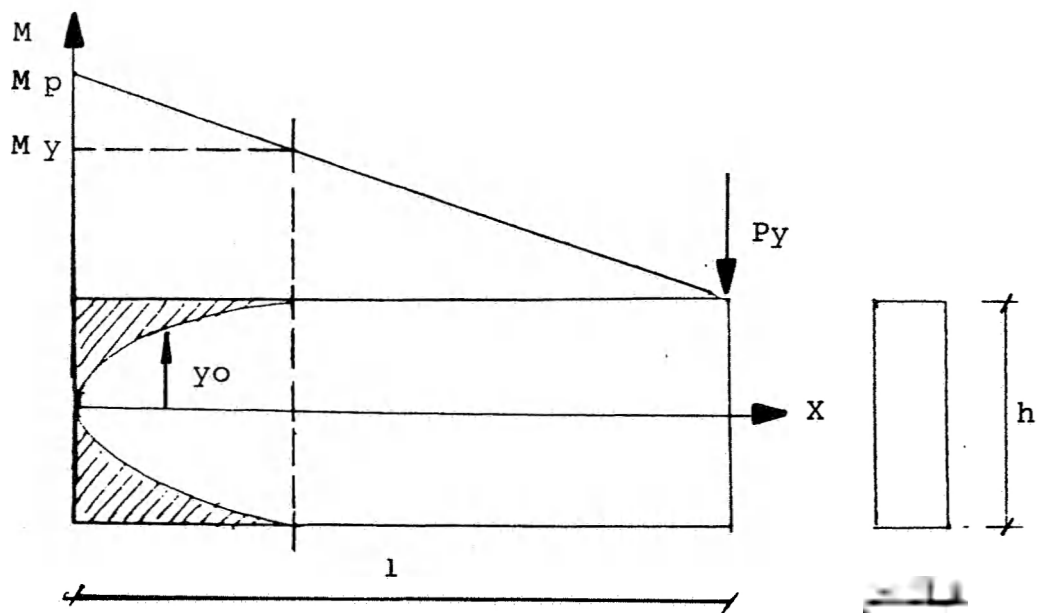


Figure 10.1 Cantilever beam

Consider the cantilever beam in Figure 10.1. The cross-section is elastic when $M < M_y$. Once $M = M_y$ yielding starts in the utmost fiber. For increasing bending moment the plastic zone spreads towards the neutral axis. At the end the whole cross-section is plastified and the bending moment attains the plastic bending moment.

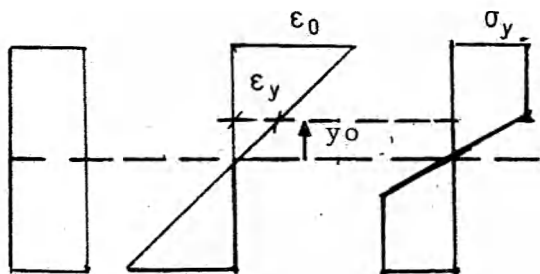


Figure 10.2 Strain distribution

The distribution of strain in the elasto-plastic section is sketched in Figure 10.2. When $\epsilon_0 \geq \epsilon_y$ the stress $\sigma = \sigma_y$ according to the assumption of linear elastic-ideal plastic behaviour. The corresponding moment is

$$M = 2 \int_0^{\frac{h}{2}} \sigma_y dy = M_p \left[1 - \frac{4}{3} \left(\frac{y_0}{h} \right)^2 \right] = M_p \left[1 - \frac{1}{3} \left(\frac{\epsilon_y}{\epsilon_0} \right)^2 \right] \quad (10.1)$$

where

$$M_p = \frac{\sigma_y h^2}{4}$$

= the plastic bending moment for rectangular cross-section.

The axial variation of the bending moment is expressed as

$$M = M_p \left(1 - \frac{x}{l} \right) \quad (10.2)$$

From Eq (10.1) and Eq (10.2) there is obtained

$$\frac{\epsilon_0}{\epsilon_y} = \frac{1}{\sqrt{3} \frac{x}{l}} \quad (10.3)$$

The rotation in the elasto-plastic zone from the onset of yielding to an arbitrary point, Δl , from the end is given by

$$\theta = \int_{\Delta l}^{\frac{1}{3}} \frac{2\epsilon_0}{h} dx = \frac{2\epsilon_y}{h} \int_{\Delta l}^{\frac{1}{3}} \frac{1}{\sqrt{3} \frac{x}{l}} dx = \frac{4l\epsilon_y}{3h} \left[1 - \frac{\epsilon_y}{\epsilon_{\max}} \right] \quad (10.4)$$

where ϵ_{\max} denotes ϵ_0 at Δl .

This shows that the rotation in elasto-plastic zone for an ideal plastic material is bounded and approaches asymptotically the value

$$\theta_{ep} = \frac{4l\epsilon_y}{3h} \quad (10.5)$$

Conversely, the maximum strain can be estimated from the total rotation

$$\epsilon_{\max} = \frac{1}{1 - \frac{3h}{4l\epsilon_y} \cdot \theta} \quad (10.6)$$

10.2.2 Tubular cross-section

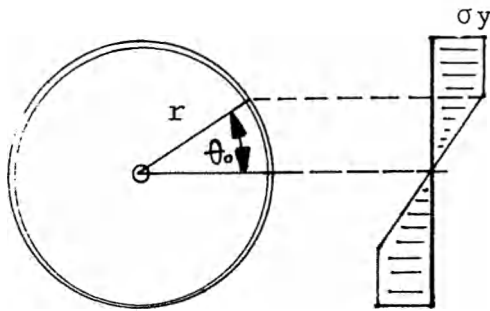


Figure 10.3 Stress distribution in tubular cross-section

Figure 10.3 shows the elasto-plastic stress-distribution in case of circular cross-section. The distance to the first yielding fiber is now described by the angle θ_0 .

The corresponding bending moment is given by

$$M = M_p \left[\frac{\theta_0}{\sin\theta_0} + \cos\theta_0 \right] / 2 \quad (10.7)$$

In the same manner as for rectangular cross-section the axial variation of the yield zone is determined by

$$\frac{\frac{\theta_0}{\sin\theta_0} + \cos\theta_0}{2} = 1 - \frac{X}{l} \quad \frac{X}{l} \in \left[1 - \frac{\pi}{4} \right] \quad (10.8)$$

Fracture Criteria

The total rotation can again be found by integrating the curvature in the elasto-plastic region

$$\theta = \int_{\Delta l}^{(1-\frac{\pi}{4})l} \frac{\epsilon_{\bar{r}}}{\bar{r}} \bar{r} d\bar{r} \quad (10.9)$$

A closed-form solution is difficult to obtain. Approximately, there is obtained

$$\theta = \frac{\epsilon_y l}{2.3r} \left[1 - \frac{\epsilon_{\max}}{\epsilon_y} \right] \quad (10.10)$$

and

$$\frac{\epsilon_{\max}}{\epsilon_y} = \frac{1}{1 - \frac{2.3 r \cdot \theta}{\epsilon_y l}} \quad (10.11)$$

10.3 ROTATION IN STRAIN HARDENING REGION

For large rotations strain hardening will occur. In the following the model shown in Figure 10.4 is used

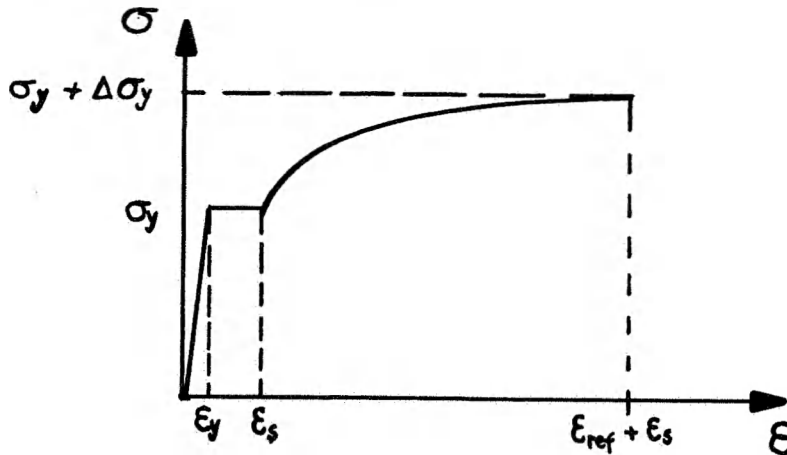


Figure 10.4 Strain hardening model

The yield strain is assumed constant in the range $\epsilon_y < \epsilon < \epsilon_s$. For strains exceeding ϵ_s strain hardening takes place with a maximum value, $\Delta\sigma_y$, for $\epsilon = \epsilon_{ref} + \epsilon_s$ where ϵ_{ref} signifies a reference strain. The hardening follows a parabolic relation given by

$$\Delta\sigma = \Delta\sigma_y \left(\frac{\epsilon - \epsilon_s}{\epsilon_{ref}} \right) \left[2 - \frac{\epsilon - \epsilon_s}{\epsilon_{ref}} \right] \quad (10.12)$$

10.3.1 Bending

For a tubular cross-section the strain hardening contributes to the bending moment as illustrated in Figure 10.5.

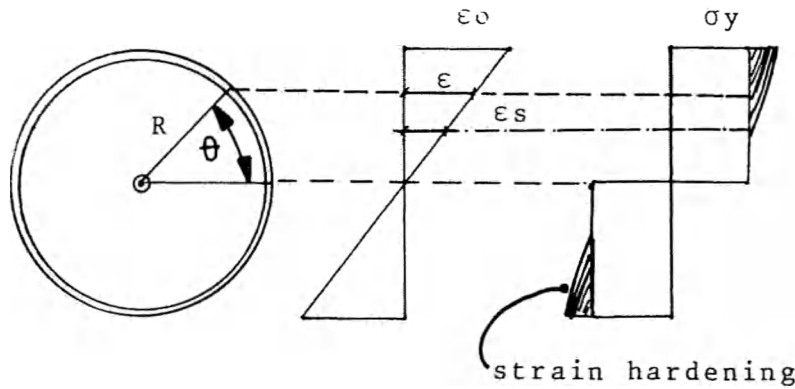


Figure 10.5 Strain/stress distribution for a tubular cross-section

The strain at an arbitrary fibre is given by

$$\epsilon = \epsilon_0 \sin\theta \quad (10.13)$$

where ϵ_0 is the maximum strain of the cross-section.

The additional moment due to strain hardening is now given by

$$\begin{aligned} \Delta M &= 4r^2 t \Delta \sigma_y \int_{\arcsin \frac{\epsilon_s}{\epsilon_0}}^{\frac{\pi}{2}} \left[\frac{\epsilon_0 \sin\theta - \epsilon_s}{\epsilon_{ref}} \right] \left[2 - \frac{\epsilon_0 \sin\theta - \epsilon_s}{\epsilon_{ref}} \right] \sin\theta d\theta \quad (10.14) \\ &= 4r^2 t \Delta \sigma_y \left\{ \left[1 + \frac{\epsilon_s}{\epsilon_{ref}} \right] \frac{\epsilon_0}{\epsilon_{ref}} \left[\frac{\pi}{2} - \arcsin \frac{\epsilon_s}{\epsilon_0} - \frac{\epsilon_s}{\epsilon_0} \left[1 - \left(\frac{\epsilon_s}{\epsilon_0} \right)^2 \right]^{1/2} \right] \right. \\ &\quad \left. - \frac{2}{3} \left[\frac{\epsilon_0}{\epsilon_{ref}} \right]^2 \left[1 - \left(\frac{\epsilon_s}{\epsilon_0} \right)^2 \right]^{3/2} \right\} \end{aligned}$$

This can also be written

$$\Delta M = 4r^2 t \Delta \sigma_y f(\epsilon_0) = 4r^2 t \Delta \sigma_y f(\epsilon_{max}) \frac{f(\epsilon_0)}{f(\epsilon_{max})} \quad (10.15)$$

It is interesting to see that the maximum attainable moment is

$$\Delta M = 4r^2 t \Delta \sigma_y \left\{ \frac{\pi}{2} - \frac{2}{3} \right\} = 3.62 r^2 t \Delta \sigma_y \quad (10.16)$$

when $\epsilon_s/\epsilon_0 \rightarrow 0$, $\epsilon_0/\epsilon_{ref} \rightarrow 1$. The constant 3.62 is, as expected, higher than 3.14, corresponding to a linear stress distribution, but smaller than 4, corresponding to a uniform stress distribution over the cross-section.

For a cantilever, the bending moment varies linearly. Introducing a local coordinate system x at the point of strain hardening initiation, $f(\epsilon_0)$ must obey the relationship

$$\frac{f(\epsilon_0)}{f(\epsilon_{max})} = \frac{x}{l_h} \quad (10.17)$$

where l_h denotes the length of the strain hardening region.

The total rotation in the strain hardening region is

$$\theta_h = \int_0^{l_h} \frac{\epsilon_0}{r} dx = \int_0^{l_h} \frac{1}{r} f^{-1} \left[f(\epsilon_{max}) \frac{x}{l_h} \right] dx \quad (10.18)$$

It is very difficult to find closed form solutions to Equation (10.21) and approximate methods will be resorted to.

Rearranging, Equation (10.21) becomes

$$\theta_h = \frac{p \epsilon_{ref} l_h}{r} \int_0^{l_h} \frac{1}{p} \left[\frac{\epsilon_0 - \epsilon_s}{\epsilon_{ref}} \right] \frac{dx}{l_h} + \int_0^{l_h} \frac{\epsilon_s}{r} dx \quad (10.19)$$

where the parameter p is given by

$$p = \frac{\epsilon_{max} - \epsilon_s}{\epsilon_{ref}} \quad (10.20)$$

ϵ_{\max} is the maximum strain occurring at the beam end. Figure 10.6 displays how the nondimensional strain is distributed over the strain hardening region.

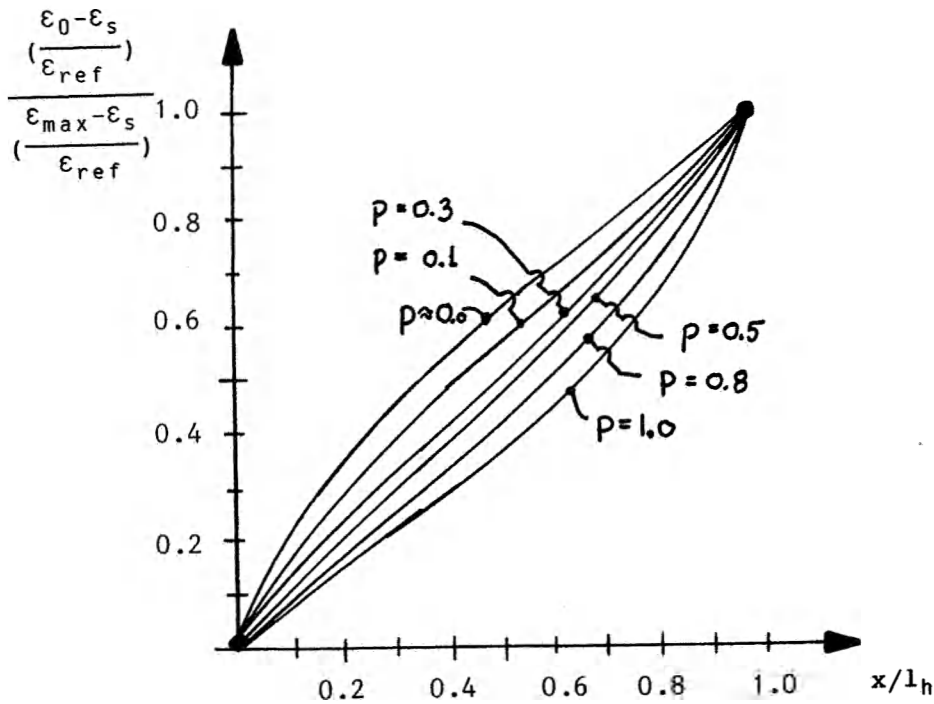


Figure 10.6 Strain distribution over hardening region

Relatively speaking, the strain intensity distribution is larger for moderate strain levels as compared with high strain levels.

A reasonable approximation to the integral in Equation (10.22) is offered by the expression

$$\int_0^{l_h} \frac{1}{p} \left(\frac{\epsilon_0 - \epsilon_s}{\epsilon_{ref}} \right) \frac{dx}{l_h} \approx \frac{1.2}{2+p} \quad (10.21)$$

The length of the strain hardening region is found from

$$\frac{l_h}{l} = \frac{\Delta M/M_p}{1 + \Delta M/M_p} = \frac{f(\epsilon_{\max}) \frac{\Delta \sigma_y}{\sigma_y}}{1 + f(\epsilon_{\max}) \frac{\Delta \sigma_y}{\sigma_y}} \quad (10.22)$$

The relationship between $f(\epsilon_{\max})$ and p is shown in Figure 10.7.

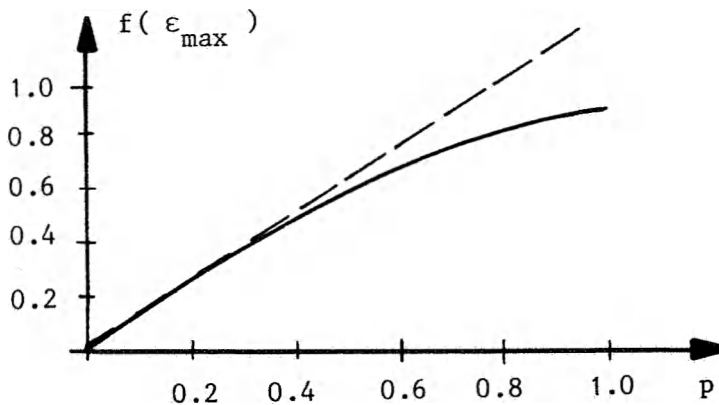


Figure 10.7 $f(\epsilon_{\max})$ versus the parameter p

The following approximation is introduced

$$f(\epsilon_{\max}) \approx \frac{1.4p}{1+0.5p} \quad (10.23)$$

The rotation in the elastoplastic region is given by Equation (10.8)

$$\theta_{ep} \approx \frac{\epsilon_y l}{2.3r} \quad (10.24)$$

and

$$\frac{l_{ep}}{l} = \frac{1 - \frac{\pi}{4}}{1 + f(\epsilon_{\max}) \frac{\Delta \sigma_y}{\sigma_y}} = \frac{0.215}{1 + \frac{1.4p}{1+0.5p} \frac{\Delta \sigma_y}{\sigma_y}} \quad (10.25)$$

Combining Equations (10.22, 10.24, 10.26, 10.27, 10.28) there is obtained

$$\theta = \theta_h + \theta_{ep} = \frac{\epsilon_{ref} \cdot 1}{r} \frac{1}{1 + \frac{\Delta\sigma_y}{\sigma_y} \frac{1.4p}{1+0.5p}} \left\{ \frac{1.2p}{2+p} \cdot \frac{\Delta\sigma_y}{\sigma_y} \frac{1.4p}{1+0.5p} + \frac{\epsilon_s}{\epsilon_{ref}} \cdot \frac{\Delta\sigma_y}{\sigma_y} \frac{1.4p}{1+0.5p} + \frac{\epsilon_s}{\epsilon_{ref}} \frac{\epsilon_y}{\epsilon_s} \frac{1}{2.3} \right\} \quad (10.27)$$

Rearranging, there is obtained a second degree equation in p

$$ap^2 + bp + c = 0 \quad (10.27)$$

where

$$a = 1.68 \frac{\Delta\sigma_y}{\sigma_y} + \left[1.4 \frac{\Delta\sigma_y}{\sigma_y} + 0.215 \right] \frac{\epsilon_s}{\epsilon_{ref}} - \frac{\theta_r}{\epsilon_{ref} \cdot 1} \left[0.5 + 1.4 \frac{\Delta\sigma_y}{\sigma_y} \right] \quad (10.28a)$$

$$b = \left[2.8 \frac{\Delta\sigma_y}{\sigma_y} + 0.86 \frac{\epsilon_y}{\epsilon_s} \right] \frac{\epsilon_s}{\epsilon_{ref}} - \frac{\theta_r}{\epsilon_{ref} \cdot 1} \left[2 + 2.8 \frac{\Delta\sigma_y}{\sigma_y} \right] \quad (10.28b)$$

$$c = 0.86 \frac{\epsilon_y}{\epsilon_{ref}} - 2 \frac{\theta_r}{\epsilon_{ref} \cdot 1} \quad (10.28c)$$

Once p is solved the maximum strain is obtained from

$$\epsilon_{max} = \epsilon_{ref} \left[p + \frac{\epsilon_s}{\epsilon_{ref}} \right] \quad (10.29)$$

10.3.2 Membrane Strain

The yield criterion formulated in terms of stress resultants takes the following form for a tubular cross-section

$$f(m, n) = 0 \quad (10.30)$$

Fracture Criteria

where $m = M/M_p$, $n = \pi/2 N/N_p$ are nondimensional bending moment and axial force, respectively. The plastic increments in rotation and axial displacement are governed by the normality criterion, i.e.:

$$d\theta_p = d\lambda \frac{\partial f}{\partial m} \frac{\partial m}{\partial M} \quad (10.31a)$$

$$d\theta_p = d\lambda \frac{\partial f}{\partial n} \frac{\partial n}{\partial N} \quad (10.31b)$$

where $d\lambda$ is the plastic increment scalar. Combining, this yields

$$d\theta_p = \frac{\partial f/\partial m}{\partial f/\partial n} \cdot \frac{\partial m/\partial M}{\partial n/\partial N} du_p \quad (10.32)$$

and

$$d\theta_p = \frac{1}{\sin n} \cdot \frac{1}{r} du_p \quad (10.33)$$

This shows that the plastic axial displacement divided by the radius can be interpreted as an equivalent rotation. This corresponds to distributing the axial displacement over the effective hinge length. Hence, the total rotation to be used in Equation (10.31a-c) is

$$\theta^{tot} = \theta_p + \frac{u_p}{r} \quad (10.34)$$

The presence of axial force increases the effective hinge length as illustrated in Figure 10.8.

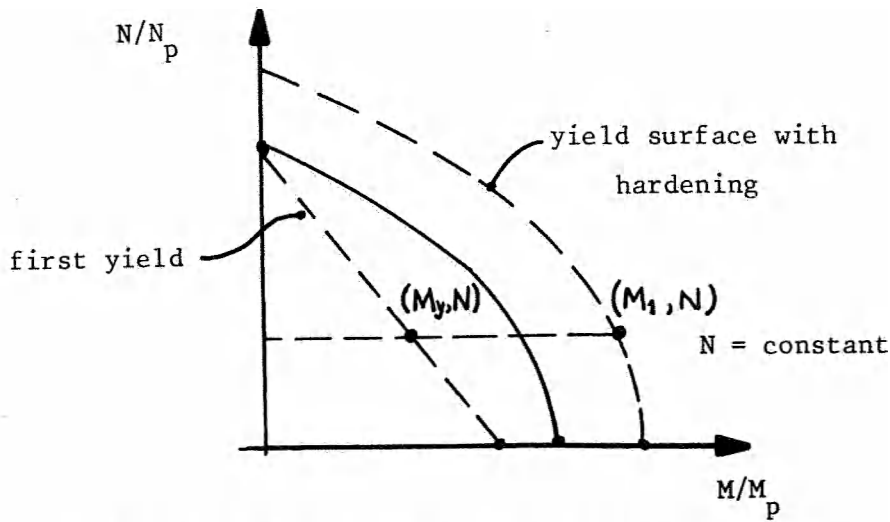


Figure 10.8 Axial force - bending moment interaction

The relative length of the plastic and elastoplastic zone is

$$\frac{l_{ep}}{l} = \left(1 - \frac{M_y}{M_1}\right) \quad (10.35)$$

Introducing the first yield Equation

$$\frac{4}{\pi} \frac{M_y}{M_p} + \frac{N}{N_0} - 1 = 0 \quad (10.36)$$

and the fully plastic surface

$$\frac{M_1}{(1+C_M)M_p} - \cos \frac{\pi}{2} \frac{N}{(1+C_N)N_p} = 0 \quad (10.37)$$

where C_M and C_N account for the hardening in the bending - and axial direction respectively. This gives

$$\frac{l_{ep}}{l} = 1 - \frac{\frac{\pi}{4} \left(1 - \frac{N}{N_p}\right)}{(1+C_M) \cos \frac{\pi}{2} \frac{N}{(1+C_N)N_p}} \quad (10.38)$$

l represent the length from member end to the inflection point and is obtained from the formula

$$\frac{l}{l_{mem}} = \frac{1}{1 + \frac{M_2}{M_1}} \leq 1 \quad (10.39)$$

Fracture Criteria

where l_{mem} is the total element length and M_2 denotes the bending moment at the opposite end.

Combining Equations (10.41 and 10.42) there comes out

$$\frac{l_{ep}}{l_{mem}} = \frac{1}{1 + \frac{M_2}{M_1}} \left(1 - \frac{\frac{\pi}{4} \left(1 - \frac{N}{N_p} \right)}{(1+C_M) \cos \frac{\pi}{2} \frac{N}{(1+C_N)N_p}} \right) \quad (10.40)$$

The augmentation of effective yield hinge length caused by the membrane force can then be obtained from

$$f = \frac{l_{ep}/l_{mem}}{l_{ep}/l_{mem} (N = M_2 = 0)} = \frac{1}{1 + \frac{M_2}{M_1}} \cdot \frac{1}{1 - \frac{\pi/4}{1+C_M}} \cdot \left[1 - \frac{\frac{\pi}{4} \left(1 - \frac{N}{N_p} \right)}{(1+C_M) \cos \frac{\pi}{2} \frac{N}{(1+C_N)N_p}} \right] \quad (10.41)$$

The bending parameter is taken as

$$C_M = f(\epsilon_{max}) \frac{\Delta\sigma_y}{\sigma_y} \quad (10.45)$$

For simplicity C_N is chosen equal to C_m .

10.4 FRACTURE CRITERION

A number of methods based upon fracture mechanics principles are available for determining the critical strain. Most of them are valid under pure elastic - or moderate yielding conditions. However, the advent of the Level 3 method /31/ allows fracture assessment to be performed on work hardening materials undergoing large strains, and is therefore appropriate for our need. The method utilizes the crack tip opening displacement (CTOD) as the fracture toughness input. The criterion is formulated as follows

$$\delta_{crit} = \frac{\pi \sigma_y \cdot a}{E} \left\{ \frac{\sigma_p}{\sigma_y} \left(\frac{a_e}{a} + \frac{E \epsilon_a}{\sigma_a} - 1 \right)^2 + \frac{\sigma_s}{\sigma_y} \right\}^2 \quad (10.43)$$

where a is the flaw size, a_e is the effective flow size given by

$$a_e = a + \frac{1}{2\pi} \frac{(K_I^p)^2}{\sigma_y^2} \frac{1}{1 + \frac{\sigma_a}{\sigma_y}} \quad (10.44)$$

The primary stress σ_p is the result of the net force and moment acting on the stress-section, the effects of stress concentrations and crack-like flaws being ignored.

The stress intensity due to the primary stress is given by

$$K_I^p \cong \sigma_p (\pi a)^{1/2} \quad (10.45)$$

The secondary stresses, σ_s , are stresses which are selfequilibrating within the cross-section, being e.g. caused by residual welding stresses. In the present calculation they are ignored, i.e. $\sigma_s = 0$.

σ_a and ϵ_a designate, respectively, corresponding values of stress and strain as obtained in uniaxial tensile test. At the critical CTOD they attain the values $\sigma_a = \sigma_{max}$, $\epsilon_a = \epsilon_{max}$. Furthermore, $\sigma_p = \sigma_{max}$. Combining Equations (10.46, 10.47, 10.48) there comes out

Fracture Criteria

$$\delta_{crit} = \frac{\pi\sigma_y a}{E} \cdot \frac{\sigma_{max}^2}{\sigma_y^2} \left\{ \frac{\sigma_{max}^2}{2\sigma_y^2} \frac{1}{1 + \frac{\sigma_{max}}{\sigma_y}} + \frac{E\varepsilon_{max}}{\sigma_{max}} \right\} \quad (10.46)$$

It is noted that for large strains Equation (10.49) is completely dominated by the second term.

The procedure for controlling fracture is as follows:

Calculate ε_{max} and corresponding σ_{max} from expressions in Section 10.3.

Assume appropriate flaw size, a . Calculate right hand side of Equation (10.49) and check whether

$$\delta > \delta_{crit} \quad (10.47)$$

If Equation (10.47) is fulfilled rupture is assumed.

11 LOCAL BUCKLING OF RECTANGULAR CROSS-SECTIONS

11.1 INTRODUCTION

This section describes the methods method for taking into account the detrimental effect of local buckling of one of the side walls on the plastic capacities for rectangular cross-sections. The implementation is based on the following assumptions:

- The reduction in plastic load-carrying capacities of unstiffened rectangular cross-sections due to local buckling of one of the side walls is calculated.
- Local buckling of stiffened rectangular cross-sections is not taken into account unless this can be adequately described by the model used for the unstiffened section.
- It is assumed that buckling takes place in one of the two principal axes of bending. Once buckling is initiated this is not allowed to occur in the other direction.
- The buckle affects the bending capacity in one direction only, the other remains unaltered.
- The interaction function used for intact cross-section is also valid for the buckled state.
- The effect of "jamming", i.e. the strength increase due to direct contact between the two surfaces exterior to the buckled section, is not taken into account.

Kecman /32/ has carried out extensive experiments with rectangular and square section tubes. Figures 11.1 and 11.2 show typical collapse modes obtained in the large rotation range.

Local Buckling of Rectangular Cross-sections

Evidently, the cross-sections undergoing this kind of local failure are no longer capable of attaining the fully plastic capacities. For a reliable simulation this must also be reflected in the large displacement/large strain calculations. Similar to the method developed for tubular cross-sections it is proposed that the local buckling effect is handled entirely within the plastic hinge concept. This is achieved by a proper reduction of the plastic capacities. The calculation of the reduced properties are based upon an assumed collapse pattern or yield line mechanism, which is entirely governed by the plastic rotation of the cross-section.

The proposed modelling of local collapse behaviour includes:

- a buckling criterion
- calculation of reduced plastic capacities under local collapse
- modification of elasto-plastic stiffness matrix in accordance with the calculated reduced properties.

Local Buckling of Rectangular Cross-sections

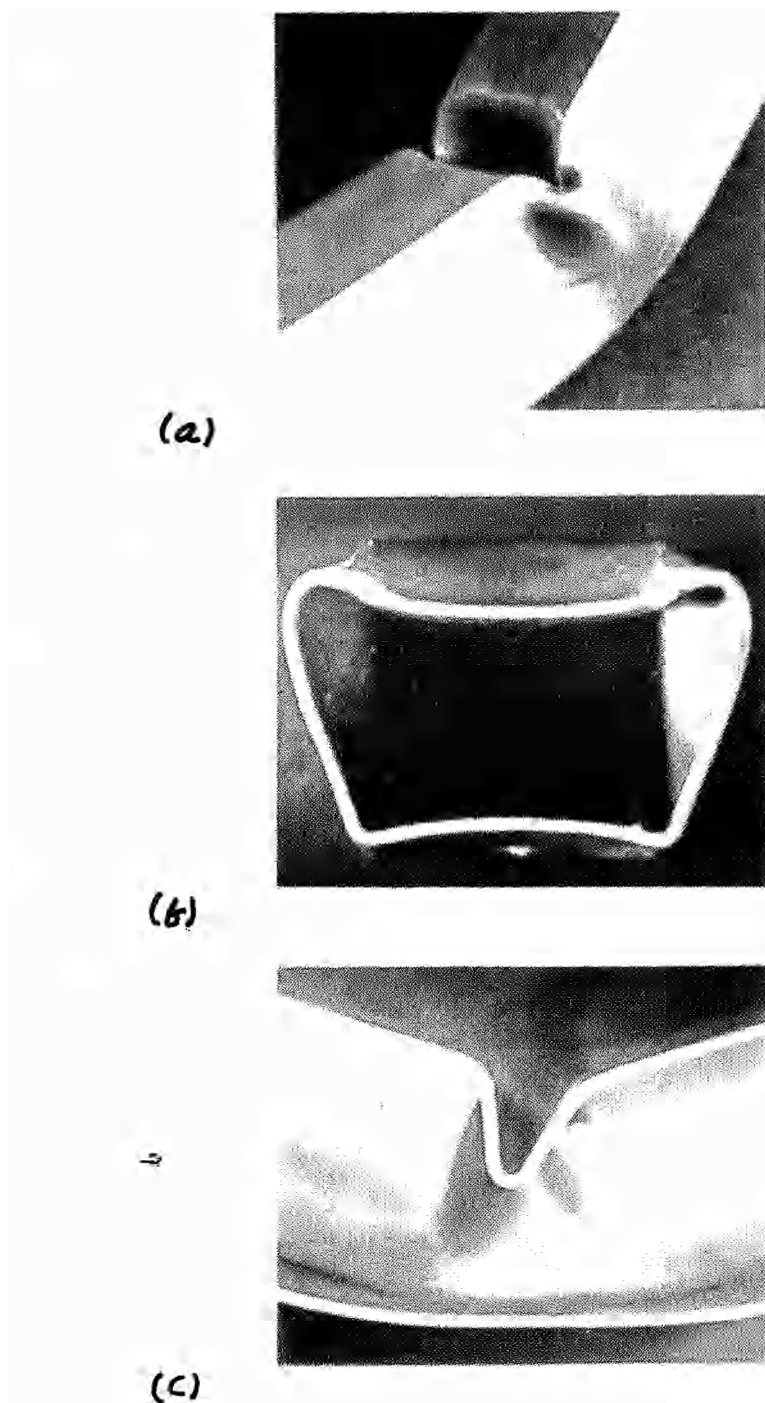


Figure 11.1 (a) A typical hinge collapse mechanism with:
(b) cross section and (c) longitudinal section.

Local Buckling of Rectangular Cross-sections

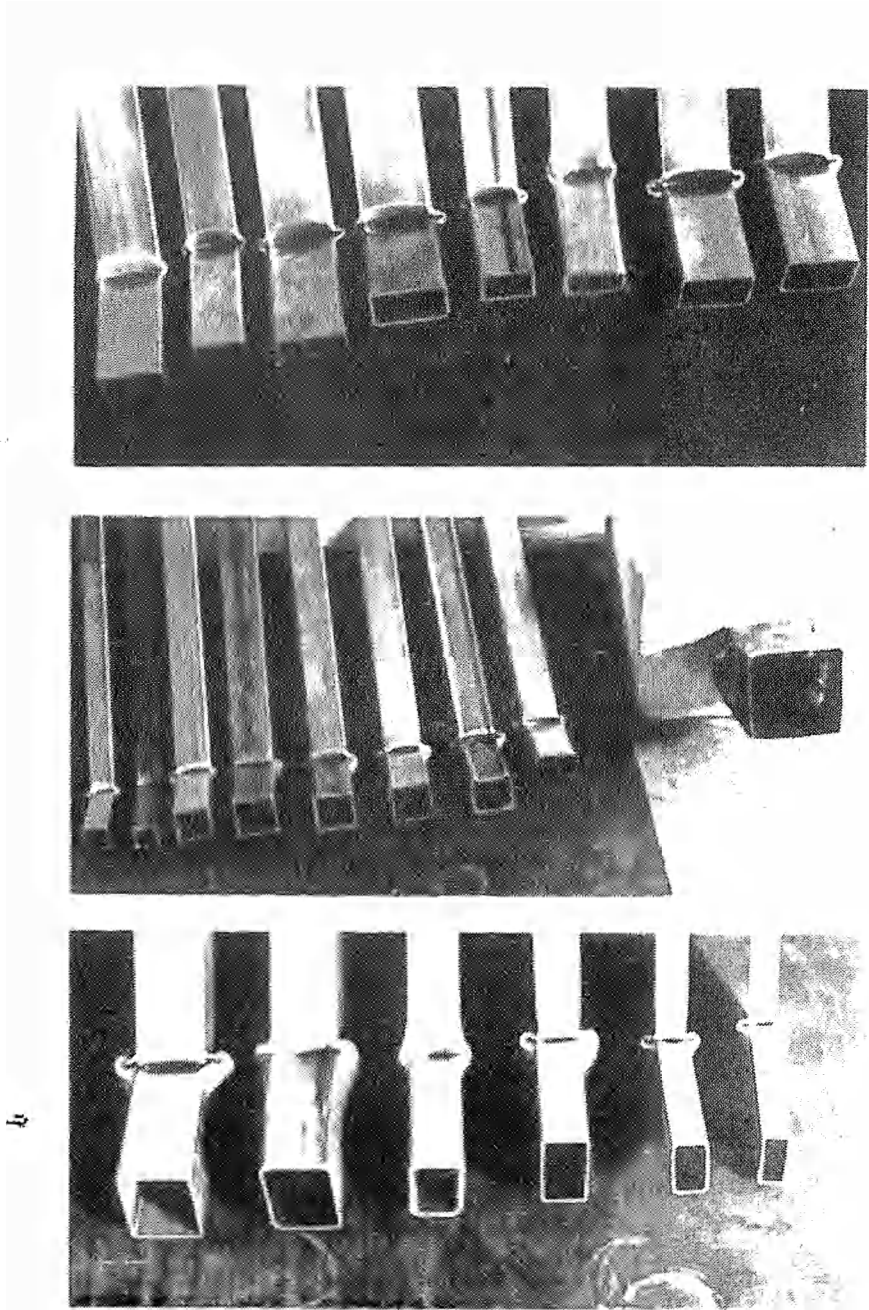


Figure 11.2 Collapse modes in various rectangular and square sections.

11.2 BUCKLING CRITERION

The collapse mechanism for the cross-section is triggered once local buckling occurs in one of the side walls, due to excessive uniaxial compression and rotation. For this purpose a buckling criterion needs to be introduced.

The criterion may be based on conventional buckling formulas for plate elements. For thin-walled members buckling is predominantly elastic and a critical stress criterion may be used. For thick-walled elements showing pronounced elasto-plastic effects a strain criterion is required. In this case the total rotation and displacement at a node need to be transferred to an equivalent axial strain e.g. by the method used in the fracture control analysis. If this method is used the conservativeness in the code formulas should be appreciated. For our purposes the mean buckling stress is relevant.

Conceivably, such a criterion is not very accurate, especially for low slendernesses. Alternatively, it may be based on experimental evidence.

The tests carried out by Keckam cover a large range of wall slendernesses and should constitute a good basis in this respect. Hopefully, these data can be provided.

Due to lack of experimental data, a simplified buckling criterion will temporarily be used. The present implementation assumes that local buckling will occur as the force state reaches the bounding surface. This results in a conservative solution as the cross sectional capacity is limited by elastic wall buckling or yielding, depending on the width to wall thickness ratio.

11.3 RESIDUAL PLASTIC CAPACITIES

The collapse mode observed during tests is by Keckam idealized by a yield line mechanism as shown in Figures 3 and 4. It consists of bending across stationary yield lines and rolling deformation across travelling hinge lines, e.g. KA, GA, by which a part of the side wall becomes a part of the "top" flange.

Local Buckling of Rectangular Cross-sections

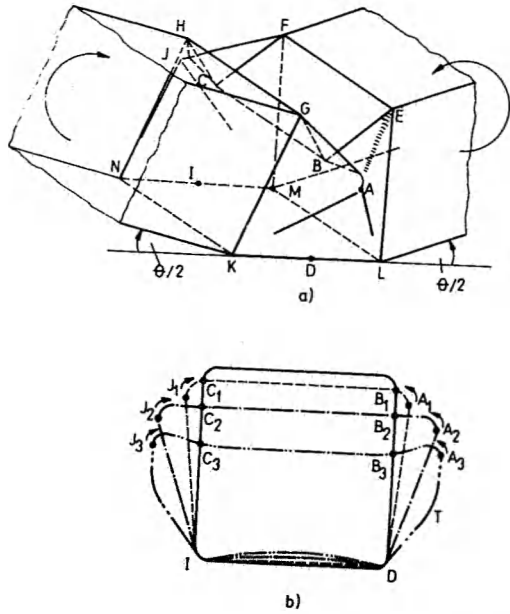


Figure 11.3 Hinge mechanism (a) at various stages of development (b).

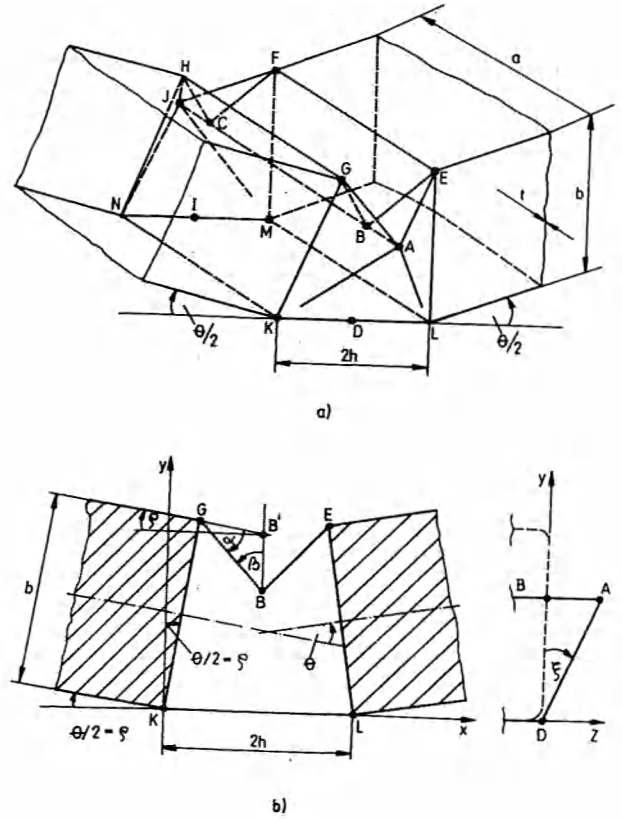


Figure 11.4 The theoretical model (a) and its longitudinal section (b).

In order to obtain the reduced bending capacity, Kecman derived the total energy absorbed by plastic deformation up to a rotation angle θ . It consists of 8 contributions (for details of derivation, confer Ref. /32/).

$$E_{EF+GH} = m_{pt}a (\pi-\theta-\mu)$$

$$E_{BC} = m_{pt}a(\pi-\mu)$$

$$E_{AB+CJ} = 2m_{pw}z_A (\pi-\mu)$$

$$E_{BG+BE+CH+CF} = 2\pi m_{pw}h$$

$$E_{GK+EL+HN+FM} = 4m_{pw}b \arctg \left(\frac{z_A}{\{(h-x_A'')^2 + (y_A''-y_B'')^2\}^{1/2}} \right)$$

Local Buckling of Rectangular Cross-sections

$$E_{GA+AE+CH+CF} = 4m_{pw}z_A \frac{h}{r}$$

$$E_{KA+LA+NJ+MJ} = \frac{8}{3} m_{pw} \frac{z_A}{r} (h^2 + y_B^2 + z_A^2)^{1/2}$$

$$E_{KN+LM+KL+MN} = m_{pw} \cdot a \left(\theta + \frac{4h}{a} \arctg \left(\frac{h}{a} \right) \right)$$

where:

$$\mu = 2 \arcsin \left(1 - \frac{b}{h} \sin \frac{\theta}{2} \right)$$

$$y_A = y_B = b \cos \frac{\theta}{2} - \left\{ b \sin \frac{\theta}{2} (2h - b \sin \frac{\theta}{2}) \right\}^{1/2}$$

$$z_A = b \sin^2 \frac{\theta}{2} - h \sin \frac{\theta}{2} + \left\{ b \sin \frac{\theta}{2} (2h - b \sin \frac{\theta}{2}) \right\}^{1/2} \cos \frac{\theta}{2}$$

$$y_A'' = \frac{h \operatorname{tg} \frac{\theta}{2} - y_B}{1 + \operatorname{tg}^2 \frac{\theta}{2}}$$

$$x_A'' = y_A'' \cdot \operatorname{tg} \frac{\theta}{2}$$

$$m_{pi} = \sigma_y \frac{t_i^2}{4} : \text{ plastic bending moment for a platestrip, dependent upon actual wall thickness } t_i \text{ (suffix } t=\text{topp, } w=\text{web, } b=\text{bottom)}$$

$$r(\theta) = \left(0.07 - \frac{\theta}{70} \right) h \text{ empirical rolling radius.}$$

The wave length is selected as the minimum of the width/height of the cross-section

$$h = \min \left\{ \frac{a}{2}, \frac{b}{2} \right\}$$

The total energy is found by summation

$$E(\theta) = \sum_{i=1}^8 E_i(\theta)$$

Local Buckling of Rectangular Cross-sections

The bending capacity is obtained by differentiation with respect to θ of the total energy. The derivative of the bending moment is also needed. Because of the complexity of differentiation this is carried out numerically, hence:

$$M_p(\theta) = \frac{E(\theta+\Delta\theta) - E(\theta-\Delta\theta)}{2\Delta\theta}$$

$$\frac{dM_p(\theta)}{d(\theta)} = \frac{E(\theta+\Delta\theta) - 2E(\theta) - E(\theta-\Delta\theta)}{\Delta\theta^2}$$

In calculation of the reduced plastic axial capacity in compression the following assumptions are introduced:

- The axial capacity in the bottom flange is not influenced by the mechanism.
- Using a finite strip approach the axial force in the top flange is determined from force equilibrium of a three hinge mechanism.
- The axial stress in the side wall is assumed to remain at yield, because the corner nodes A,J constitute very stiff points with significant in-plane deformations. The reduction of axial load-carrying is thus only due to the geometric effects.

The axial force in the lower flange is accordingly:

$$N_{NK} = \sigma_y \cdot t_b \cdot a$$

and in the upper flange,

$$N_{HG} = \frac{\overset{\rightarrow}{2m_p t} \cdot a}{h \cos\left(\frac{\theta}{2} + \frac{\mu}{2}\right)} = \sigma_y \cdot t_t \cdot a \frac{t_t}{2 h \cos\left(\frac{\theta+\mu}{2}\right)}$$

To avoid numerical problems this term is approximated to a straight line from zero rotation to the "jamming angle".

In the side walls:

Local Buckling of Rectangular Cross-sections

$$N_{KG+NH} = 2 \sigma_y \cdot t_w \cdot b \cos \left\{ \arctg \left[\frac{z_A}{\{(h-x_a'')^2 + (y_A''-y_B'')^2\}^{1/2}} \right] \right\}$$

The total plastic axial force is

$$N_p(\theta) = N_{NK} + N_{HG} + N_{KG+NH}$$

The reduced capacity of the upper flange causes an excentricity, which is given by

$$e = y_e = \frac{(N_{HG} - N_{NK})a}{N_p(\theta)} \quad (\text{negative for present choice of axis system})$$

The gradient of the plastic axial capacity is found by numerical differentiation

$$\frac{dN_p(\theta)}{d\theta} = \frac{N_p(\theta+\Delta\theta) - N_p(\theta-\Delta\theta)}{2\Delta\theta}$$

The axial force contributes to the bending moment through the excentricity

$$M = M + Ne$$

Correspondingly, the partial derivative of the yield function with respect to axial force becomes

$$\frac{\partial f}{\partial N} = \frac{\partial f}{\partial N} + \frac{\partial f}{\partial M} e$$

The calculation procedure described above results in a singularity in the calculation of plastic capacities at zero plastic rotation. In order to avoid this problem a transition curve (a straight line) is chosen to define the plastic moment capacity from onset of buckling to a specific collapse hinge rotation, denoted θ_T , see Figure 11.5.

θ_T represents the plastic rotation when the straight transition line becomes tangential to the moment capacity curves respectively defined by the energy formulations in Section 11.3. This approach corrolates well with experimental results /32/.

Local Buckling of Rectangular Cross-sections

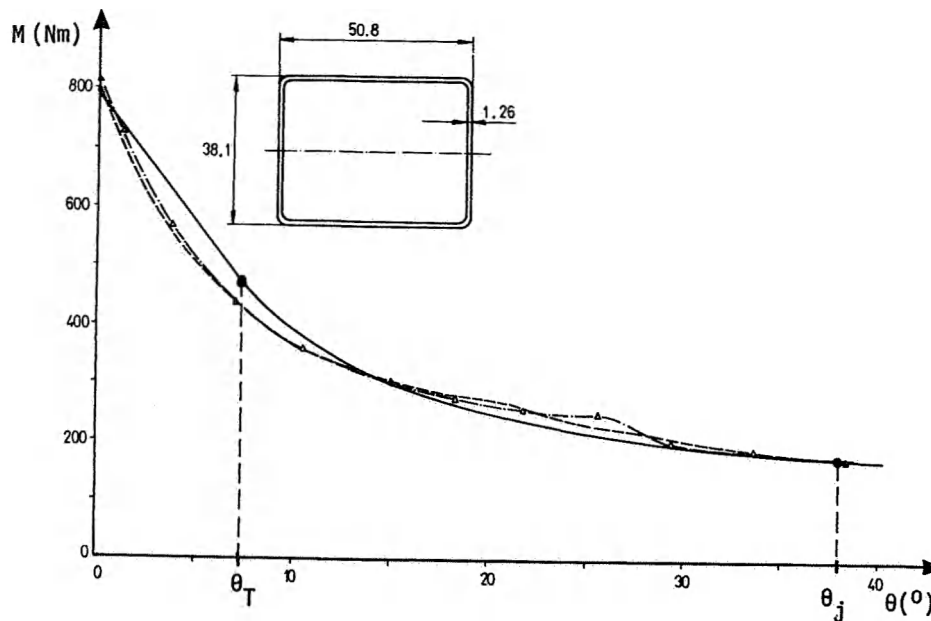


Figure 11.5 Plastic moment capacity degradation curve due to local buckling.

11.4 INTERACTION FUNCTION FOR STRESS RESULTANTS

The interaction function for the stress resultants for an intact cross-section is supposed to remain valid for a buckled cross-section. Thus, the only influence of the buckle is to reduce the available capacities in bending and axial compression (full capacity in tension).

The plastic capacity for bending in the other direction is assumed to be unaffected by the buckle. This is reasonable for moderate rotations. Further, the initiation of a local buckle is so dramatic that it is likely to govern the behaviour in the post-collapse region.

11.5 ELASTO-PLASTIC CONSTITUTIVE EQUATIONS

A basic assumption for the following derivations is that the buckling phenomenon is entirely confined to the hinges. The behaviour of the hinges are in turn governed by the plastic flow theory which states that

Local Buckling of Rectangular Cross-sections

$$F(N, Q_y, Q_z, M_x, M_y, M_z) = 0$$

$$dF = \begin{bmatrix} \frac{\partial F}{\partial N} & \frac{\partial F}{\partial Q_y} & \frac{\partial F}{\partial Q_z} & \frac{\partial F}{\partial M_x} & \frac{\partial F}{\partial M_y} & \frac{\partial F}{\partial M_z} \end{bmatrix} \begin{bmatrix} dN \\ dQ_y \\ dQ_z \\ dM_x \\ dM_y \\ dM_z \end{bmatrix}$$

$$= \mathbf{g}^T d\mathbf{S} = 0$$

$$d\mathbf{v}^p = \Delta\lambda \mathbf{g}$$

The yield criterion may also be written as

$$F \left(\frac{N}{N_p}, \frac{Q_y}{Q_{yp}}, \frac{M_x}{M_{xp}}, \frac{M_y}{M_{yp}}, \frac{M_z}{M_{zp}} \right) = 0$$

It is now necessary to incorporate also a possible change of plastic capacities in the consistency criterion.

Accordingly,

$$dF = \frac{\partial F}{\partial \mathbf{S}} d\mathbf{S} - \frac{\partial F}{\partial \mathbf{S}_p} d\mathbf{S}_p = 0$$

where $\mathbf{S}_p^T = [N_p, Q_{yp}, Q_{zp}, M_{xp}, M_{yp}, M_{zp}]$ is the vector of plastic capacities.

Local Buckling of Rectangular Cross-sections

Further,

$$\frac{\partial F}{\partial S_p} dS_p = \frac{\partial F}{\partial S} \left(\frac{\partial S}{\partial S_p} dS_p \right) = \frac{\partial F}{\partial S} \begin{bmatrix} - \frac{N}{N_p} dN_p \\ - \frac{Q_y}{Q_{yp}} dQ_{yp} \\ - \frac{Q_z}{Q_{zp}} dQ_{zp} \\ - \frac{M_x}{M_{xp}} dM_{xp} \\ - \frac{M_y}{M_{yp}} dM_{yp} \\ - \frac{M_z}{M_{zp}} dM_{zp} \end{bmatrix} = 0$$

In accordance with the previous paragraph it is assumed that the change of plastic capacities is governed by the kinematics of the cross section, in other words by the change of plastic displacement (Plastic rather than total displacements seems to be a logical choice. This also renders a simpler calculation). This yields

$$\begin{bmatrix} - \frac{N}{N_p} dN_p \\ - \frac{Q_y}{Q_{yp}} dQ_{yp} \\ \vdots \\ - \frac{M_z}{M_{zp}} dM_{zp} \end{bmatrix} = - \begin{bmatrix} \frac{N}{N_p} \frac{\partial N_p}{\partial u_p} & \frac{N}{N_p} \frac{\partial N_p}{\partial v_p} & \dots & \frac{N}{N_p} \frac{\partial N_p}{\partial \theta_{zp}} \\ \frac{Q_y}{Q_{yp}} \frac{\partial Q_{yp}}{\partial u_p} & \frac{Q_y}{Q_{yp}} \frac{\partial Q_{yp}}{\partial v_p} & \dots & \frac{Q_y}{Q_{yp}} \frac{\partial Q_{yp}}{\partial \theta_{zp}} \\ \vdots & \vdots & & \vdots \\ \frac{M_z}{M_{zp}} \frac{\partial M_{zp}}{\partial u_p} & \frac{M_z}{M_{zp}} \frac{\partial M_{zp}}{\partial v_p} & \dots & \frac{M_z}{M_{zp}} \frac{\partial M_{zp}}{\partial \theta_{zp}} \end{bmatrix} \begin{bmatrix} du_p \\ dv_{yp} \\ dv_{zp} \\ \partial \theta_{xp} \\ \partial \theta_{yp} \\ \partial \theta_{zp} \end{bmatrix}$$

or

Local Buckling of Rectangular Cross-sections

$$\begin{bmatrix} -\frac{N}{N_p} dN_p \\ -\frac{Q_y}{Q_{yp}} dQ_{yp} \\ \cdot \\ \cdot \\ -\frac{M_z}{M_{zp}} dM_{zp} \end{bmatrix} = -C_p \cdot d\mathbf{v}_p$$

Introducing these equations into the consistency criterion there is obtained

$$dF = \mathbf{g}^T dS - \mathbf{g}^T C_p d\mathbf{v}_p = 0$$

Further

$$dS = \mathbf{k}_e (d\mathbf{v} - d\mathbf{v}_p)$$

$$d\mathbf{v}_p = d\lambda \mathbf{g}$$

and

$$dF = \mathbf{g}^T \mathbf{k}_e (d\mathbf{v} - d\lambda \mathbf{g}) - \mathbf{g}^T C_p d\lambda \mathbf{g} = 0$$

The plastic increment becomes

$$d\lambda = \{\mathbf{g}^T (\mathbf{k}_e - C_p) \mathbf{g}\}^{-1} \mathbf{g}^T \mathbf{k}_e d\mathbf{v}$$

and the reduced plastic stiffness matrix

$$dS = \mathbf{k}_e (d\mathbf{v} - d\lambda \mathbf{g}) = [\mathbf{k}_e - \mathbf{k}_e \mathbf{g} \{\mathbf{g}^T (\mathbf{k}_e - C_p) \mathbf{g}\}^{-1} \mathbf{g}^T \mathbf{k}_e] d\mathbf{v}$$

This means that the contraction of the yield surface due to local buckling enters the scaling factor, given by the bracket expression, in the same manner as does the hardening effect. It is noted that there are only two non-vanishing

terms in C_p for the present mechanism, namely $\frac{\partial N_p}{\partial \theta_{zp}}$, $\frac{\partial M_{yp}}{\partial \theta_{zp}}$ or $\frac{\partial M_{zp}}{\partial \theta_{zp}}$.

Local Buckling of Rectangular Cross-sections

The partial derivatives are to be determined on the basis of the reduced plate properties derived in section 11.3. However, except for a few terms they are all zero.

In the present implementation of local buckling behaviour of rectangular sections, cyclic material behaviour is not considered. This implies that repeated plasticity in the yield lines of the local mechanism due to sequences of loading and unloading do not trigger rupture of the structural element. However, this option may be implemented in a later extension of the program.

The introduction of rotation dependant local buckling effects into the beam element stiffness formulation is shown in detail in Section 4.

4

12. DECK PLATING ELEMENT

A four node membrane element is implemented in USFOS. The local node numbering and local coordinate system are described in figure 12.1.

The element has 2 degrees of freedom per node and should be used in combination with beam elements (to avoid zero stiffness terms).

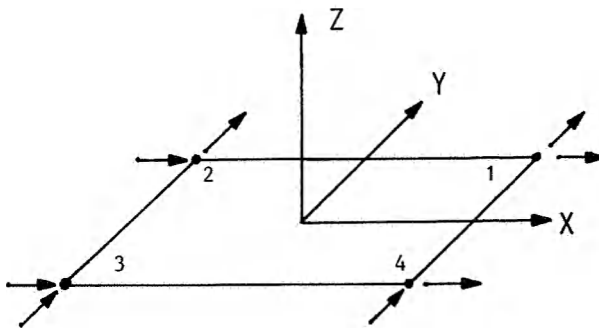


Figure 12.1 Membrane element

The element nodes may be eccentric connected to the system nodes.

The midnode of the beam element is not connected to the edge of the membrane element, see figure 12.2.

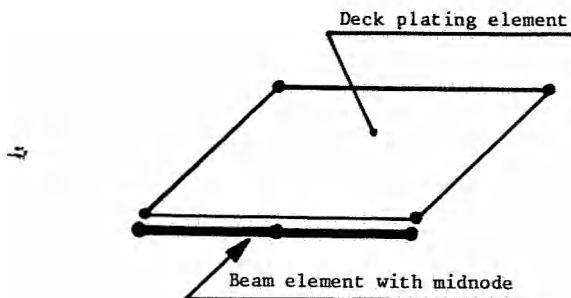


Figure 12.2 Membrane element connected to beam with midnode

In addition the element acts as a "load-element" for pressure loading. The total element load, (pressure x area of element), is distributed to the element nodes, (1/4 to each node), and transformed to the system nodes. The pressure is directed parallel to the current local Z-axis of the element, (non-conservative load).

The element is elastic until Von mises yield criterion is fulfilled at one of the four nodes and will then become plastic.

Buckling is not accounted.

13. SHIP COLLISION

13.1 INTRODUCTION

The collision response of fixed offshore structures can be divided in the following deformation modes :

- Local deformation of the tube wall at the point of impact
- Beam deformation of the hit member
- Global deformation of the structure

Calculation of beam deformation and global deformation of the platform is included in the ordinary USFOS calculations.

13.2 LOCAL DENTING OF TUBE WALL

The load-indentation curves recommended by DnV /32/ is shown in Figure 13.1.

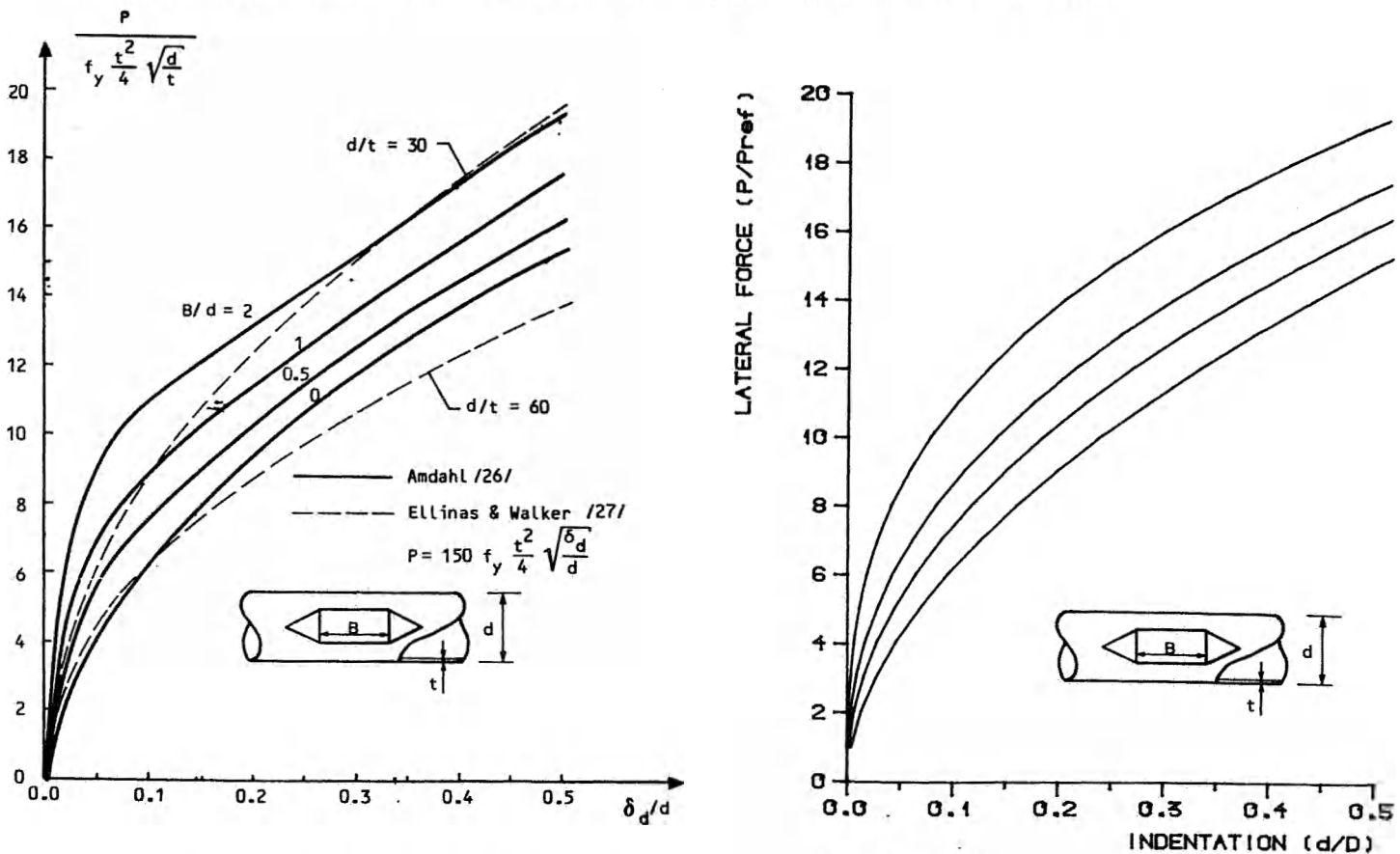


Figure 13.1. Load indentation, DnV

USFOS model

In USFOS, the curves were parametrized, and the following formulas were implemented:

$$\frac{P}{P_{ref}} = C_1 \left(\frac{\delta}{D}\right)^\alpha \quad (13.1)$$

$$P_{ref} = \sigma_y \frac{t^2}{4} \sqrt{\frac{D}{t}}$$

$$C_1 = 22 + 1.2 \frac{B}{D}$$

$$\alpha = \frac{1.925}{3.5 + \frac{B}{D}}$$

The resulting load indentation relationships are shown in Figure 13.1.

To account for the influence of axial force on the dent growth, the following correction was introduced.

$$\frac{P}{P_{ref}} = C_1 \left(\frac{\delta}{D}\right)^\alpha \frac{4}{3} \sqrt{1 - \frac{1}{4} \left[1 - \frac{N}{N_p}\right]^2}, \quad -0.5 \leq \frac{N}{N_p} \leq 1.0 \quad (13.2)$$

where N and N_p are the axial force and the axial capacity of the member, respectively. Effects of this correction is indicated in Figure 13.2.

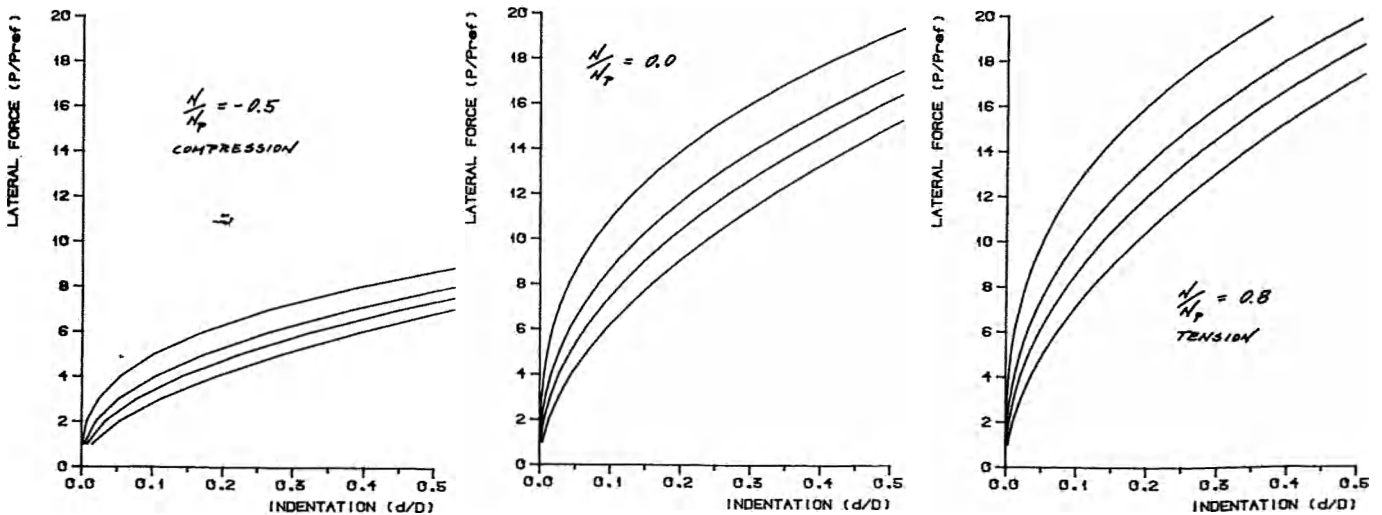


Figure 13.2. Correction for membrane action

This gives the following expression for dent depth as a function of lateral impact load and axial member force.

$$\frac{\delta}{D} = \left[\frac{\frac{P}{P_{ref}}}{\frac{4}{3} C_1 \sqrt{1 - \frac{1}{4} \left[1 - \frac{N}{N_p} \right]^3}} \right]^{1/\alpha} \quad (13.3)$$

13.3 IMPLEMENTATION IN THE PLASTICITY FORMULATION

The local indentation, and subsequent dent growth, cause a shrinkage of the yield surface. For members with plastic hinges, this shrinkage will cause the stress resultants to depart from the yield surface. However, this effect can be accounted for, by including in the consistency criterion Eq. (4.111) an additional term, which represents the change of the yield surface due to the temperature increment:

$$\Delta F = \Delta F_{t=\text{constant}} + \Delta F_{\Delta \delta} = 0$$

The second term takes the form

$$\Delta F_{\Delta \delta} = \frac{\partial F}{\partial \delta} \frac{\partial \delta}{\partial N} \Delta N + \frac{\partial F}{\partial \delta} \frac{\partial \delta}{\partial P} \Delta P \quad (13.4)$$

where P is the lateral component of the impact load, and N is the axial force in the member.

Comparing Eq. (13.4) to Eq. (4.103), it is seen that the first term can be considered as a contribution to the elasto-plastic incremental stiffness, and the second term as a contribution to the increment in consistent nodal forces.

13.4 SHIP INDENTATION CHARACTERISTICS

The strength and load-indentations characteristics of the ship are based on the curves given in /32/. Figure 13.4

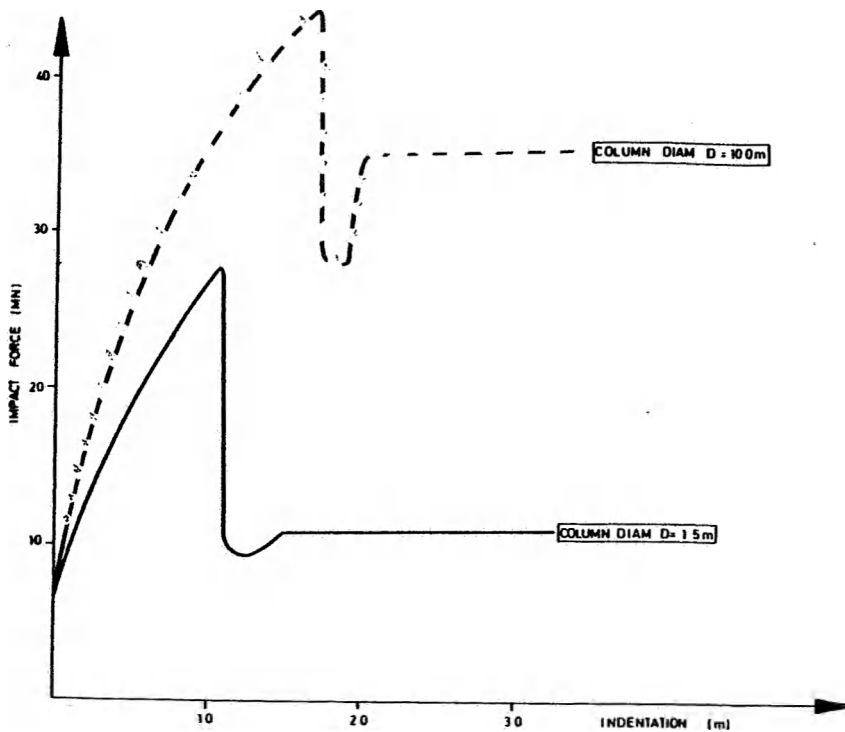


Figure 13.4 Load indentations curves for ship impact

The curves apply to broad side impact of a 5000 tonnes vessel. Post-collapse deformations of the ship are not included in the ship impact algorithm. That is, no energy absorption is calculated after the max ship impact force is reached.

14 DYNAMIC COLLAPSE ANALYSIS

14.1 Dynamic equations of motion

The dynamic equilibrium equation may be written as

$$\mathbf{F}^i(t) + \mathbf{F}^d(t) + \mathbf{F}^r(t) = \mathbf{R}(t) \quad (14.1)$$

where

$\mathbf{F}^i(t) = \mathbf{M}\dot{\mathbf{r}}$ vector of inertia forces

$\mathbf{F}^d(t) = \mathbf{C}\dot{\mathbf{r}}$ vector of damping forces

$\mathbf{F}^r(t) = \mathbf{K}\mathbf{r}$ vector of structural restoring forces (linear case)

\mathbf{R} vector of external loads

14.2 Mass matrix

The mass matrix of the discretized system may be given either as a consistent mass or a lumped mass. The consistent mass matrix is given by the expression :

$$\mathbf{M} = \int_{i=1}^{nel} \mathbf{a}_i^T \int_{V_i} \rho_i \mathbf{N}^T \mathbf{N} dV \mathbf{a}_i \quad (14.2)$$

where ρ is the density and \mathbf{N} the element interpolation polynomial.

Using a third order polynomial shape function the consistent mass matrix takes the following form for a 4 DOF beam element:

$$\mathbf{m} = \frac{\bar{m}l}{420} \begin{bmatrix} 140 & 0 & 0 & 70 & 0 & 0 \\ 0 & 156 & -22l & 0 & 54 & 13l \\ 0 & -22l & 4l^2 & 0 & -13l & -3l^2 \\ 70 & 0 & 0 & 140 & 0 & 0 \\ 0 & 54 & -13l & 0 & 156 & 22l \\ 0 & 13l & -3l^2 & 0 & 22l & 4l^2 \end{bmatrix} \quad (14.3)$$

The lumped mass matrix reads:

$$m = \frac{\bar{m}l}{420} \text{diag} [210, 210, \alpha l^2, 210, 210, \alpha l^2] \quad (14.4)$$

Concentrated masses may be specified at nodes.

14.3 Damping

Based on distributed material damping property a_i , the well-known equivalent viscous damping model is given by:

$$F^d = C \cdot \dot{r} \quad (14.5)$$

where the damping matrix is given by:

$$C = \int_{i=1}^{nel} a_i^T \int_{i=1} C_i N^T N dV a_i \quad (14.6)$$

For computational reasons the damping matrix is commonly expressed in terms of the Caughey-series:

$$C = \sum_k \alpha_k M (M^{-1}K)^k \quad (14.7)$$

where M and K are the mass and stiffness matrix respectively. This expansion reduces to the Rayleigh-damping form when the series is truncated after the two first terms. The weight-factors α_k are calculated from modal damping data available for the structure.

14.4 The α -method of time integration

The so-called HHT- α method for time integration proposed by Hilber, Hughes and Taylor /34/ is adopted. This method employs some sort of time averaging of the damping, stiffness and load term expressed by the α -parameter. A beneficial feature of the method is that it introduces artificial damping of higher frequency modes without degrading the accuracy. The governing equilibrium equation reads:

$$M\ddot{r}_{n+1} + (1+\alpha)C\dot{r}_{n+1} - \alpha C\dot{r}_n + (1+\alpha)K r_{n+1} - \alpha K r_n = (1+\alpha)R_{n+1} - \alpha R_n \quad (14.8)$$

$$\dot{r}_{n+1} = \dot{r}_n + \Delta t(\gamma)\ddot{r}_n + \Delta t\gamma\ddot{r}_{n+1} \quad (14.9)$$

The factors γ and β are the free parameters in the Newmark- β method which, along with α ,

$$r_{n+1} = r_n + \Delta t \dot{r}_n + \frac{\gamma \Delta t^2}{2} (1-2\beta) \ddot{r}_n + \Delta t^2 \beta \ddot{r}_{n+1} \quad (14.10)$$

determine the stability and accuracy of the quadrature formula. In the original Newmark- β method ($\alpha=0$) γ is set equal to 0.5 to avoid artificial damping. Depending on the value of β different integration methods are retrieved, such as second central difference method ($\beta=0$), linear acceleration ($\beta=1/6$) and constant average acceleration ($\beta=1/4$). Only the integration with constant average acceleration is unconditionally stable, otherwise the method is conditionally stable. In the HHT- α method unconditional stability is obtained when the following conditions are satisfied:

$$\begin{aligned} -\frac{1}{3} < \alpha < 0 \\ \gamma &= \frac{1}{2} (1 - 2\alpha) \\ \beta &= \frac{1}{4} (1 - \alpha)^2 \end{aligned}$$

Incremental equations are developed as follows:

$$\begin{aligned} M(\dot{r}_{n+1} - \dot{r}_n) + (1+\alpha)C(\dot{r}_{n+1} - \dot{r}_n) + (1+\alpha)K(r_{n+1} - r_n) &= (1+\alpha)(R_{n+1} - R_n) \\ &+ R_n - M\dot{r}_n - C\dot{r}_n - Kr_n \end{aligned} \quad (14.11)$$

$$\Delta \dot{r}_{n+1} = \dot{r}_{n+1} - \dot{r}_n = \frac{1}{\Delta t^2 \beta} \Delta r_{n+1} - \frac{1}{\Delta t \beta} \dot{r}_n - \frac{1}{2\beta} \ddot{r}_n \quad (14.12)$$

$$\Delta \dot{r}_{n+1} = \dot{r}_{n+1} - \dot{r}_n = \frac{\gamma}{\Delta t \beta} \Delta r_{n+1} - \frac{\gamma}{\beta} \dot{r}_n - \Delta t \left(\frac{\gamma}{2\beta} - 1 \right) \ddot{r}_n \quad (14.13)$$

Combining equations (14.11-13) yields

$$\begin{aligned} \left[\frac{1}{\Delta t^2 \beta} \Delta r_{n+1} - \frac{1}{\Delta t \beta} \dot{r}_n - \frac{1}{2\beta} \ddot{r}_n \right] M + (1+\alpha) \left[\frac{\gamma}{\Delta t \beta} \Delta r_{n+1} - \frac{\gamma}{\beta} \dot{r}_n - \Delta t \left(\frac{\gamma}{2\beta} - 1 \right) \ddot{r}_n \right] C \\ + (1+\alpha) [\Delta r_{n+1}] K = (1+\alpha) (R_{n+1} - R_n) + \alpha R_n - M\dot{r}_n - C\dot{r}_n - Kr_n \end{aligned} \quad (14.14)$$

The only unknown is Δr_{n+1} . Collecting all unknown on left hand side yields

$$\begin{aligned} \left[(1+\alpha)K + (1+\alpha) \frac{\gamma}{\Delta t \beta} C + \frac{1}{\Delta t^2 \beta} M \right] \Delta r_{n+1} = \\ (1+\alpha)(R_{n+1} - R_n) + \alpha R_n - M\dot{r}_n - C\dot{r}_n - Kr_n + \\ \left(\frac{1}{\Delta t \beta} \dot{r}_n + \frac{1}{2\beta} \ddot{r}_n \right) M + \left[(1+\alpha) \left(\frac{\gamma}{\beta} \dot{r}_n + \Delta t \left(\frac{\gamma}{2\beta} - 1 \right) \ddot{r}_n \right) \right] C \end{aligned} \quad (14.15)$$

In the subsequent derivation proportional damping is assumed:

$$\mathbf{C} = \mathbf{C}_0 + \alpha_1 \mathbf{M} + \alpha_2 \mathbf{K} \quad (14.16)$$

Consequently, the governing equation can be written as

$$\mathbf{K}^* \Delta \mathbf{r}_{n+1} = \Delta \mathbf{R}_{n+1} \quad (14.17)$$

where the effective stiffness becomes

$$\mathbf{K}^* = (1+\alpha) \left(1 + \frac{\alpha_2 \gamma}{\Delta t \beta} \right) \mathbf{K} + (1+\alpha) \frac{\gamma}{\Delta t \beta} \mathbf{C}_0 + \left[\frac{1}{\Delta t^2 \beta} + (1+\alpha) \frac{\alpha_1 \gamma}{\Delta t \beta} \right] \mathbf{M} \quad (14.18)$$

or

$$\mathbf{K}^* = a_K \mathbf{K} + a_C \mathbf{C} + a_M \mathbf{M} \quad (14.19)$$

where the definition of a_K , a_C , a_M is evident from equation (14.18). The effective load vector takes the form:

$$\begin{aligned} \Delta \mathbf{R}_{n+1} = (1+\alpha) & \left[\mathbf{R}_{n+1} - \mathbf{R}_n + \left(\frac{\gamma}{\beta} \dot{\mathbf{r}}_n + \Delta t \left(\frac{\gamma}{2\beta} - 1 \right) \ddot{\mathbf{r}}_n \right) \mathbf{C} \right] \\ & + \left(\frac{1}{\Delta t \beta} \dot{\mathbf{r}}_n + \left(\frac{1}{2\beta} - 1 \right) \ddot{\mathbf{r}}_n \right) \mathbf{M} + \mathbf{R}_n - \mathbf{C} \dot{\mathbf{r}}_n - \mathbf{K} \mathbf{r}_n \end{aligned} \quad (14.20)$$

or

$$\Delta \mathbf{R}_{n+1} = (1+\alpha) (\mathbf{R}_{n+1} - \mathbf{R}_n + \mathbf{C}_C \mathbf{C}) + \mathbf{C}_M \mathbf{M} + \mathbf{R}_n - \mathbf{C} \dot{\mathbf{r}}_n - \mathbf{K} \mathbf{r}_n \quad (14.21)$$

where again the definition of \mathbf{C}_C and \mathbf{C}_M is obvious from equation (14.20).

The total acceleration, velocity and displacement at step $n+1$ become:

$$\mathbf{r}_{n+1} = \mathbf{r}_n + \Delta \mathbf{r}_{n+1} \quad (14.22)$$

$$\dot{\mathbf{r}}_{n+1} = \frac{\gamma}{2\beta} \Delta \mathbf{r}_{n+1} + \left(1 - \frac{\gamma}{\beta} \right) \dot{\mathbf{r}}_n - \Delta t \left(\frac{\gamma}{2\beta} - 1 \right) \ddot{\mathbf{r}}_n \quad (14.23)$$

$$\ddot{\mathbf{r}}_{n+1} = \frac{1}{\Delta t^2 \beta} \Delta \mathbf{r}_{n+1} - \frac{1}{\Delta t \beta} \dot{\mathbf{r}}_n + \left(1 - \frac{1}{2\beta} \right) \ddot{\mathbf{r}}_n \quad (14.24)$$

14.5 Equilibrium iteration

In general, unbalance will be introduced during each load increment. To achieve equilibrium the following iterative scheme is introduced:

$$\Delta R_{n+1}^{j+1} = \Delta R_{n+1}^j + \Delta_{n+1}^{i+1} \quad (14.25)$$

$$\Delta R_{n+1}^{j+1} = \Delta R_{n+1}^j + \dot{\Delta}_{n+1}^{i+1} \quad (14.26)$$

$$\Delta R_{n+1}^{j+1} = \Delta R_{n+1}^j + \ddot{\Delta}_{n+1}^{i+1} \quad (14.27)$$

where Δ_{n+1}^{i+1} , $\dot{\Delta}_{n+1}^{i+1}$, $\ddot{\Delta}_{n+1}^{i+1}$ denote increments in displacement, velocity and acceleration during iterative step number $i+1$.

From equations (14.12-13) the following relationships are obtained:

$$\Delta_{n+1}^{i+1} = \frac{\gamma}{\Delta t \beta} \Delta_{n+1}^{i+1} \quad (14.28)$$

$$\dot{\Delta}_{n+1}^{i+1} = \frac{1}{\Delta t^2 \beta} \Delta_{n+1}^{i+1} \quad (14.29)$$

The only unknown is the displacement increment, which is determined from:

$$K^* \Delta_{n+1}^{i+1} = \Delta R_{n+1}^{i+1} \quad (14.30)$$

where K^* is given by equation (14.18). The right hand side represents the unbalance between external loads and internal forces and is given by:

$$\begin{aligned} \Delta R_{n+1}^{i+1} &= (1+\alpha) R_{n+1} - \alpha R_n \\ &- M F_{n+1} - (1+\alpha) C f_{n+1} + \alpha C f_n - (1+\alpha) K r_{n+1} + \alpha K r_n \\ &= (1+\alpha) (R_{n+1} - C f_{n+1} - K r_{n+1}) - M F_{n+1} \\ &- \alpha (R_n - C f_n - K r_n) \end{aligned} \quad (14.31)$$

As soon as equilibrium is achieved the load term vanishes. In practice, convergence is assessed on the basis of iterative displacement increments in the same way as for static analysis.

14.6 The predictor-corrector method

An alternative to the above procedure is to use the predictor-corrector approach. Then the equations (14.9-10) are split into two parts:

$$\dot{r}_{n+1} = \dot{r}_{n+1}^p + \dot{r}_{n+1}^c \quad (14.32)$$

$$\dot{r}_{n+1}^p = \dot{r}_n + \Delta t (1-\gamma) \ddot{r}_n \quad (14.33)$$

$$\dot{r}_{n+1}^c = \Delta t \gamma \ddot{r}_{n+1} \quad (14.34)$$

$$r_{n+1} = r_{n+1}^p + r_{n+1}^c \quad (14.35)$$

$$r_{n+1}^p = r_n + \Delta t \dot{r}_n + \frac{\Delta t^2}{2} (1-2\beta) \ddot{r}_n \quad (14.36)$$

$$r_{n+1}^c = \Delta t^2 \beta \ddot{r}_{n+1} \quad (14.37)$$

The first part r_{n+1}^p and \dot{r}_{n+1}^p are called the predictors. They depend upon values at step previous step and can be determined without solving of incremental equations. Thus, the displacements at step $n+1$ is first estimated on the basis of the predictors (implicitly assuming the acceleration \ddot{r}_{n+1} equal to zero). Then, the corrector terms, r_{n+1}^c and \dot{r}_{n+1}^c , which only depend upon the total acceleration at step $n+1$, \ddot{r}_{n+1} , are determined during equilibrium iterations as described above. The displacement, acceleration and velocity are updated as follows:

$$\begin{aligned} r_{n+1}^{i+1} &= r_{n+1}^i + \Delta r_{n+1}^{i+1} \\ \ddot{r}_{n+1}^{i+1} &= \left(\ddot{r}_{n+1}^{i+1} - \ddot{r}_{n+1}^p \right) / \Delta t^2 \beta \\ \dot{r}_{n+1}^{i+1} &= \dot{r}_{n+1}^p + \ddot{r}_{n+1}^{i+1} \Delta t \gamma \end{aligned} \quad (14.38)$$

14.7 Time step scaling

An important concept in the static solution algorithm is scaling of the step length to avoid large overshooting of the yield surface during load incrementation.

It is considerably more complex to perform scaling in dynamic analysis. The natural parameter to scale is the time step Δt . However it is seen from equations 12 and 14 that both the effective stiffness as well as the effective load are (nonlinear) functions of Δt . In addition the various components of the displacement increment vary non-proportionally during the time step.

A better way to achieve some degree of scaling and thereby prevent large overshooting of yield surfaces is to use the predictor-corrector method. In the predictor phase scaling of Δt is easily performed by the same algorithm used in static analysis. As noted above this involves no solution of the dynamic equilibrium equations. Once the scaled time increment is determined, the new plastic hinge is introduced and the dynamic equilibrium equation is solved in the corrector phase keeping Δt constant. The corrector displacements cause drift-off from the yield surface of existing hinges and new hinges may also form. However, repeated equilibrium iterations ensure that the force state in yield hinges return to the yield surface.

15 EXTERNAL HYDROSTATIC PRESSURE

15.1 Introduction

An option is included in USFOS to account for large hydrostatic pressures on the capacity of tubular beam elements. Such a load situation may occur for structural components such as bracing members of deep sea offshore platforms in which water is sealed off.

The external pressure exerted by water introduces compressive stresses in the circumferential direction. This action reduces both the cross sectional plastic capacities as well resistance to local wall buckling.

15.2 Tube section interaction curves

Figure 15.1 depicts a typical set of interaction curves with respect to axial force and bending moment for a tube section with $D/t = 48$, exposed to external pressure. It is observed that as the pressure increases, the size of the interaction function decreases. From numerical simulations /35/ it has been concluded that the interaction functions for different levels of external pressure have almost identical shapes.

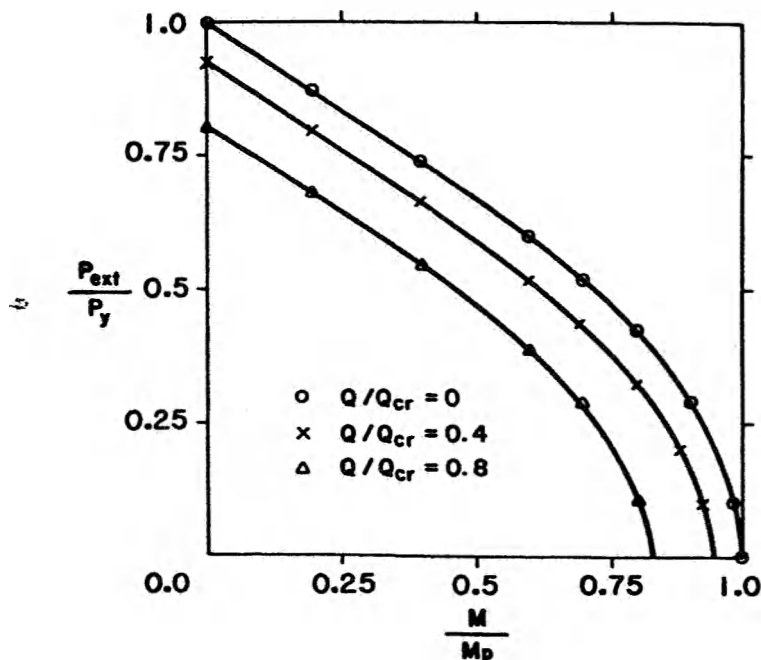


Figure 15.1 Tube section interaction curves for various levels of external pressure Q

The plastic capacities with respect to axial force P_{PQ} and bending moment M_{PQ} , including the effect of external pressure, are given by /35/:

$$N_{PQ} = N_p[1.0 - A_p(Q/Q_{cr})^{1.2}] \quad (15.1)$$

$$M_{PQ} = M_p[1.0 - A_m(Q/Q_{cr})]$$

where

$P_p = A \cdot \sigma_y$ and $M_p = W_p \cdot \sigma_y$ are the cross sectional plastic capacities without the effect of external pressure. The normalized pressure is given by Q/Q_{cr} where Q_{cr} is the elastic collapse pressure:

$$Q_{cr} = \frac{2E(tD)^3}{(1-\nu)^2} \quad (15.2)$$

A_p and A_m are geometry dependent modification factors for the axial and moment capacity, respectively, /35/:

$$A_p = 0.18 + 1.09 \cdot 10^5 / (D/t)^{3.65} \quad (15.3)$$

$$A_m = 0.15 + 4.30 \cdot 10^4 / (D/t)^{3.51}$$

P_{PQ} and M_{PQ} are plotted in Figure 15.2 as a function of the relative pressure Q/Q_{cr} .

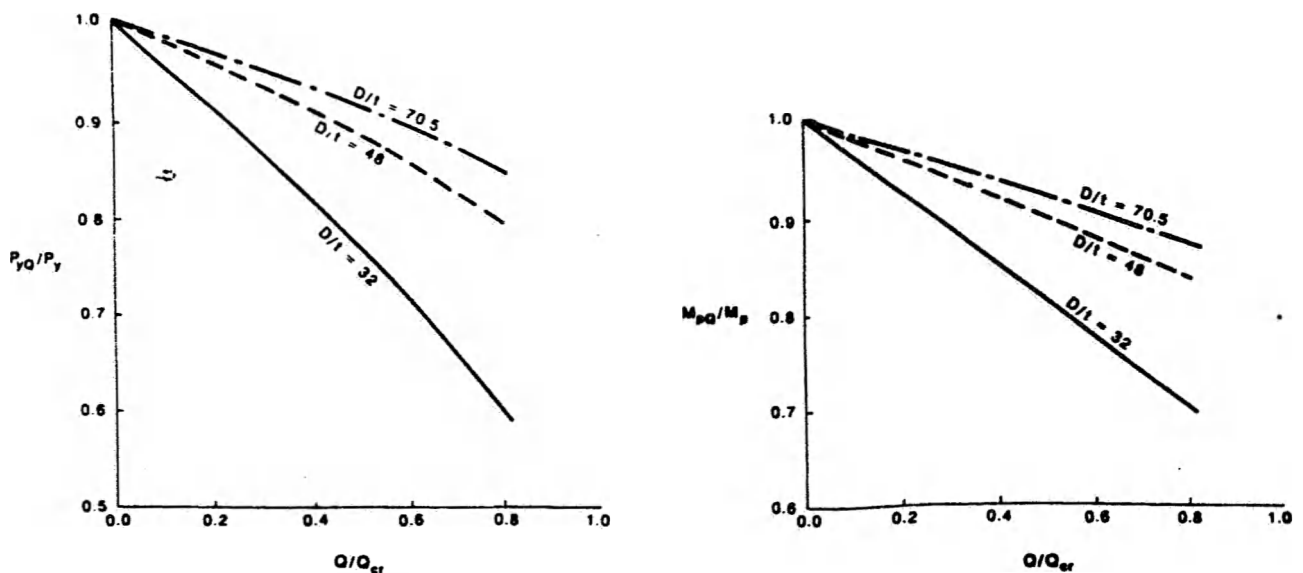


Figure 15.2 Plastic capacities as a function of relative pressure Q/Q_{cr}

The interaction function for the tube section, when accounting for external pressure, is given by:

$$(1 - m_x^2)^{1/2} \cdot \cos\left(\frac{\pi}{2} \frac{n}{(1 - m_x^2)^{1/2}}\right) - (m_y^2 + m_z^2)^{1/2} = 0$$

(15.4)

where

$$n = \frac{N}{N_{PQ}}, \quad m_x = \frac{M_x}{M_{Px}}, \quad m_y = \frac{M_y}{M_{PQy}}, \quad m_z = \frac{M_z}{M_{PQz}}$$

From Eq 15.4 it is observed that the effect from the external pressure on the plastic torsional capacity M_{Px} is neglected.

15.3 Implementation in the plasticity formulation

The effect of the external pressure on the plastic cross sectional behaviour is implemented in the two-surface model. The size of the bounding surface corresponding to full plastification of the cross section is reduced according to Eq 15.1. It is for convenience also assumed that the size of the yield surface, corresponding to initial yielding, is given by Eq 15.1. Figure 15.3 shows the yield and bounding surface for a compressed member located at 300 m water depth.

The effects of external pressure only enters the plasticity formulation which implies that the elastic behaviour of tubular components is unaffected. This is clearly illustrated in Figure 15.4 which shows the buckling load of two compressive members with slenderness of 60 and 120 respectively. For the column with slenderness equal to 120, it is seen that the peak compressive load is the same for zero and 300 m water depth, respectively.

The external hydrostatic pressure is calculated by USFOS at both ends of the beam element as well as the midspan, i.e. at the positions where a yield hinge may occur. The external pressure is calculated on basis of the initial geometry of the structure neglecting the pressure changes caused by structural deformations.

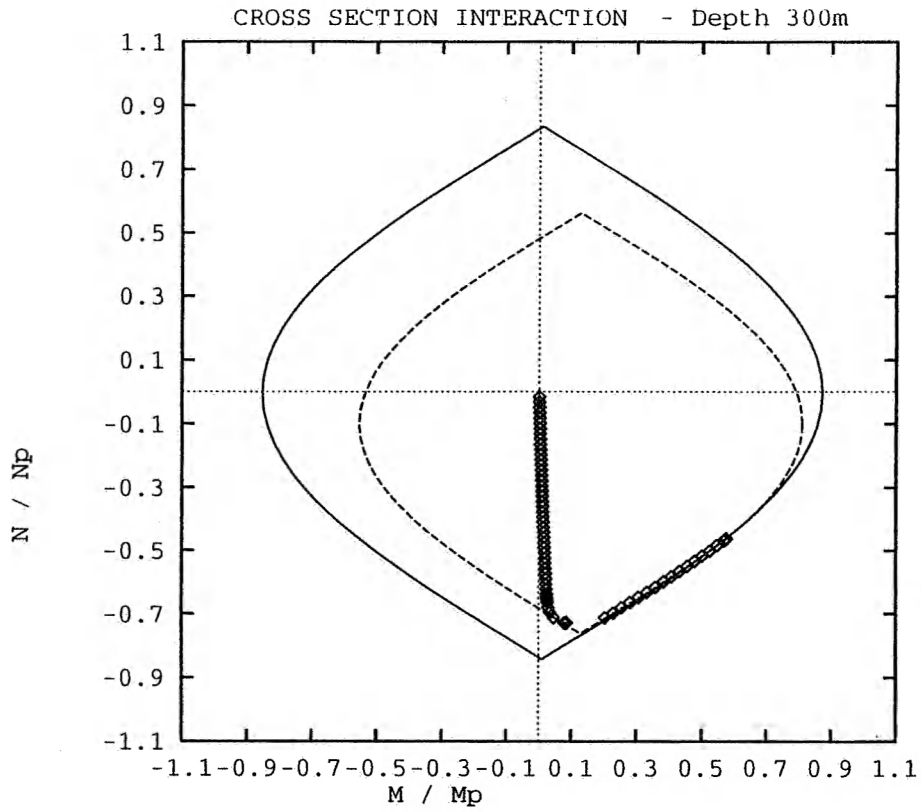


Figure 15.3 Plasticity model including effect of external pressure

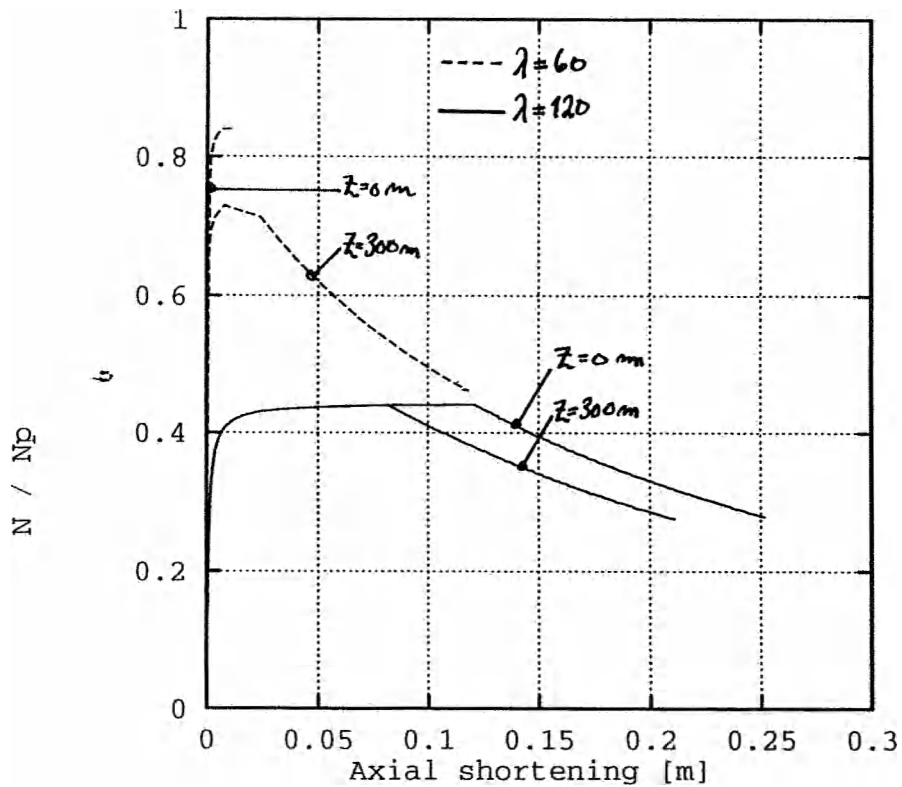


Figure 15.4 Axial force is axial displacement for columns with different slenderness

15.4 Limitations

It should be noticed that the accelerating effect of the hydrostatic pressure on the local dent growth is **not** realistically modelled. This implies that USFOS may predict the local dent growth unconservatively for the case when the tube section is exposed to external hydrostatic pressure.